Resolution Requirements for the Spatial Sampling of Rainfall

Paul Evan Shucksmith

A thesis submitted in fulfilment of the requirements
for the degree of Doctorate of Philosophy in Physics

The University of Auckland
2013

Abstract

Spatial rainfall information is used for a wide variety of applications. The resolution at which this information is sampled can have a significant impact on its usefulness to these applications. This research is directed towards assessing the magnitude of this impact. Using a high resolution radar dataset of three months' duration, rainfall is degraded in spatial and temporal resolution to a range of spatial and temporal scales so that—from a comparison with the original high resolution data—the error arising from lower resolution sampling can be quantified.

On average, across all significant events in the dataset, this sampling error (expressed in RMSE normalized to the mean average rainfall accumulation) was observed to be approximately 0.2 for 2000 m/300 s sampling. A relationship was found between the mean characteristic length scale of an event and spatial sampling error magnitude, allowing prediction of sampling error using only low resolution data. By simulating a rain gauge network using the same dataset, the contribution that sampling error makes to the total radar/rain gauge bias was estimated to be, at a minimum, approximately 30%. Gauge correction of radar data in light of these sampling errors was also assessed and a correction scheme that would minimize the impact of sampling errors was proposed. Additionally, the impact of sampling error on a distributed rainfall runoff model (GSSHA) was examined. The magnitude of this error was fairly substantial (a variation of 14–30% in peak flow for conventional radar resolutions) and was found to be greater for less saturated initial soil moisture conditions.

THE UNIVERSITY OF AUCKLAND
SCHOOL OF GRADUATE STUDIES

Co-Authorship Form

Graduate Centre
ClockTower – East Wing
22 Princes Street, Auckland
Phone: +64 9 373 7599 ext 81321
Fax: +64 9 373 7610
Email: postgraduate@auckland.ac.nz
www.postgrad.auckland.ac.nz

This form is to accompany the submission of any PhD that contains research reported in published or unpublished co-authored work. **Please include one copy of this form for each co-authored work**. Completed forms should be included in all copies of your thesis submitted for examination and library deposit (including digital deposit), following your thesis Abstract.

Please indicate the chapter/section/pages of this thesis that are extracted from a co-authored work and give the title and publication details or details of submission of the co-authored work.

Chapter 2 includes significant extracts from 'The spatial and temporal sampling errors inherent in low resolution radar estimates of rainfall' by Shucksmith, P. E., Sutherland-Stacey, L. and Austin, G. L.

Nature of contribution by PhD candidate	Participated in obtaining data, wrote most code, conducted analyses, wrote text
Extent of contribution by PhD candidate (%)	96%

CO-AUTHORS

Name	Nature of Contribution
Luke Sutherland-Stacey	Participated in obtaining data, minor contributions to code and text
Prof. Geoff Austin	Assisted with general overview, minor contributions to text

Certification by Co-Authors

The undersigned hereby certify that:

- the above statement correctly reflects the nature and extent of the PhD candidate's contribution to this work, and the nature of the contribution of each of the co-authors; and
- in cases where the PhD candidate was the lead author of the work that the candidate wrote the text.

Name	Signature	Date
Luke Sutherland-Stacey		12/09/2012
Geoff Austin		22/09/2012

Acknowledgements

I would first and foremost like to thank my wife Ann for her patience and support over the four years of this PhD study. Thanks also must go to my supervisor Professor Geoff Austin whose guidance and insight made this work possible. I would also like to thank fellow members of the Atmospheric Physics Group especially fellow PhD candidate Luke Sutherland-Stacey with whom the field work for this research was carried out. Thanks also go to technicians Steve Warrington, Murray Hollis and the late Kevin George, for their vital assistance with the radar field work. I am also thankful my family for their support while I undertook this degree.

Contents

List of Figures

List of Tables

Introduction

Rainfall is one of the oldest quantifiably observed atmospheric phenomena, with its measurement dating back to at least the 4th Century BC. The reason for this is that rainfall is so easy to measure, place a cup or a bucket outside and it is a simple task to determine how much it has rained just by looking at how much water there is in the container. If the same container is used each time then the rainfall can be easily quantified.

At first glance, it may appear that the job is pretty much done; one would just record the amount of water in the bucket every n hours/days to obtain a rainfall record at the required temporal frequency. To add convenience, a gauge that automatically records and then empties the rainfall could be invented. This stage was reached in the 17th Century and not much has changed with rain gauges in the hundreds of years since.

While the rainfall at the point where the rain gauge is sited may be measured reasonably well, one quickly finds that another rain gauge located a certain distance away will record a different total. One then notices that this difference can vary considerably between (and during) storms. If the intention is to estimate the rain falling over an area (to estimate the volume of rain fallen into a catchment, for example), it is likely several gauges should be used. But how many? Is there a minimum decorrelation length (say 1 km) at which it would be 'safe' to space the gauges apart by? It turns out that even gauges that are very close together (< 10 m) do not exactly agree. Even for 1 km spacing, to cover a decent sized catchment, one would require what would usually be considered an infeasible number of gauges.

Weather radar, made feasible with the invention of the cavity magnetron in 1940, provided a revolutionary change in the way rainfall could be measured. As it measures rainfall in a spatial manner, radar is presumably an ideal solution for obtaining areal

rainfall information. However, a radar does not directly measure rainfall, but an integration of the radar cross sections of all of the particles within its sampling volume. Additionally, this sampling volume is not at ground level but at some distance above the ground.

Yet again, as it was for gauges, the spatial variation of the rainfall field causes sampling issues with the measurement. Any variation on a scale that is smaller than the sampling volume will be smoothed over, reducing the intensity of peaks and possibly giving an indication of rainfall in a location where there is none at all. To add to this, any variation of rainfall intensity inside of the radar's sampling volume will lead to a bias in the converted rainfall estimate. Another problem is introduced by the fact that a radar takes a certain amount of time to complete a measurement (or a set of measurements). Any change in the rainfall field that occurs between these measurements will not be observed, leading to a different estimate of rainfall accumulation depending upon the sampling period.

It is these sampling issues that are the focus of this thesis. What is the magnitude of this error? How does it vary with sampling resolution? With rainfall event? What is the impact on the many applications of the data? How much resolution is 'enough' for rainfall measurement? It is the aim that answers to these questions will be more informed after the completion of this work.

Although the investigation of this thesis is based predominantly on radar observations, many of the inferences resulting from this work are also applicable to satellite observations of rainfall.

The thesis will be set out as follows:

Chapter 1 gives an overview of rainfall observation: how it is performed, the problems associated with it, qualities of rainfall data and details many of the applications of rainfall data as well as predicting which of these applications will be most affected by sampling error. The applications deemed most affected will then be examined in the following chapters.

Chapter 2 describes the issue of sampling error in greater detail and, through the analysis of a high resolution radar dataset, simulates the effect of low resolution sampling to estimate its magnitude relating to quantitative precipitation estimation (QPE) by radar.

Chapter 3 details the other sources of radar error, attempting to place sampling error into context with all contributions to radar rainfall uncertainty.

Chapter 4 assesses the impact of sampling error on the procedure of gauge correcting radar data.

Chapter 5 introduces hydrological modelling, describes the use of and issues with radar in hydrology and looks at the variation in output that occurs when running a rainfall runoff model with lumped or distributed rainfall input. The variation of modelled rainfall runoff with input rainfall accumulation period is also assessed.

Chapter 6 assesses the impact of sampling error on the distributed rainfall runoff model GSSHA for an infiltration excess runoff scheme. The effect that sampling error in gauge correction has on this model is also examined.

Chapter 1

How Much Resolution is Enough for Rainfall Measurement?

A reply of "it depends" could be given to the question posed above. It depends upon the application of the rainfall data, it depends upon the characteristics of the rainfall system being measured and it depends upon the instrument which performs the measurement. For these reasons, an overview of rainfall sources, applications of rainfall data and rainfall data properties will be given in the subsequent sections. Following this, an exploration into error resulting from the choice of observation temporal and spatial resolution will be made using data from the University of Auckland's high resolution X-band radar. We should then be in a better position to discuss the resolutions necessary for rainfall observation.

1.1 Rainfall Sources

To understand rainfall data, it is important to understand where it comes from. The primary sources of rainfall data are rain gauges, radar and weather satellites. Alternative sources include LIDAR (Shipley et al., 1974, Lewandowski et al., 2009) and the more recently investigated use of microwave links (Upton et al., 2005, Rahimi et al., 2003, Leijnse et al., 2010); utilizing the microwave links from commercial telecommunications networks is a promising area of study (Overeem et al., 2011). Forecasts, from numerical prediction models or from radar nowcasts, can also be considered a source of

rainfall information, however, they are not an observation and will not be covered here. A brief history and outline of each data source will be given in the following sections.

1.1.1 Rain Gauges

The rain gauge can come in several different forms and is formally defined as "a device for the measurement of rainfall". Under this definition, radar and satellite systems could also be included, however, we shall limit the coverage of this term to devices which measure the rainfall at the location of that device (i.e. not consider 'remote sensing' devices).

The conventional form of the rain gauge, in a form which may date back to 15th Century Korea (although it existed in some form or other much earlier), consists of an upright cylinder with a funnel at its top end which channels water into a narrower cylinder that has gradations down its length in order for rainfall depth to be read off. Such a device is very inexpensive to make but requires a human observer to record rainfall amount and empty the gauge at a specified interval.

The need for an observer was removed for the first time in 1662 by Sir Christopher Wren who invented the first tipping bucket rain gauge (Biswas, 1967). Modern tipping bucket gauges store tip information (each tip is usually registered electronically using a reed switch) onto internal memory and/or communicate this information to a central receiving location. These communicating 'telemetered' gauges are usually much more expensive to install and operate than gauges that store data locally but they allow real-time rainfall data of quite high resolution (dependent on the rainfall rate).

Tipping bucket gauges can display underestimation of high rainfall rates due to the finite time for the tipping mechanism to oscillate between states. Rainfall can also be misrepresented by the fact that rainfall from a previous event which filled the bucket almost to capacity will be falsely attributed to a new event which *does* completely fill the bucket, resulting in a tip.

Other designs of automatically recording rain gauges also exist. Weighing gauges continuously measure the weight of gathered fallen precipitation. These are especially used for measurement of solid precipitation, usually with the addition of a heater or antifreeze. Tipping bucket gauges can also be used for this purpose if they include a heated funnel to first melt the precipitation. Such a heating system does introduce

Figure 1.1: Tipping bucket rain gauge mounted on fence post, Ardmore, Auckland.

evaporation and wetting losses, however (Savina et al., 2012). Weighing gauges are even more costly than tipping bucket gauges and involve increased service requirements relating to emptying of the gauge and replacement and disposal of antifreeze (if used).

Drop counting gauges (eg. Stow et al., 1998) provide an increase in resolution over tipping bucket gauges, being able to measure rainfall in far smaller quanta than the typical 0.1 mm or 0.254 mm equivalent rainfall buckets. These devices operate by collecting rainfall in a funnel which is then routed between a pair of electrodes as a water drop of specific volume. The time of each drop is then recorded similarly to how each 'tip' is recorded by a tipping bucket gauge. There is some uncertainty in the requirement of a constant drop volume and issues with the recording of heavy rainfall when the drops can turn into a constant stream of water. The device also requires much more power than a tipping bucket gauge as the detection mechanism (the electrodes) requires a power source to operate.

Impact gauges measure the force imparted by hydrometeors as they impact the surface of the gauge. This design is usually used for disdrometers (whose primary purpose is the measurement of the size distribution of hydrometeors) but they also function as rain gauges and are commercially available as such.

A benefit of this design is that solid and wet precipitation can often be separately distinguished. A shortfall in the design is the requirement of knowledge about the velocity

of the impacting hydrometeor so as to ascertain its mass related to its observed momentum. The velocity can vary significantly in the presence of wind. The observed force of hydrometeor impact can also vary with direction of impact and the location of impact on the gauge surface. The surface area of the gauge must also be made small enough so that multiple impacts are not likely to occur simultaneously for a desired maximum observable rainfall rate. A 'dead-time' exists between drops where the impact recording mechanism reattains equilibrium.

Acoustic gauges (really just a different form of the above impact gauge) measure the intensity of sound pressure level resulting from hydrometeors impacting a 'drum-like' surface. This surface can be as simple as an upside down paint tin with a microphone inside (Manley, 2006). The design removes the problem of clogging that can occur in funnel designs whereby debris can accumulate in the inlet of the gauge preventing or restricting rainfall from entering. The acoustic properties of the gauge would, however, alter if the surface of the gauge became severely contaminated.

Acoustic gauges can also be realized using bodies of water and a hydrophone. This would remove drum surface contamination issues and could allow the use of a much greater surface area of measurement. Acoustic gauges can suffer from false positive detection from sources such as wind, wildlife and other ambient sound. Many of these false positive detections can be removed by software algorithms, however.

Optical gauges exist that consist of an infrared emitter directed towards an infrared sensor located tens of centimetres away. The intensity of this signal is attenuated in the presence of rainfall which can be related to rainfall rate.

All of these gauges suffer from issues relating to wind. The fact that a gauge which is placed at some certain height above the ground records less rainfall than a gauge which is placed at a lower height has been noted since the 18th century (Heberden, 1769). It was discovered in the 19th century that this is due to the difference in wind speed at ground level (which approaches zero) and at the height of the gauge. Hydrometeors, especially those of low mass, may be prevented from entering the gauge due to alteration of the wind flow by the presence of the gauge. This effect on average leads to underestimation of rainfall by 5–10% and can lead to even greater underestimation for individual events (Neff, 1977).

To obtain a gridded rainfall product from a network of gauges, interpolation tech-

niques must be utilized. The simplest such method would be for each point in the grid to use the rainfall from the closest gauge. This is known as the Thiessen polygons or nearest neighbour method. Slightly more complex methods are bilinear interpolation and inverse distance weighting. More complex methods involve geostatistical techniques, for example: simple Kriging, ordinary Kriging and Kriging with external drift. For modern reviews and evaluations of these methods, the reader is referred to Haberlandt (2007), Zhang and Srinivasan (2009) and Grimes and Pardo-Igzquiza (2010).

That the measurement of rainfall at a particular point in space does not necessarily represent the rainfall occurring in the surrounding area of that point is discussed later in this chapter.

Rain gauges remain one of the most popular devices for rainfall measurement and are often utilized as a reference source when rainfall measurement from other sources are to be calibrated and assessed.

1.1.2 Radar

History

Before World War II, Radar (an acronym for radio detection and ranging) was limited to frequencies of up to ~ 200–400 MHz. Whilst able to detect large targets such as aeroplanes, these radars were unable to observe precipitation. Higher frequencies were able to be generated although only at very low intensities, unsuitable for use with radar. This changed with the invention of the cavity magnetron at the University of Birmingham in 1940, which made the construction of radars with centimetre wavelengths a reality.

As Britain did not have sufficient manufacturing capabilities during the war, the technology was given to the United States in exchange for its support. This resulted in the formation of the Radiation Laboratory at MIT which was responsible for the majority of the radar development in the latter part of WWII.

S-band (3 000 MHz) and X-band (10 000 MHz) radars were developed primarily for military uses; for instance, on anti-aircraft guns to assist in targeting aircraft and on aeroplanes for use in hunting submarines. A meteorological use that was also of military application was the ability to determine wind speed by the tracking of weather balloons, which greatly improved the targeting accuracy of artillery guns.

It was noticed early on that echoes from rain were being detected by the shorter wavelength radars which were not observable by the longer wavelength (200–400 MHz) radars. In Atlas (1990) it is stated that "the first detection of precipitation on radar probably occurred in the United Kingdom in late 1940 or early 1941."

Major theoretical work on the effect of weather on radar performance was performed by the Rydes (eg. Ryde and Ryde, 1944, Ryde, 1946). From their work they obtained analytic relations for the expected attenuation and scattering due to meteorological targets. Relations were found over a range of radar frequencies and drop sizes varying from cloud size to rain drop size hydrometeors in both liquid and solid phases. They also determined that the change in reflectivity as snow melted to rain was the likely cause of the bright band.

It was not until after the war that quantitative measurements of reflectivity were carried out, notably by Marshall et al. (1947) and Marshall and Palmer (1948) at the Stormy Weather Group at McGill University. In these papers, a power law relationship was found between radar reflectivity (Z) and rainfall rate (R). The Z-R relationship found by Marshall and Palmer (1948) is still used to this day, although in the slightly altered form of $Z = 200R^{1.6}$ and bears their names.

Great improvements in the technology of radars took place after the war. Logarithmic receivers started to be used in the late 50s providing vast improvements to dynamic range. The CAPPI (constant altitude plan position indicator) was introduced by Langleben (1956) at McGill University. Digitization of weather radars occurred in the late 60s and early 70s. Significant research was carried out on Doppler weather radar between 1965–75. By the end of this period, most issues had been solved and use of Doppler radars became more widespread.

Since their invention, radars have been used to provide detailed information on the structure of weather events such as tropical cyclones, tornadoes and thunderstorms which could not otherwise have been observed.

For a more complete history of meteorological radars the reader is recommended to read Atlas (1990).

Description

The most common form of radar for observation of rainfall operates by emitting a pulse of microwave energy, focused and directed by reflecting off a large parabolic dish, and recording the energy from this pulse that is backscattered by hydrometeors in its path. The distance from the radar to the observed 'target' (ideally the target is precipitation but can also be terrain, trees, birds, etc.) is determined by the difference between the time at which the pulse was transmitted and the time at which the backscattered energy is received. Many such pulses must be averaged to obtain a reasonable estimate of radar reflectivity (Z) due to the randomly varying distribution of scatterers in the beam volume causing the returned radar signal to be incoherent and exhibit a random fluctuation (Marshall, 1953).

The dish is rotated constantly in a single direction—or scanned back and forth—so as to form a 2D plan image (known as plan position indicator or PPI) of reflectivity. The dish is also often altered in elevation to obtain a 3D 'volume' scan of the surrounding precipitation. This is performed in part to minimize ground clutter at short ranges by using high elevation scans and to reduce the height of the radar beam at long ranges to avoid beam overshooting (whereby the radar beam's path is such that it passes above lower altitude precipitation leading to non-detection).

Reflectivity is then related to rainfall rate using the Z-R relationship described earlier. The general relationship takes the form $Z = aR^b$, where Z is radar reflectivity, R is rainfall rate (in mm hr^{-1}) and a and b are constants. The basis for the power law form of the Z-R relationship is that reflectivity is proportional to $\sum_n D(n)^6$, where $D(n)$ is the diameter of the n^{th} hydrometeor. Assuming that the hydrometeors' diameters are exponentially distributed (the Marshall-Palmer distribution, Marshall et al., 1947), the Z-R power law results. While raindrop size distributions on average tend towards the Marshall-Palmer distribution, there can be variation from this distribution in individual storms (Ohtake, 1970). While other distributions have been suggested, the simplicity of the Z-R relationship based on the Marshall-Palmer distribution, has lead to its widespread adoption for radar rainfall estimation.

The wavelength of the emitted pulse of microwave energy from radars used for the measurement of precipitation usually falls into one of the following microwave bands: S-band (2–4 GHz, 15–7.5 cm), C-band (4–8 GHz, 7.5–3.8 cm) or X-band (8–12 GHz,

Figure 1.2: C-band radar with radome. MetService radar located in Wellington, New Zealand. Picture taken in 2011.

3.8–2.5 cm).

Shorter wavelengths are much more likely to be scattered by hydrometeors (due to the $\frac{1}{\lambda^4}$ nature of Rayleigh scattering [Strutt, 1871]) which on the one hand decreases the transmission power required while on the other hand reduces the signal intensity quite dramatically in the presence of heavy rainfall (leading to attenuation of the signal behind such heavy rainfall). To avoid significant levels of attenuation when observing most precipitation systems, C-band or S-band wavelengths are most often used.

Shorter wavelength X-band radars are typically used for portable weather radar systems (for instance, on aeroplanes) and for research purposes due to their smaller size and lower power requirements. Due to the attenuation problem, X-band radars are typically assigned lower range scans (< 50 km) and must be carefully interpreted in the presence of heavy rainfall—greater than around 40 dBZ where attenuation reaches ~ 0.24 dB k^{-1} (Burrows and Attwood, 1949).

Cost is a major factor in the choice of radar transmitter wavelength as longer wavelengths translate to larger dishes and higher power. There is a balance between cost, resistance to attenuation and beam width.

There are many sources of error involved with radar estimation of precipitation and these will be discussed more fully in Chapter 3. The error source that is a focus of this thesis is sampling error. This is defined here as errors relating to the manner in which precipitation is sampled by the observing instrument, focusing on spatial and temporal resolution.

Radar reflectivity is a volume measurement, the size of this volume being determined by the duration of the transmitted pulse (the pulse length) and the angular distribution pattern of radiation emanating from the radar's dish (characterized by a beam width, a measure of angular width of the beam at which radiation intensity falls below 3dB of the peak). The pulse length is fairly trivial to alter in modern radar systems, meaning that the real limit on spatial resolution is the beam width.

Beam width is primarily determined by the diameter of the radar dish and the wavelength of the transmitted pulse. The longer the wavelength, the larger the dish must be to achieve a given beam width.

Dish sizes are typically designed to provide 1–2° beam widths for the particular wavelength of the transmitter. Due to the diverging nature of the beam, higher spatial resolution is obtained closer to the radar than is obtained at far ranges. For instance, for a radar with a 1° beam width, the beam spread is ~870 m at 50 km while at 200 km it reaches 3500 m. It is important to note that this spread is in the vertical as well as the horizontal, which leads to the vertical profile of reflectivity (VPR) being averaged out in relation to range from the radar. This can have some beneficial effect in that bright band contamination is often smoothed out, reducing its impact on rainfall estimates which have not been VPR corrected (a correction made on precipitation measurements observed at altitude to estimate the surface precipitation at that position). If VPR correction is performed, however, it is greatly desirable to possess knowledge of the VPR at all locations in the domain. The knowledge of the VPR at long range is much poorer due to beam spreading. While the many different VPR correction procedures can account for the mean VPR with various degrees of success, the substantial fluctuation around the mean VPR remains as a significant source of random error (relating to sampling) in a radar rainfall estimate.

A radar's temporal resolution is determined by the rate of pulses transmitted (the pulse repetition frequency, or PRF), the radar dish's rotation frequency (or arc sweep

time, if not a continuously rotating mechanism), the desired signal to noise ratio (determined by the number of pulses averaged per bin as described earlier) and the number of elevation angles it is desired to observe at.

That there is a time difference between the observation of precipitation at the beginning of a scan and that at the end of that scan while at the same time the precipitation field is likely advecting also introduces complication to this operation. This effect is often ignored and this may be reasonable if rotation rate/sweep time is not too long compared to the advection speed of the precipitation and the size of the radar sampling volume. The unknown evolution (variation of precipitation intensity in a Lagrangian sense, i.e. after taking into account advection) of the precipitation system between scans is the greatest source (Tsonis and Austin, 1981, Bellon and Austin, 1984, Seed, 2003) of uncertainty arising from differences in temporal resolution (holding the number of pulses per azimuth bin constant).

A variety of compromises can be made between the parameters governing temporal resolution: PRF can be increased, the sweep time can be varied fairly trivially, the number of scan elevations can be altered and the desired signal to noise ratio is also flexible. Increasing the PRF necessarily decreases a radar's maximum range. A new pulse is transmitted before backscatter from targets past a specific range (defined as $\frac{c}{2\mathrm{PRF}}$) makes it back to the radar, being potentially misidentified as being from the new pulse. Increasing the PRF does, however, increase the maximum unambiguous Doppler velocity able to be observed by a Doppler capable radar.

Having a large number of scan elevations is beneficial as much more information about the precipitating system can be obtained. Knowledge of the variation of radar reflectivity with altitude allows long range observations to be more effectively VPR corrected as well as providing insight into the physical processes involved in the precipitating system. Multiple elevations angles are also used, as stated earlier, to allow low scan elevations to be used to observe precipitation at long range while using higher elevations at short range to avoid ground clutter contamination. The benefit of a large number of elevation sweeps can be outweighed by the reduction in temporal resolution at any one elevation angle. Radars around the world are operated with many differing sweep patterns, for instance, in the United States, 9–14 elevation angles are used depending on precipitation type, in New Zealand, 13 elevation angles are used from

$0.5°$–$20°$ and in Switzerland, 20 elevation angles are used from $-0.3°$ to $40°$ (Germann et al., 2006).

The number of pulses 'n' per azimuth bin is given by $n = \frac{\Delta\theta}{\theta'}\mathrm{PRF}$ where $\Delta\theta$ is the azimuth bin width and θ' is the rate of rotation of the dish. There is little value in increasing the angular *bin* width $\Delta\theta$ above the angular *beam* width, as bins finer than this will be highly correlated to their neighbours (samples which are not independent). Angular resolution can, however, be sacrificed for temporal resolution by increasing the angular bin size and increasing the scan rate.

The signal to noise ratio also plays an important role here, it can be decreased by averaging fewer pulses per azimuth bin (usually by increasing the scan rate while holding PRF and azimuth bin width constant). It may well be beneficial to reduce signal to noise ratio to improve temporal resolution so that evolution in the precipitating system is better captured.

A radar's PRF is usually chosen to allow for a particular compromise between range and Doppler velocity ambiguity, which are typically valued higher than temporal resolution. Doppler velocity ambiguity can be improved by use of dual or tri PRF schemes (Jorgensen et al., 2000).

The algorithms for producing rainfall products from radar data are continuously being developed and enhanced. Some currently used systems are detailed in the following articles: Fulton et al. (1998), Seo et al. (2011) and Ventura and Tabary (2013).

1.1.3 Satellite

History

The first weather satellite was launched on the 1st of April, 1960 and was named TIROS-1 (Television Infrared Observation Satellite). This satellite was placed in an inclined orbit—at $50°$—at a height of around 725 km and carried two television cameras which relayed visible imagery of cloud systems back to one of two ground stations. TIROS-1 was operational for only 78 days but it proved the feasibility of weather observing satellites leading to several other TIROS satellites carrying more advanced instruments (including various radiometers).

In 1964, Nimbus-1—launched into a polar orbit—first demonstrated the ability to

make high resolution cloud cover observations at night utilizing the HRIR (High-Resolution Infrared Radiometer). TIROS-9, the first TIROS satellite launched into a sun-synchronous near polar orbit obtained the first complete daily coverage of the entire sun-illuminated portion of the Earth.

The first operational weather satellite used for forecasting—launched in February, 1966—was ESSA-1 (Environmental Science Services Administration) which operated in a near polar orbit and carried two redundant TV cameras for observing cloud formations. A geostationary weather satellite was first demonstrated in December 1966 with the launch of ATS-1 (Applications Technology Satellite) carrying, among other instruments, a spin scan cloud camera which could provide visible full disc imagery of the Earth every 20 minutes (NASA, 2012). The ATS series of satellites, which allowed cloud motion to be observed, led to the dedicated weather satellite program GOES (Geostationary Operational Environmental Satellite) run by NOAA which is still operating today.

The previously mentioned satellites were all launched by the USA but it wasn't only the Americans who operated weather satellites; the USSR launched its first fully operational weather satellite in 1969, Meteor 1-1 (carrying dual cameras and a scanning radiometer), the European Space Agency launched its first weather satellite, Meteosat 1, into a geostationary orbit in 1977, the Japanese also launched their first weather satellite in 1977 named GMS-1. India, China and Korea also operate weather satellites.

Description

Meteorological satellites are most often placed in one of two different orbits, each orbit having its advantages and disadvantages. Satellites in geostationary orbit are located at a height of 35786 km above the Earth's equator. This orbit gives the satellite an orbital rotation period equal to that of the Earth's so that the satellite appears stationary to an observer on the Earth's surface. This allows the satellite to have the same view of the Earth at all times which permits high temporal resolution observations to be made. For instance, GOES-15 (a NOAA satellite also known as GOES-West, located at 135° W longitude) has a 15 minute update period over the continental United States. MTSAT 2 (a JMA (Japanese Meteorological Agency) satellite located at 145° E longitude) provides Northern hemisphere coverage every 30 minutes and a full disc scan every hour.

The downside to geostationary orbits is that they allow only comparatively low spatial resolution due to their great distance from the Earth's surface. This means that it is of little benefit to place a conventional precipitation radar on such a satellite as these instruments typically have wide beam widths and lack the power required to operate at such a distance (due to power supply limitations on satellites). Similarly, microwave imagers are also not suited for operation in geostationary orbit as they operate with wide view angles and are not sensitive enough to function at this range.

The instrument that can be used to make precipitation estimates on a geostationary satellite is the vis/IR imager. The GOES satellites provide vis/IR imagery ranging in resolution (cross beam at nadir) from 1 km for visible, to 4 km for two shortwave and two longwave IR channels to 8 km for the moisture channel (6.5–7μm).

Vis/IR imagers do not directly measure precipitation but provide information relating to cloud location, thickness and height. Cloud thickness is inferred from the visible channel, generally the thicker the cloud the more visible light is scattered toward the satellite. Cloud height is inferred from the IR channels. The higher a cloud is, the colder it is. From Wien's law it follows that the wavelength radiated from the cloud is longer for clouds of lower temperature and therefore for those of higher altitude. The visible and IR imagery can be combined to select clouds which are both thick and extend to high altitude. These clouds are considered more likely to be precipitating clouds. It is difficult, however, to retrieve a quantitative rainfall value using this method (Lovejoy and Austin, 1979, Kidd, 2001). Vis/IR precipitation estimation can be improved by determining relationships between vis/IR channel intensities and surface radar precipitation estimates which can then be applied to vis/IR estimates outside of radar domains (Bellon et al., 1980).

Satellites placed in near-polar solar synchronous orbits orbit in an approximately north/south direction passing by the poles so that they always cross a particular line of latitude at the same local mean solar time. This provides consistent lighting for observations. Polar orbiting satellites typically have a period of around 96–100 minutes and orbit at an altitude of around 800–900 m (WMO, 2012). As the Earth rotates under the satellite during its orbit, polar orbiting satellites can observe the entire Earth twice per day (once in the daytime and once in the nighttime). These satellites are often operated in pairs to provide four observations per day (such as the POES and METOP-

A pair). The benefit of this orbit is the much lower altitude (which provides the ability to observe at higher resolution and to observe much weaker signals) combined with repeated observations globally at fixed intervals. The trade off that comes with a lower altitude is a more limited field of view on each pass. In addition to the benefit that vis/IR imagers operate at a much higher resolution in this orbit is the ability to use microwave imagers.

Microwave imagers measure the net emitted microwave energy from the Earth's surface after losses in the atmosphere. Over the oceans (which have a fairly predictable emissivity compared to land), it is possible to obtain knowledge of the water vapour profile and of rainfall. Beam filling (spatial sampling error) is a significant problem with microwave imagers as, even at low altitude orbits, resolution is on the order of tens of kilometres. For instance, resolution is stated as 50 km for the AMSU-A (advanced microwave sounding unit A, 24–89 GHz) on NOAA-19 (a POES satellite) and 16 km for AMSU-B (89–183 GHz) on the same satellite. Precipitation gradients inside a 50 km pixel are not usually able to be ignored, however, some correction can be made to account for this problem (Wentz and Spencer, 1998, Petrenko, 2001, Kubota et al., 2009).

Meteorological satellites are also placed in other orbits. For example, the Tropical Rain Measurement Mission (TRMM) satellite is placed in a non sun-synchronous low Earth orbit (originally 350 km altitude, later 'boosted' to 402.5 km in 2001) at an inclination of 35°. The reason for such an orbit is to allow for the operation of the first satellite borne microwave precipitation radar. TRMM's radar operates at K-band radar (at 13.8 GHz) and has a horizontal resolution of 4.3 km at nadir, expanding to 5 km at scan edge. The swath width is around 220 km. The minimum detectable reflectivity is 20.8 dBZ which increased to around 22 dBZ after boost.

The radar allows investigation of beam filling effects on the also carried microwave imager, which has a coarser resolution as well as being a source of validation for the rainfall algorithms used by the microwave imager and the vis/IR imager for precipitation estimation. The major downfall of the radar is attenuation due to the radar's high frequency. This frequency was necessary so as to limit the beam width to 0.71° and limit the power requirements of the radar to make it feasible as a satellite package. While the upsides to TRMM's orbit are increased resolution and sensitivity with the precipitation

radar and microwave imager, the downside is that measurements are taken at irregular intervals over particular areas. The information from the satellite is, therefore, primarily used as a calibration or verification for other satellite instrument measurements or for investigating climate processes and trends involving rainfall in the tropics. In the near future, a new TRMM inspired satellite (the Global Precipitation Measurement (GPM) mission Core Observatory) carrying a dual-frequency precipitation radar will be sent into orbit. This satellite will be placed into an orbit with a higher inclination than TRMM so as to allow measurement over mid and high-latitude areas and not just over the tropics (Neeck et al., 2010).

1.2 Data Qualities

There are several important qualities of rainfall data that are of differing levels of significance to the many applications of the data. In no particular order these can be listed as: timeliness, coverage, completeness, lead-time, representativeness, resolution and accuracy. To understand where resolution fits in with these other properties it is of use to discuss them here.

Timeliness

Timeliness here is meant as the time between when rainfall data is observed and recorded and when this data is disseminated to the end user(s). For most sources of rainfall data in the present day this can be near instantaneous with the only limiting factor being the cost of a telecommunications system (ignoring data licensing/access permission issues).

The only data source for which instantaneous data transmission is not extensively realized in operation is the rain gauge. Although most electronically logged rain gauge stations operated by meteorological organizations usually have telecommunication capability, manually recorded stations (often more numerous in many countries), rely on human logging usually with a daily time period. The importance of instantaneous communication of data at such a coarse temporal resolution is greatly diminished. Timeliness of data is important if predictions of a very short time scale (< 24 hours) are to be made using the data. This is applicable to hydrologists and to operational meteorologists who may wish to assess quality in their models or assimilate this data into their

next model run to improve model skill.

Coverage

Coverage concerns the spatial completeness of data inside the desired domain. It is often the case that rainfall observation can prove difficult in certain types of terrain. For observation by rain gauge this would include any terrain which is difficult to access (for servicing, data retrieval, etc.). As a result, rain gauges are usually placed near roads and are most often sparsely distributed in mountainous and forested areas except at great expense to the installer/operator.

The coverage of a radar on the other hand is predominantly limited by obstructions to its view. This is particularly affected by mountains, with the result that radar observation in mountainous regions is often poor (or expensive, as the solution is often an increase in the number of radars in the region). The coverage of a radar is also dependent upon the characteristics of the precipitation systems that are currently being observed. Intense systems extending many kilometres into the atmosphere can be detected at much greater distances from the radar than less intense and shallow precipitation systems. Additionally, while an echo from some system at range might just be able to be detected by the radar, the relationship between this echo and the surface rainfall might be so weak so as to render the measurement of no use. Satellite based observations do not suffer from any of these issues and have, therefore, the greatest spatial coverage of any of the rainfall data sources over very large domains (essentially over the entire globe regarding polar orbiting satellite data).

Data coverage is of great significance to hydrological application as catchments can be very large and include the aforementioned difficult terrain. If gaps in coverage are present, interpolation must be implemented to adequately represent the rainfall volume falling into the catchment. Such interpolation methods are less than ideal for precipitation fields due to their non-continuous nature. Satellite measurements can be used to aid in interpolation of other instruments due to their satisfactory ability to detect rain/no-rain conditions (Todd et al., 1999).

Completeness

Completeness of record refers to the temporal completeness of the data over a desired time period. Dropouts in telecommunications, instrument malfunction or relocation/removal of instruments are the likely causes of data 'holes' in long term rainfall records. For instance, radar records can be prone to this issue if stations are remote and rely on microwave links or satellite connections which can drop out in bad weather (the very weather we wish to have a record of). While this would not necessarily lead to data loss if temporary on-site storage is utilized, this capability is often absent as radar operators are more concerned with the real-time output of data than with keeping complete records. In addition to communication dropouts, radars can also suffer from malfunctions which require on-site human assistance that also may not be available to remote stations during hazardous weather events.

With respect to rain gauges, it is often the case that gauges are retired from locations and never replaced or are relocated elsewhere. This is particularly the case in many countries where manually logged gauges are being replaced with fewer electronically logged gauges due to financial considerations. Dense gauge networks that can often be implemented for a particular project or purpose also do not remain longer than the duration of that project or purpose.

Data outages can particularly be a major problem to users of extreme rainfall information as under these conditions outages are more likely. These users include hydrologists who require long records in order to calibrate their rainfall-runoff models and are often interested in extreme events for risk analysis. Interruption of the real-time transmission of extreme event data is arguably more important than completeness of an historical record as it affects disaster management and warning systems. This is another area where satellites have an edge over terrestrial observation systems as weather systems cannot influence a satellite's operation making them no more likely to experience a fault during extreme weather than at any other time.

Lead-time

Lead-time is a property of a forecast, being the time between when a forecast is generated and/or disseminated and the time for which the forecast is being made. There are three major divisions that the range of possible lead-times can be divided into: very

short forecasts (< 6 hours), that are best made from extrapolation of current observations of precipitation (eg. radar nowcasts) (Austin et al., 1987, Golding, 1998), short to medium range forecasts (6 hours to 14 days), which are generated from numerical weather prediction models and long range climate forecasts, best made from climate averages or from climate models (when considering climatic change) (AMS, 2007).

As lead time increases, only coarser scale precipitation can be accurately forecasted. To understand this, consider that an individual precipitation cell has a lifespan of the order of 30–50 minutes (Weisman, 2002). If a radar were to observe such a cell over a period of say 10 minutes, a nowcast could be made utilizing that cell's observed intensity and velocity. The accuracy of this nowcast degrades quite substantially for lead times longer than tens of minutes as the cell goes through its life cycle, often disappearing within the hour. If this cell were part of a larger organization of precipitation, such as a front, then we would expect new cells to be generated which replace those which dissipate. A nowcast of this organization of cells would therefore have much greater accuracy if we ignore the exact placement of each of the cells (lowering the forecast resolution). It is important, therefore, to consider that high resolution precipitation *observations* may often be of little additional benefit to a precipitation *forecast* than observations made at lower resolutions (as long as the character of the precipitation can be determined, eg. scattered storms can be distinguished and are not lumped into one observation pixel).

Lead-time has great considerations for the application of forecast data. The duration of lead time required or desired varies considerably with application. Flash flood forecasts by their very nature will require short lead times to be accurately predicted in time and space in most circumstances. For an operator of a hydroelectric dam, 24 hours or more may be required for dam levels to be reduced in expectation of a storm. If one were staging an outdoor event, however, a week or more may be required to shift the event indoors or for it to be postponed.

Representativeness

Representativeness refers to how well the observed precipitation represents the actual precipitation over the desired domain. To not overlap with the other qualities of accuracy and resolution, this term will be confined here to mean the ability of rainfall point

measurements to represent the precipitation field surrounding that measurement. The representativeness of a gauge network depends on its density, the characteristic length scale(s) of the observed precipitating system(s) and the accumulation period of interest. For example, for sub-hourly accumulations, under highly uniform stratiform rainfall, rainfall rates from a single gauge might be expected to be extrapolated tens of kilometres without dramatic loss of accuracy. Under sparse convective systems, however, a density of one gauge per square kilometre may be required to provide accurate rainfall estimates over a domain.

For longer accumulation periods, accumulated rainfall is much less variable in space as larger scale processes dominate. Berne et al. (2004b) found the relationship between decorrelation range (r) and time resolution (Δt) to be well modelled by

$$r = 4.5\sqrt{\Delta t} \tag{1.1}$$

This means that for longer accumulation times, a gauge will have a wider area of representativeness. It is important to note, however, that this is not necessarily the case in areas of complex terrain where orographic effects are significant.

Representativeness plays an important role for users of rain gauge information, although it can sometimes be overlooked. Rain gauges are the mainstay for the hydrological community as the source for rainfall information. This is because the data records are often long with high completeness and the data is usually easily wielded due to its small size (relative to radar information for example). Although gauge density or just distance to gauge (if there is only one near the catchment of interest) is usually considered of significance, very low density networks or gauges far from catchments are still often used in preference to other available data sources (such as radar which is seen as unreliable, not always unfairly). Representativeness is important when determining the number of gauges required for a specific application. For instance, a farmer may wish to record the daily rainfall accumulation his crops receive so as to estimate future crop yield. If the farm is large, several gauges may be required to obtain reliable estimates, especially if located in an area which experiences frequent scattered precipitation systems.

Resolution

Resolution can be split into three components: spatial, temporal and quantitative. Spatial resolution is defined as the ability to distinguish between two closely located objects in space. Temporal resolution can be split further into observing frequency and integration period. Many rainfall products are integrations (such as hourly accumulations) of more frequently observed data. The rainfall volume accumulated in a given integration period can depend upon the observation frequency when considering observing systems that take 'snapshots' of precipitation at a particular location at a given instant (such as radar or satellite products).

For a radar, the integration period is accumulated by summing the individual radar frames of rainfall rate multiplied by the observation period. Although some improvement can be made to the accumulation by also allowing for the movement of rainfall echoes between radar frames, the missing knowledge of echo evolution between observations leads to an inaccuracy in the final accumulation. Parallels can be drawn between this 'interpolation' in time and the spatial interpolation used with gauge network data.

Of spatial resolution, a distinction can also be made between the resolution of volume/areal data (from radar, satellite and NWP) and from the resolution of an interpolated field made from individual point measurements (i.e. from a gauge network). While the 'image' created from such an interpolation shows increasing detail with increase in the density of point observations, revealing smaller length scales of the data, the term resolution in this case differs from areal/volume measurements in that gauge networks can fail in detecting precipitation at all if the system does not pass over at least one gauge in the network. This is related to the representativeness discussed previously.

Quantitative resolution is the smallest detectable variation in the measurement of rainfall that an instrument can make. For instance, for a tipping bucket rain gauge, the smallest measurement of rainfall is related to the size of the bucket, typically 0.1 mm or 0.254 mm. A radar can make much finer observations of rainfall at lower rainfall rates than at higher rainfall rates due to sampling from a logarithmic receiver. A change of 1 dB from 20 dBZ to 21 dBZ is around 0.1 mm h^{-1}, a change from 50 dBZ to 51 dBZ is around 7.5 mm h^{-1}. The resolution is determined by the analog to digital converter after the logarithmic receiver and by the number of bits used to store the data. Storage limitations in the past meant that radar data was often stored using 4 bits giving only

16 levels. With modern hard drive technology, this is no longer a constraint and data is usually stored with 8 or 16 bits.

Accuracy

Accuracy is quite a broad quality and reflects the quantitative difference in the estimated rainfall accumulation over a certain time period in a particular location or area and the true value of rainfall accumulation. While rain gauges are usually used as this "true" value, as discussed earlier, the representativeness of this "truth" can become suspect when comparisons to areal rainfall estimates are made. Along with this, the inaccuracy in gauge point measurements themselves can be on average 5–10% as mentioned earlier. Without comparison to rain gauges, the accuracy of other data sources can be estimated based on a comparison with data obtained using a similar instrument. Satellite measurements are usually compared to radar estimates as they are of a similar (spatially averaged) form.

Quantitative accuracy is only really important for quantitative uses of the data (eg. as input into models), for many applications, qualitative accuracy (meaning one could only say 'heavy rain' or 'light rain' rather than putting numbers to it and specifying uncertainty) may be considered to be sufficient. For instance, if one is deciding to participate in a future outdoor activity, it is not important to know the accuracy of the future rainfall to any great extent but rather just the knowledge of whether there will be light, medium or heavy rainfall and the rough duration and timing of this precipitation. As an input to a hydrological model, however, the rainfall volume reaching the surface of a catchment is of vital importance to the functioning of the model. The practice of dividing past days into wet days, rain days or dry days for climate information also doesn't require data of great accuracy, as long as precipitation that occurs is observed to at least some extent.

1.3 Applications of Rainfall Data

The application of rainfall data is of vital importance regarding the necessary resolution of the data. For instance, the rainfall data requirements of an agriculturalist, for whom weekly rainfall accumulations in the locality of his or her farm would likely be suffi-

cient, are not the same as those of an urban hydrologist for whom five minute (or less) accumulations may be required over an entire urban area.

The applications of rainfall data can be placed into two categories relating to the fields of meteorology/climatology and hydrology. Under the first category, it is the rainfall reaching the surface of the Earth—as well as that still in the atmosphere—which is usually of interest. What happens to the water after reaching the Earth's surface is of concern to applications in the second category, hydrology. Some examples of users under the first category are: the general public, researchers, operational meteorologists, event organizers, construction companies, shipping companies, pilots and emergency aid providers.

The rainfall products which the general public most often use seem to be forecasts and climate history. This is supported by the abundance of time allocated to forecasts in daily news programs. The forecasts required would generally be fairly low resolution with citywide scale being sufficient in most cases. Higher resolution would involve higher inaccuracies as to the timing and location of events until short lead times so as to be of limited use to a member of the public who wants to know if it will rain in their location at a particular time of the day. One would think resolution sufficient to determine scattered rain/showers with an update period of 30–60 minutes or so would be adequate for such use.

Lazo et al. (2009) performed a survey of the public's interest in and use of weather forecasts for U.S. citizens in 2006. The survey found that people were most interested in rainfall information over other forecast products and that this related mainly to the location, timing and chance of precipitation as well as precipitation type and intensity. This interest was focused mainly on their own city or on other cities in their respective states. Use of the information was primarily "simply knowing what the weather will be like", followed by determining clothing requirements, planning outdoor activities and transport.

High resolution short lead time forecasts (nowcasts) are applicable to the public when regarding extreme weather such as tornadoes and flash flooding. It is not possible to predict such extreme weather with great spatial and temporal accuracy essentially until the weather system has begun to form. Sub 2 km spatial resolution would likely be required for flash flood forecasting, temporal resolution must be high enough so as to

observe quickly developing convective systems and sufficiently track their movement. Spatial resolutions of the order of hundreds of metres are required to directly observe most tornadoes although indicative 'hook echoes' can be observed at lower resolutions (Brown et al., 2005). High movement speeds combined with often erratic motion and variable intensity make temporal resolution of high importance when observing tornadoes. Precise knowledge of tornado location is likely to be of little use to the public as there is nothing additional that can be done to avoid the tornado's effects if a tornado warning for the area has already been made. Aeroplanes, on the other hand, could make use of high resolution tornado information to make flight manoeuvres to avoid a tornado.

Climate history would be of interest to the public when travelling or relocating to other locations. This may indicate whether or not one may wish to travel there or what items of clothing are required to be taken with them. Other uses may be event planning and gardening.

Event organizers, for example, those involved in the management of concerts, sports events and myriad other outdoor events, would require accurate forecasts as well as climate history of a location. The accuracy of forecasts is vital in this application, especially the spatial and temporal aspect, as it is of little concern if precipitation occurs after an event or occurs 10 km away from the event's location. Lead time is also important, as long as the forecast remains accurate. Keenan et al. (2003), a report on the Sydney 2000 Forecast Demonstration Project that operated during the 2000 Olympic Games states that "users of the forecast product considered product "effectiveness" in terms of timeliness and comprehensibility and suitability for decision-making". Climate history could be used to predict probability of rain occurring for the time of year the event is held, or for assistance in choosing the time of year that the event is held.

The construction industry uses rainfall data and forecasts in a very similar manner to event organizers when predicting the number of "rain days" they might expect on a project. This is done in order to calculate completion dates, which can often be costly if overrun (El-Rayes and Moselhi, 2001). While climate statistics would be utilized for this estimation for long projects, shorter term forecasts are also useful for short term decision making (when to lay concrete etc.). Resolution would not be of great importance compared with forecast accuracy (especially intensity and timing [El-Rayes

and Moselhi, 2001]) in the same manner as event organizing.

There are several applications of rainfall information to aviation. Precipitation is a factor in 6 percent of commercial air carrier accidents and approximately 10 percent of general aviation accidents (Kulesa, 2003). Rainfall causes a reduction in visibility due to attenuation as well as due to raindrops impacting on the aircraft's windscreen (WMO, 2007). Thunderstorms are associated with turbulence, lightning and hail, all of which can be damaging to aircraft. Because of these dangers, commercial aircraft are fitted with forward facing X-band rain radar to assist in avoiding such situations. Aircraft mounted radar have downsides such as range problems, attenuation issues and ground clutter contamination. The issues with range leave pilots little time to make corrective manoeuvres due to the high speeds of aeroplanes.

Intense convective storms provide the most danger to the aircraft on take off and landing. It is because of this that weather radar are often installed at airports to detect such weather systems and provide automated warnings to airport personnel. High resolution measurements are important here as convection can be more accurately detected and tracked. This need for high resolution data is seen by the operation of radar systems such as the TDWR (Terminal Doppler Weather Radar) which provides high resolution (150 m downrange, 0.55° beamwidth, 1 minute sampling interval for surface scan) at numerous airports in the United States.

Operational meteorologists use rainfall information in a number of different ways. Real-time rainfall data can be used to assess or modify numerical weather prediction models (validation and data assimilation) as well as to assist operators in qualitative decision making. Historical data is also used for validation of models and observed bias between observation and prediction is sometimes used to statistically post-process future forecasts based on location (McCollor and Stull, 2008). Resolution of data is important when making observations of thunderstorms and tornadoes (< 2 km and < 5 minutes would be preferable). Spatial, temporal and quantitative accuracy are all important for these applications.

Researchers use all forms of rainfall data in a multitude of different ways. Decision making based on forecasts is not usually the focus in contrast to most of the previously mentioned applications. Historical model runs are often made to analyze physical processes occurring in meteorological phenomena. Different sources of rainfall data are

often compared to one another for calibration, verification or for creating merged data products. Common examples are comparisons of satellite to radar, radar to rain gauge, NWP to radar and NWP to rain gauge.

When making these comparisons, often one of the sources is considered to observe the 'true' rainfall accumulation. This is where resolution becomes important, especially for comparisons to rain gauges, the most accurate source for rainfall accumulations at a particular point in space. Radar data can often be 'gauge adjusted' by making bias corrections with gauges located within range of the radar. As shown in Chapter 4, this correction can vary considerably relative to the resolution of the radar over the site of the rain gauge (as well as from several other factors). Most of the data properties listed earlier are of importance to researchers, with the possible exclusion of timeliness. This is because research is generally focused on the analysis of historical data.

For most of these non-hydrological users and applications of rainfall data, it could be argued that having high resolution (sub 2×2 km and 5 minutes) real-time data may often not be of great use unless quantitative methods are to be employed or rainfall extremes are considered. Most future decision making using rainfall forecasts is specific to a location of interest. For the long lead times that can often be required for decision making, spatial and temporal accuracy is not sufficient to allow high resolution prediction to be of benefit.

Where high resolution measurement does come into play in this area is when rainfall data from differing sources are to be compared. In anything but uniform rainfall, a rain gauge observation will often be unrepresentative of the rainfall falling in say a 5×5 km area. This raises issues for the use of gauge based bias corrections (to account for systematic errors in rainfall estimates) to areal rainfall data sources (eg. radar, satellite, NWP). It should be said here that geostatistical techniques (see, for example, Wang and Wolff, 2010) can be used to account for scale differences when comparing two differently sampled observations, however, many assumptions must be made of the precipitation field that are frequently violated, especially on time scales of hours or less.

Extreme weather can also require high resolution measurements as extreme rainfall intensities are often associated with large gradients of intensity with distance and can be quickly evolving in time.

Examples of users in the second category, those who are concerned about the rainfall

once it reaches the ground, include hydrologists for local/regional/national government or private industry/consultants who may manage rivers, sewers and drains, farmers, construction companies, hydro electric power companies and drinking water suppliers.

For many of these users the application of rainfall data is the same. The rainfall data is input into hydrological models (along with a multitude of additional data regarding topography, soil and ground and surface water) which calculates the desired output. Examples of this output could be soil moisture (for crop farmers or construction companies), channel flow and level (for managers of rivers), pipe flow (for sewerage/drainage managers) or sediment transport.

River flow forecasting will be explored in greater detail in Chapter 5 and 6. For the hydrologist concerned with river flow simulation, one of the greatest concerns with regards to rainfall data is the length of an at least somewhat accurate data record (Schilling, 1991). This is desired so as to establish a 'calibration' of a hydrological model that is representative of many types of rainfall events so that the average catchment response (averaging over the many unknowns involved in the non-rainfall parameters) can be determined. Accuracy of this rainfall data is of near equal importance, with quantitative accuracy (of rainfall intensity/volume) being perhaps of most importance as catchment outflow is greatly affected by quantity of input rainfall volume.

Spatial and temporal accuracy is of increasing importance for decreasing catchment size. Both spatial and temporal accuracy have greater bearing on the timing of flood peaks than on the peak value itself. This is, until spatial inaccuracy is of a comparable magnitude to the size of the catchment. Quantitative difference in output flow from temporal and spatial inaccuracies can be observed due to differences in infiltration and interception properties of the terrain upon which the rain falls.

It could be assumed that infiltration would be affected by averaging in space and time due to the nature of rainfall excess calculation; peak rainfall values would be reduced by the averaging process and thus more likely infiltrated rather than resulting in runoff. Higher resolution in space and time could be assumed to be of greater importance for smaller catchments. Higher resolution data is often thought necessary for urban hydrology (Berne et al., 2004b).

Rainfall data can be used in the agriculture industry for estimating crop yields. Of great importance to this application is data that is representative of the rainfall which

fell in the field in which yield is to be estimated. High resolution data would not be of as great a necessity as for flood forecasting as it is the volume of infiltration that is of interest rather than the volume of runoff. The former is usually much greater than the latter in a rural environment which means that the total volume of infiltration would vary much less percentage wise under the effect of peak smoothing that occurs with lower resolution measurement. Effective use of satellite rainfall products has been applied in this field for famine prediction in sub-Saharan Africa (Verdin and Klaver, 2002).

The hydrological uses of rainfall in the construction industry are associated with soil moisture and ground water flow modelling with application to earthworks and drainage. Similar to crop farmers, resolution is not of great importance and representativeness is paramount.

All of these hydrological applications discussed require quantitative (rather than qualitative) rainfall input, as such, resolution may be of more importance than for many of the meteorological (decision making) applications previously mentioned. It is necessary to quantify this importance in the context of other rainfall properties (notably, accuracy). It may be that the integrating nature of catchments reduces the impact that low resolution rainfall input has on the output of hydrological models. A question could thus be asked here: "To what extent does the integrating nature of a catchment reduce the model impact of coarse resolution rainfall data input?". To answer this question we will first find out how the error introduced by sampling at coarse resolutions is diminished by spatial integration (in Chapter 2). In Chapter 6, the question will then be answered directly.

With regards to these many applications of rainfall data (both observed and predicted), the areas in which high resolution observation appears to be of some significant benefit are for those applications that require precise rainfall quantity, especially those requiring this quantity distributed over a domain. This involves: all uses of hydrological models where rainfall is the dominant input water source (with regard to rainfall volume estimation and any bias correction), any comparison between an areal measurement and a pointwise measurement (such as radar bias correction by rain gauge or satellite to rain gauge/radar) and short term forecasting (nowcasting), especially of severe weather.

Chapter 2

Radar Sampling Error — Impact on QPE

There are many sources of error associated with the retrieval of surface rainfall rate from radar reflectivity measurements made aloft (see Chapter 3 for an overview). Not all have been investigated to the same extent.

Some of these sources of error, for example, the uncertainty in the observed rainfall's drop size distribution and the resulting effect on the estimation of rainfall rate (Twomey, 1953, Battan, 1973, Atlas et al., 1999), beam blocking (Harrold et al., 1974, Andrieu et al., 1997) and uncertainty in the knowledge of the vertical profile of reflectivity (VPR) (Fabry et al., 1992, Kitchen et al., 1994, Joss and Lee, 1995) have been researched extensively over the past decades.

Fewer studies, however, have focused on the fundamental sampling error associated with the measurement of precipitation at spatial resolutions and at sampling intervals that are coarse compared to precipitation systems' decorrelation length and time (Fabry et al., 1994, Jordan et al., 2000, Piccolo and Chirico, 2005). Many more studies have focused on the sampling problems associated with rain gauges, however (Morrissey et al., 1995, Steiner, 1996, Nystuen, 1998, Villarini et al., 2008).

That both rain gauges and radar exhibit quite different sampling errors is also often ignored when utilizing gauges as 'ground truth' for validation of radar precipitation estimates. This has been criticized by some researchers (Kitchen and Blackall, 1992, Tees and Austin, 1991). This particular impact of sampling error will be assessed in

Chapter 4.

Quantifying this sampling error, which has been alluded to throughout the previous chapter, would provide a significant contribution to answering the question posed in the title of the previous chapter: "how much resolution is enough?".

The following text has been heavily drawn from the paper Shucksmith et al. (2011) of which this author was primary author.

The existing studies on radar sampling errors indicate that this scale related error is significant and may well dominate other sources of error in many cases. For instance, Fabry et al. (1994) studied one hour of high resolution data, downgrading it to a range of spatial and temporal resolutions. They reported that on average a 39% error was introduced into a 5 minute rainfall accumulation solely from downgrading a radar's spatial and temporal resolution to 2 km and 5 minutes, using a rain field initially observed at 250 m spatial and 20 second temporal resolution.

Similar results were obtained by Piccolo and Chirico (2005), who considered error due to temporal sampling at three different accumulation spatial scales and by Jordan et al. (2000), who found that the error due to decreasing sampling resolution from 100 m and 10 s to 5 minute sampling averaged over 1 km pixels was between 30% to 40% of the mean rainfall rate for 5 and 10 minute accumulations.

Lack of attention to this error source could perhaps be because there is little which can be done to improve the spatial sampling of existing fixed radar networks without increasing the density of the network or changing the fundamental parameters of the radars. Decreasing the sampling interval of a radar also compromises the information obtained about precipitation at range as discussed in Section 1.1.2.

As well as affecting a radar's ability to measure fine scale structure in precipitation systems, the spatial resolution of a radar, if it is coarser than the length scale at which an observed rain field exhibits variation, can also lead to an overestimation of precipitation area and intensity. These latter effects are due to both non-uniform and incomplete beam filling problems (Zawadzki, 1982).

The temporal resolution, dependent upon the radar's sampling rate, determines a radar's ability to observe a rain field's evolution as well as to better track its movement. Fabry et al. (1994) found this to be particularly important when estimating short duration (5 minute) rainfall accumulations.

A theoretical background on the local averaging of random fields, which explains the basis for some of previously mentioned results, is given in Vanmarcke (2010). One must be wary, however, to examine the appropriateness of the necessary assumptions made about the rainfall field when applying this theory.

The hierarchical spatio-temporal models described by Cressie and Wikle (2011) could also be utilized to examine this problem. A review of the literature suggests that this has not been applied with relation to rainfall as of yet, however.

A geostatistical method that has received considerable attention in that of Ciach and Krajewski (1999) who proposed a method for determining the radar error variance in light of the spatial averaging of radar observations and the point-area problem with comparisons to rain gauges. This method has been used in verifying satellite based rainfall measurements (e.g. Wang and Wolff, 2010) and determining the spatial error covariance of radar rainfall estimates (e.g. Mandapaka et al., 2009), among other uses. Though this method is not being applied in this thesis, it is worth providing the theory of the method so as to contrast it with the more experimental method that *is* used in the chapter.

The error separation method (ESM) of Ciach and Krajewski (1999) relies on the separation of the variance in the difference between the radar measured areal rainfall (R_t) and the gauge measured rainfall (R_g) which is considered a point measurement of the true rainfall field. This separation is performed as follows:

$$\begin{aligned} \mathrm{Var}\left\{R_t - R_g\right\} &= \mathrm{Var}\left\{\left(R_t - R_a\right) - \left(R_g - R_a\right)\right\} && (2.1)\\ &= \mathrm{Var}\left\{R_t - R_a\right\} - 2\mathrm{Cov}\left\{R_t - R_a, R_g - R_a\right\} + && (2.2)\\ &\quad \mathrm{Var}\left\{R_g - R_a\right\} && (2.3) \end{aligned}$$

where R_a is the true area-averaged rainfall accumulation for a specified time and area. By assuming that the difference between the radar estimate and the true areal rainfall and the difference between the rain gauge estimate and the true areal rainfall are uncorrelated, the covariance term can be eliminated. Rearranging for the radar error variance ($\mathrm{Var}\left\{R_t - R_a\right\}$) gives

$$\mathrm{Var}\left\{R_t - R_a\right\} = \mathrm{Var}\left\{R_t - R_g\right\} - \mathrm{Var}\left\{R_g - R_a\right\} \quad (2.4)$$

meaning that the variance in the radar rainfall error can be determined from the variance in the difference between the radar and gauge rainfall estimates and the variance in the

difference between the gauge rainfall and the true areal rainfall. Ciach and Krajewski (1999) state that the radar rainfall error estimation using this equation can be subject to large estimation errors when the terms cannot be assessed with sufficient accuracy.

The first term, the variance in the radar-gauge difference is calculated simply from

$$\mathrm{Var}\left\{R_t - R_g\right\} = \frac{1}{N}\sum_{i=1}^{N}\left[R_r(i) - R_g(i)\right]^2 \tag{2.5}$$

with the precision primarily determined by the number of samples N.

The second term in Equation 2.4 is much more difficult to determine. This term is related to the area-point difference between the rain gauge estimate and the true areal average of the field.

By assuming that the rain gauges measurements are "of good quality and properly calibrated", one can write

$$R_a = \frac{1}{A}\int_A R_g(x)dx^2 \tag{2.6}$$

with the further assumption that the rainfall field is second order homogeneous (i.e. having finite variance, constant mean and covariance that depends only on the spatial lag) the area-point difference variance can be written as

$$\mathrm{Var}\left\{R_g - R_a\right\} = \mathrm{Var}\left\{R_g\right\} - 2\mathrm{Cov}\left\{R_g, R_a\right\} + \tag{2.7}$$

$$\mathrm{Var}\left\{R_a\right\} \tag{2.8}$$

Substituting R_a with equation 2.6 the covariance term for the locally homogeneous field can be written

$$\mathrm{Cov}\left\{R_g, R_a\right\} = \frac{1}{A}\int_A E\left\{\left(R_g(x_g) - \mu_g\right)\left(R_g(x) - \mu_g\right)\right\}dx^2 \tag{2.9}$$

$$= \frac{\sigma_g^2}{A}\int_A \rho(x_g, x)dx^2 \tag{2.10}$$

where ρ is the correlation function. The variance of R_a can be written in a similar manner as

$$\mathrm{Var}\left\{R_a\right\} = E\left\{\left(R_a - \mu_g\right)^2\right\} \tag{2.11}$$

$$= \frac{\sigma_g^2}{A^2}\int_A\int_A \rho(x, y)dx^2dy^2 \tag{2.12}$$

with $\mathrm{Var}\{R_g(x)\} = \sigma_g^2$, the point area difference variance is written as

$$\mathrm{Var}\{R_g - R_a\} = \sigma_g^2\left(1 - \frac{2}{A}\int_A \rho(x_g, x)dx^2 \right. \tag{2.13}$$

$$\left. + \frac{1}{A^2}\int_A\int_A \rho(x, y)dx^2dy^2\right) \tag{2.14}$$

Therefore, the radar error variance can be calculated with knowledge of the rainfall field's spatial correlation function and the observed variance in the difference between the radar rainfall estimates and gauge measurements. The spatial correlation function is usually determined by fitting a correlation model to the gauge measurements. Ciach and Krajewski (1999) fit an exponential model with a 'nugget' to account for microscale variation.

This method relies upon a host of assumptions: zero covariance between the $(R_g - R_a)$ variance and the $(R_t - R_a)$ variance, second order stationarity of the rainfall field, R_g and R_t being free of bias. To estimate the correlation structure, a sufficiently dense (for the desired accumulation period) gauge network must also be present. Correlation estimation techniques frequently assume isotropy and apply a limited set of models (e.g. exponential, spherical, etc.) which often do not fit the observations sufficiently (e.g. Wang and Wolff, 2010).

The method described below avoids these assumptions while also looking at the how temporal sampling rate affects radar sampling error. A limitation with this method is that the smallest scale spatial and temporal variability are not observed by the high resolution radar, meaning we can only get a lower bound estimate on the sampling error.

2.1 Quantifying Sampling Error

To explore the errors introduced by sampling at these lower spatial and temporal resolutions, high resolution (200 m, 50 s) X-band radar data is downgraded in spatial and temporal resolution by means of spatial averaging and temporal subsampling and then compared to the original high resolution form. The effect that sampling error has on the overall distribution of rainfall rates is explored as well as the relationship that these scale dependent errors have with the characteristic length scale of the precipitating systems.

This study fills a gap in the published literature with the application of Fabry et al.'s technique to a larger dataset than has ever been analyzed in this way before. This allows for more certainty in the results for the average case as well as allow investigation into the variation of sampling error across different rainfall systems.

This method only looks at spatial resolution in the horizontal, no spatial averaging is performed in the vertical. The vertical profile of reflectivity can often vary substantially within a rainfall system (although there is less variation than in the horizontal).

The radar data collected for this study did not possess sufficient vertical resolution so as to apply this method in the vertical. Indeed, it would not be possible to use this method to look at both spatial resolution in the horizontal and vertical as well as temporal resolution. To achieve higher vertical resolution, more elevation angles are required, limiting the temporal resolution. A fast-scanning phased array radar system would be able to achieve this, however, sadly no such radar was available for this study.

As the following analysis is based on radar observations, it is not directly comparable to other areal measurements such as those from vis/IR or microwave radiometer based satellite measurements as averaging is performed specifically for radar assuming the validity of the Z-R relationship. A qualitative interpretation of the results could, however, be representative of measurements from other areal precipitation observations as similar averaging occurs with these observations.

Now would be an appropriate time to list some hypotheses:

1. Error—as measured in comparison to rainfall accumulations made from observations of a particular (higher) resolution—increases when observation spatial and temporal resolution is decreased.

2. Sampling error is greater for more fine scale (spatially and temporally variable) rainfall than for more large scale (spatially uniform and temporally persistent) rainfall.

3. Coarse spatial scaling diminishes high intensity peaks in the rainfall field.

2.1.1 Dataset

The data used for the analysis presented here were collected using the University of Auckland Trailer Radar (Figure 2.1). The radar is designed to be portable, being towable

by a standard four-wheel drive vehicle and provides short range (20 km) high resolution rainfall measurements. The radar's high resolution capability has allowed the characterisation of small scale weather phenomenon such as tornadoes (Sutherland-Stacey et al., 2010).

Figure 2.1: The University of Auckland Trailer Radar situated in a field near Mangakino during the 2009 field deployment

During the winter of 2009, the radar was deployed near the town of Mangakino in the central North Island of New Zealand for a period of three months. Over this period, 48 rainfall events were selected as being significant (having a duration longer than one hour and the sum of the mean rainfall depth per radar scan over the event being 5 mm or greater) and were used for the following analysis.

The radar was operated to observe precipitation out to a range of 20 km. The short range reduces the requirements for a comprehensive multiple elevation scan regime which minimises the radar's sampling period to around 50 s. At these near ranges, the radar's 1.8° beam stays relatively narrow over the data domain, expanding to 800 m at 20 km (when an adjustment for the rotation speed of the dish is included). The data from a single scan elevation of 6°, being the lowest elevation sweep with minimal ground clutter, were processed onto a Cartesian grid with a pixel length of 200 m. Across the whole domain, an average pixel length of around 400–500 m is a more representative estimate of the radar's spatial resolution.

2.1.2 Method

To investigate quantifiably how sampling errors can affect the estimation of the true rainfall accumulation, spatial temporal sampling error statistics of 10 minute rainfall accumulations were calculated for the 48 selected events in the dataset using a method similar to that of Fabry et al. (1994).

The spatial temporal sampling error statistics are calculated assuming that the high resolution radar images represent a possible instance of a 'true' rain field. This 'true' rain field is then progressively downgraded in spatial and temporal resolution with the resulting lower resolution rain fields being accumulated into 10 minute rainfall maps at each particular combination of spatial and temporal resolution. The accumulation maps are then compared to the 'true' 10 minute accumulation.

The spatial resolution of the radar images used to generate the accumulations is downgraded by averaging radar reflectivity (Z) in space, in a manner physically analogous to increasing the sampling volume (assuming reflectivity is uniform with height within the beam volume). In this way we model how a theoretical radar might observe the same field at a lower spatial resolution. The rainfall rate for each scan is then retrieved by use of the standard Z-R relationship (with the parameters a = 200 and b = 1.6) (Marshall and Palmer, 1948).

Temporal resolution is downgraded by sampling every n^{th} (for n = 2,3,...) radar scan when aggregating the 10 minute accumulation, simulating an increase in the sampling period of n times the original interval. The accumulation is then estimated using an advection based interpolation scheme similar to that of Method 1 from Fabry et al. (1994). The rainfall accumulation between consecutive radar scans is generated by translating the n^{th} frame in the direction of diagnosed echo motion for half of the sampling period whilst accumulating at each one second step of the translation. The $(n+1)^{\text{th}}$ frame is translated in the reverse direction for the second half of the period in the same manner.

Echo motion is determined using a phase correlation approach and applying smoothing in time using an exponential weighting.

The comparison between the downgraded accumulation and the original high reso-

lution accumulation is made according to

$$\text{NRMSE} = \frac{\sqrt{\left\langle (L_i - H_i)^2 \right\rangle_{H>T \vee L>T}}}{\langle H_i \rangle_{H>T}} \tag{2.15}$$

Where L_i and H_i represent rainfall depth (in mm) in a single pixel from the downgraded and original resolution accumulations respectively, $\langle ... \rangle_{H>T \vee L>T}$ indicates calculating the mean over all pixels with intensities greater than T mm in either the downgraded or original resolution accumulations. This gives the per pixel root mean squared error (RMSE) as a fraction of the mean per pixel rainfall accumulation for all pixels with intensities over a certain threshold and is hereafter referred to as normalized root mean squared error (NRMSE). The threshold T was set to 0.167 mm. NRMSE was selected as the comparison metric so as to be more consistent with previous literature (eg. Jordan et al., 2000) so that results can be more readily compared.

2.1.3 Spatial Temporal Error Diagrams

The mean radar sampling error as a function of spatial and temporal scale for all 10 minute accumulations over the 48 significant events is shown in Figure 2.2. The diagram shows that the magnitude of the error due to sampling can be significant. For example, it can be seen for 1 km and 5 minute sampling, the sampling error compared to the high resolution data is of a magnitude of 20% of the mean rainfall accumulation. For 2 km and 10 minute sampling this error reaches a magnitude of 35%.

It is evident from this diagram that when generating accumulation maps from data with coarser spatial resolutions, it becomes less important to have shorter temporal sampling intervals and it is actually more beneficial to have slightly longer sampling intervals than the minimum 50 s for spatial resolutions coarser than approximately 1000 m. This relationship may be due to the nature of the advection interpolation method used as well as the fact that the rainfall field, when observed at a lower spatial resolution, would also appear to vary at a slower rate. Small variation could, however, appear in neighbouring (large) observation pixels resulting in them possessing non-zero rainfall even though a large fraction of that pixel would be observed to have zero rainfall if it had been observed at a higher resolution. This would lead to a greater number of non-zero pixels being compared to zero rainfall pixels in the higher resolution map, increasing the

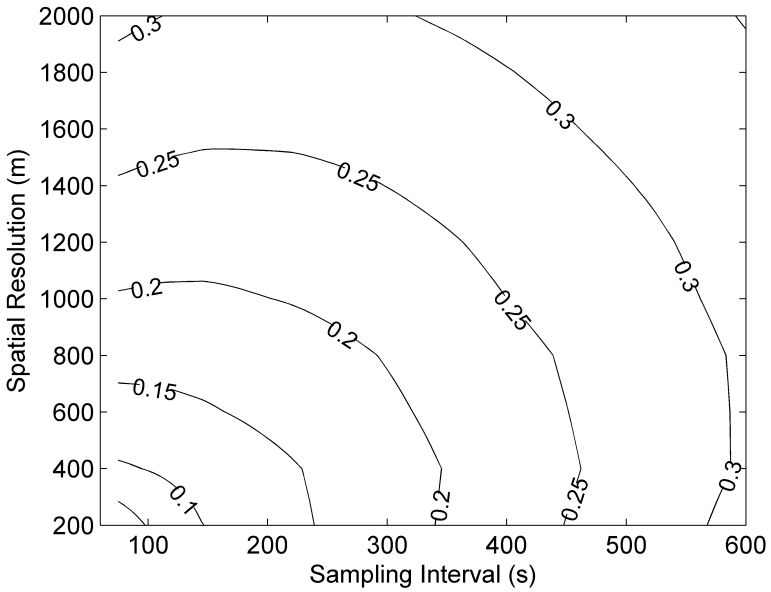

Figure 2.2: Average spatial temporal error diagram for 10 minute rainfall accumulations for all 48 significant events. Contours are NRMSE as defined in Equation 2.15.

sampling error. For lower temporal resolution observation, less of this variation would be captured, conceivably reducing the sampling error.

Similarly, if the sampling interval is longer than around 5 minutes, it is more beneficial to have slightly coarser spatial resolution than the finest 200 m. For instance, with 600 s sampling intervals, using a spatial resolution of 800 m provides a measurement of greater accuracy than when using a spatial resolution of 200 m. This supports the observation by Fabry et al. (1994) who explained this as being due to small scale evolution, which changes at a pace too rapid to observe at the particular sampling frequency, being observed instead as noise superimposed on the more well sampled larger scale evolution. This noise is reduced due to the averaging which is inherent in coarser spatial resolution observation.

This diagram is also rather symmetrical, showing that decreasing the resolution in space and time by a certain factor (the diagram has been produced so that the maximum spatial resolution and maximum sampling interval is around 10 times the highest resolution) results in a similar increase in the error.

2.1.4 Case Studies

Two case studies are considered to demonstrate the variance in the form of these spatial temporal error diagrams between different precipitation events. The first case examined (C1) is a predominantly stratiform rainfall event beginning on 2 July 2009. Representative radar images of C1 are shown in Figure 2.4. C1 consists of moderately heavy rainfall and has an average characteristic length scale of around 9 km. 'Characteristic length scale' here is defined as the average distance for the radar image's radially averaged spatial autocorrelation to fall to a factor of 1/e of the maximum. The characteristic length scale of 9 km was one of the longest of all those recorded in the three month time period (see Figure 2.3).

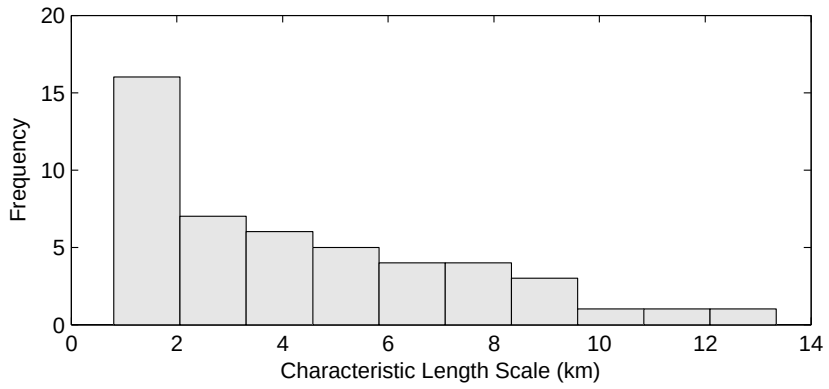

Figure 2.3: Histogram of characteristic length scales of the 48 events looked at in this analysis.

C1 has lower NRMSE than for the average case depicted in Figure 2.2. For example, for 2 km 5 minute sampling, the resulting error is less than 20% (Figure 2.5) compared to near 30% in the average case. The variation of sampling error with spatial resolution is also reduced for this case compared to the average case. This is more pronounced when the sampling interval is longer.

The second case (C2) is a predominantly convective event beginning with moderately intense convective cells early in the event leading to very intense small scale convective cells in the last hour of rainfall (Figure 2.6). The characteristic length scale is 2.5 km.

The error diagram (Figure 2.7) is dramatically different from that seen in both the

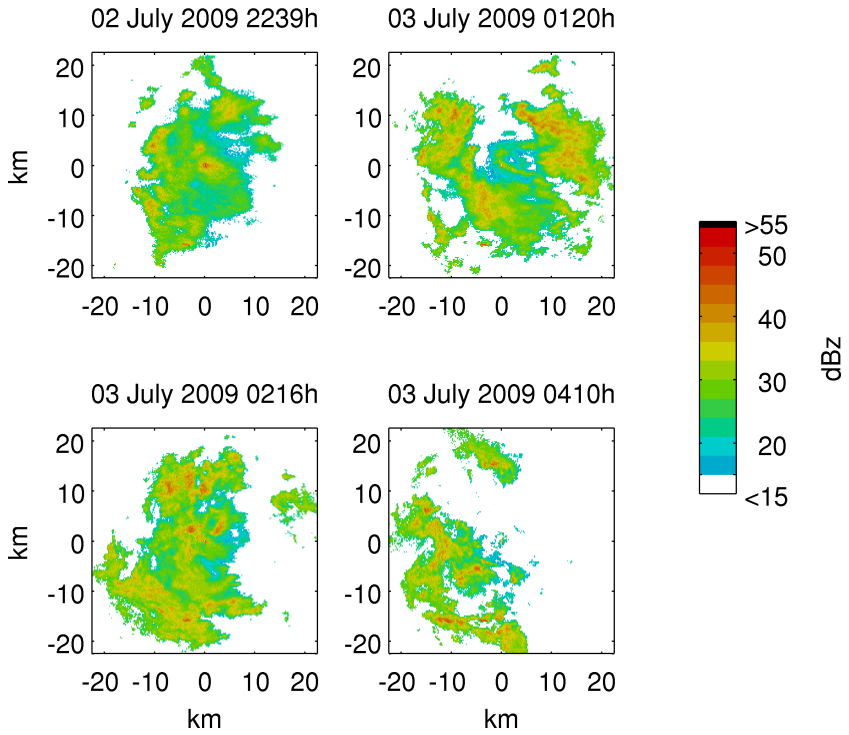

Figure 2.4: Representative radar images throughout a predominantly stratiform rainfall event (C1) on 2 July 2009. Indicated time is UTC+12.

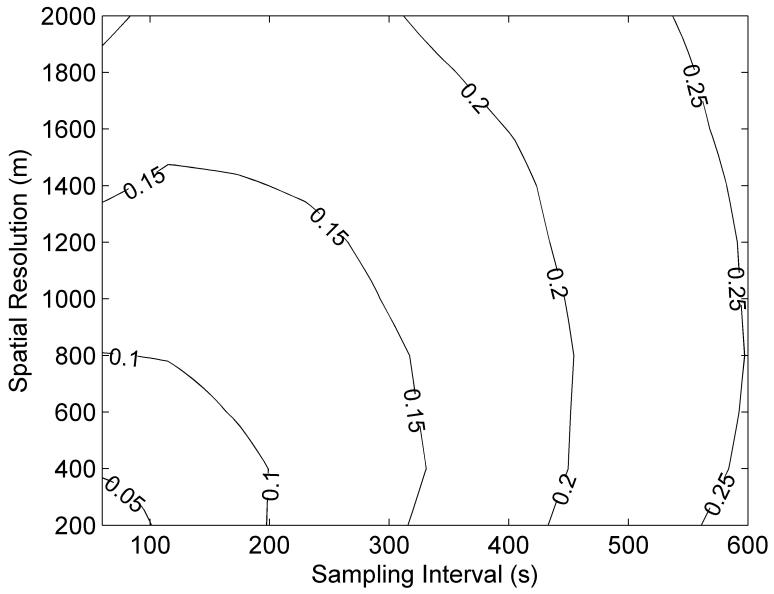

Figure 2.5: Spatial temporal error diagram for the rainfall event beginning 2 July 2009 (C1). The contours are NRMSE.

average of the 48 cases (Figure 2.2) and in C1. The magnitude of the error is greater, sampling at 2 km and 5 minutes results in near 55% error. Spatial resolution also becomes of greater importance for C2 with error increasing faster for multiplicative decreases in spatial resolution than the same multiplicative decrease in temporal resolution (increase in sampling interval).

Just as for the study average, but being more pronounced, there are benefits to increasing the sampling interval for coarser spatial resolutions. There is, however, little benefit in decreasing the spatial resolution for longer sampling intervals.

It is apparent from C1, C2 and the other 46 events (not individually shown) that the sampling errors are generally greatest for rainfall with shorter characteristic length scales. This is because the overestimation in precipitation area seen with a low spatial resolution observation is more severe for rainfall with length scales closer to or smaller than the size of the low resolution pixel. Also, small scale precipitation possesses much shorter temporal evolution times Venugopal et al. (1999) so that the radar sampling rate is much more important for capturing evolution of the rainfall field at these scales.

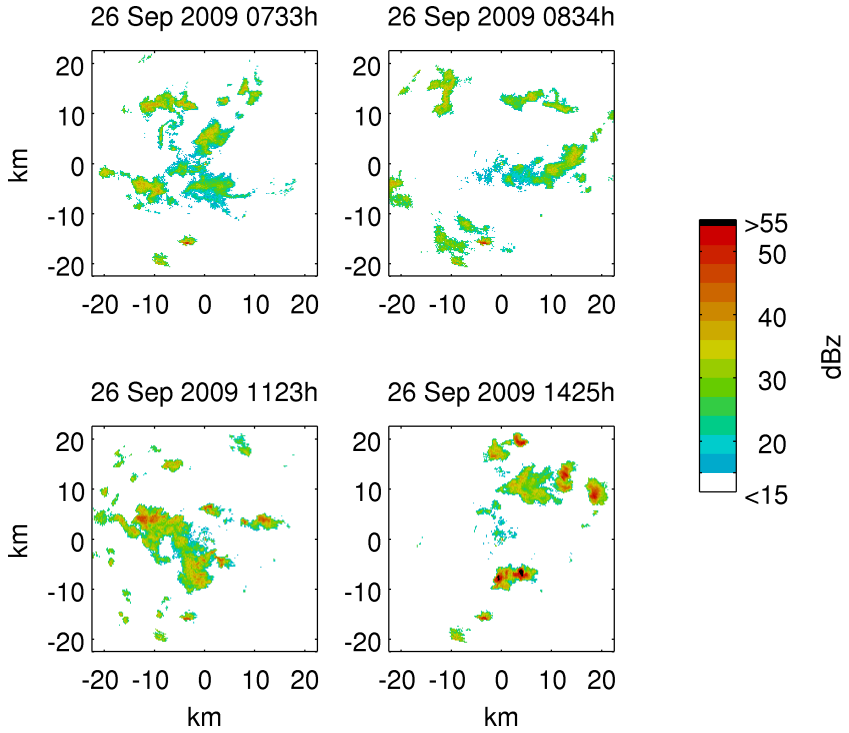

Figure 2.6: Representative radar images of the predominantly convective event (C2) on 26 September 2009. Indicated time is UTC+12.

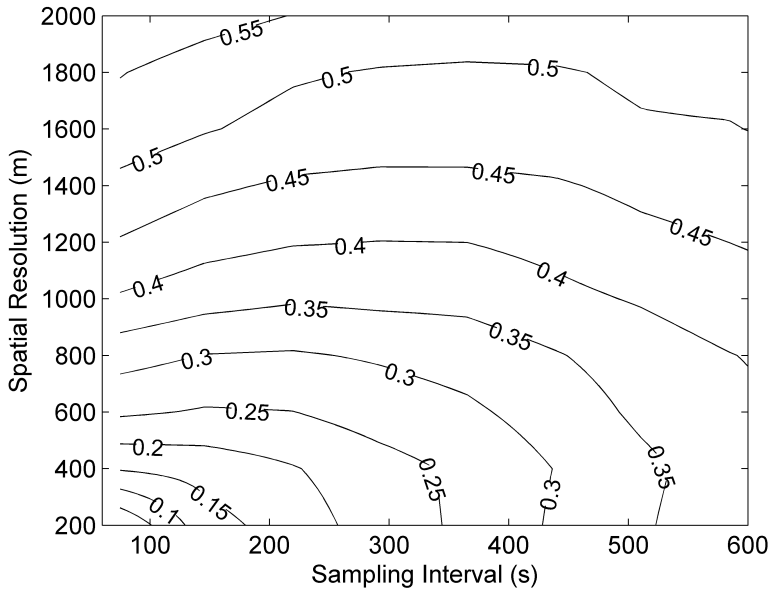

Figure 2.7: Spatial temporal error diagram for the rainfall event beginning 26 September 2009 (C2). The contours represent NRMSE.

2.1.5 Relationship to Length Scale

The presented cases imply a relationship between the characteristic length scale of the precipitating system and the sampling error. This is explored by comparing the mean NRMSE introduced by downgrading the high resolution data's spatial resolution to 2000 m for each of the 48 events to the mean characteristic length scale for each of the same events. The relationship is shown in Figure 2.8.

Generally, the longer length scale events have lower error but this is not always the case, with short length scale events also having lower error. Fitting this data against the logarithm of the length scale, we find that we are able to account for 52% of the variance in the mean error with a threshold in the rainfall accumulation amount corresponding to rainfall rates of greater than 1 mm hr^{-1}. This relationship provides insufficient information for the parameterisation of error using data from a coarser resolution instrument.

This fit is improved using a relationship of form:

$$\mathrm{NRMSE} = a \log L + bR + c \tag{2.16}$$

where a, b and c are coefficients of proportionality, R is the rainfall intensity that most

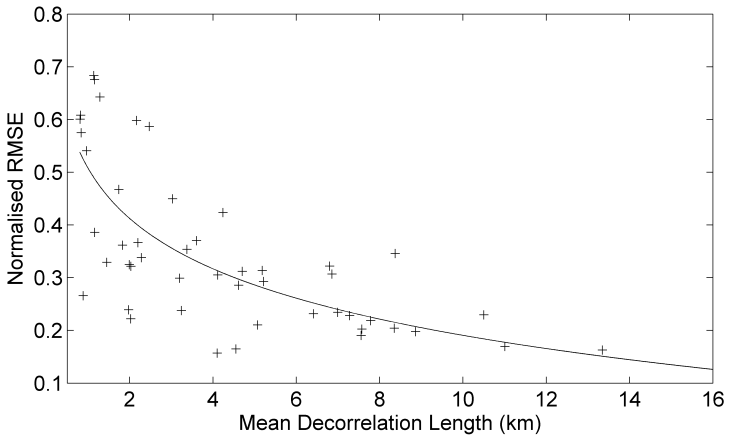

Figure 2.8: Mean NRMSE of an event related to that event's characteristic length scale. Adjusted R-squared is 0.52. Fit is of the form $\mathrm{NRMSE} = a \log L + b$, where a is negative.

contributed to the total rainfall accumulation and L is the mean decorrelation length of the two-dimensional rainfall pattern as observed by the radar. The coefficient a is negative and the new coefficient b is positive, meaning that for greater intensity rainfall we have more error due to sampling. Using this relationship, 82% of the variance in NRMSE is explained (shown in Figure 2.9). The value of R in Equation 2.16 is calculated by first finding the rainfall rate which contributes most to the rainfall accumulation for each radar frame.

The rainfall volume accumulation in each radar frame is given as

$$R_{\text{accum}} = A \times T \sum_{k} N_k r_k \tag{2.17}$$

where k spans the possible number of gradations of rainfall rate measured by the radar, A is the area of a radar pixel, T is the time between radar frames and N_k represents the total number of pixels with rainfall rate r_k. The rainfall rate that corresponds to the largest term in the summation in Equation 2.17 is classified as that which is the largest contributor to rainfall accumulation. For each precipitation event the mean of this value is calculated over all radar frames with rainfall covering an area of more than 10 km^2 to obtain the value of R used in Equation 2.16. This specific metric of rainfall intensity, was found to be a better indicator of RMSE than other intensity metrics such as mean rainfall rate or the 90^{th} percentile rainfall rate.

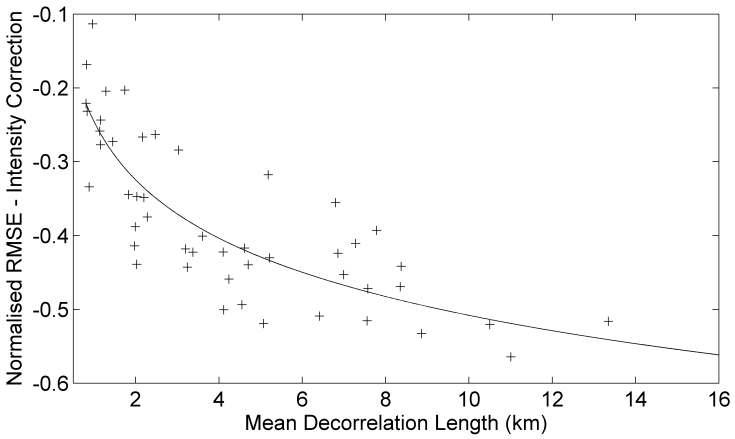

Figure 2.9: Relationship of sampling error with mean decorrelation length after taking into account a linear correction for rainfall intensity most contributing to accumulation. Adjusted R-squared is 0.82.

The relationship of NRMSE with rainfall intensity may be due to the relationship that rainfall intensity has with spatial scale, i.e. higher rainfall intensities usually occur at smaller spatial scales than lower rainfall intensities. This would suggest that the relationship with intensity may just be a proxy for a relationship with length scale information that is not present in the mean characteristic length scale over an event.

2.1.6 Effect on Intensity Distribution

The spatial averaging in reflectivity, Z, affects the distribution of rainfall intensities by reducing the number of highest intensity pixels and increasing the number of moderate and lower intensity pixels. On investigation of this process it was found that the modal reflectivity is also shifted lower by several dBZ. The total rainfall accumulation is increased by 10% and 20% on average over the 48 events when resolution is reduced to 1000 m and 2000 m respectively. This overestimation varied from 3% to 26% across the 48 cases at 1000 m resolution and from 4% to 54% at 2000 m resolution.

This bias is due to the heterogeneity of the rainfall rates inside the averaging pixel combined with the nonlinearity of the Z-R relationship. A particular case is depicted in Figure 2.10. As the overall mass of water is not conserved when averaging in Z, this figure is not normalized into a probability density function (as this could be some-

what misleading). Most of the increase in rainfall accumulation for this particular event comes from the increase in the number of pixels with reflectivities of between 22 dBZ and 35 dBZ. This more than accounts for the reduction in the number of pixels over 38 dBZ and therefore results in an increase in the total accumulation. This event is characteristic of the other 47 events. It should be noted that the reflectivity data was thresholded to a maximum of 55 dBZ before averaging was carried out, this may have some bearing on the conclusions drawn from this averaged data at the highest intensities.

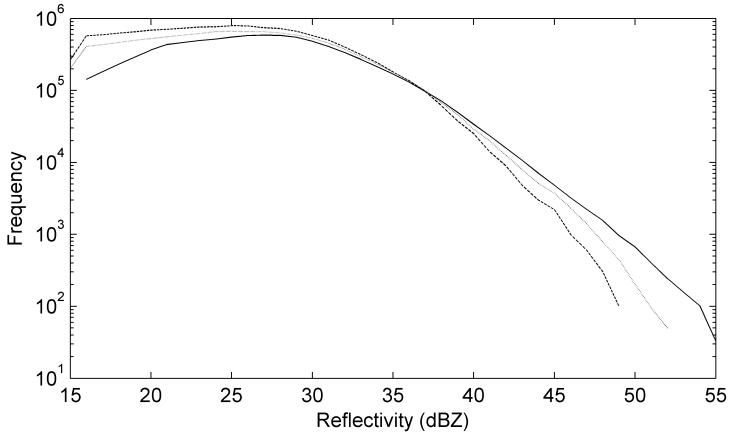

Figure 2.10: Number of pixels over a particular event by reflectivity (dBZ). Solid line is for 200 m resolution data, dotted is for 1000 m, dashed is 2000 m.

2.1.7 Conclusion

Spatial temporal sampling error statistics have been calculated for 48 mid-latitude winter rainfall events to determine the normalized root mean square error due to sampling effects for 10 minute rainfall accumulations. These errors were of significant magnitudes, varying from 17% to 64% of the mean accumulated rainfall for scales characteristic of operational weather radar networks (2 km and 5 minute sampling).

In support of hypothesis 1, sampling error *was* found to generally increase when rainfall fields were degraded in spatial and temporal resolution. However, for low spatial resolutions, a *decrease* in sampling error is often seen when longer sampling intervals are used.

The spatial and temporal error analysis was used, along with a metric of rainfall intensity, to determine a relationship between the magnitude of the sampling error caused by low spatial resolution observation and the characteristic length scale of a precipitation event. This relationship showed that an increase in spatial length scale resulted in a decrease in the sampling error and an increase in the rainfall intensity resulted in an increase in sampling error. This supports hypothesis 2, although no such relationship was found between temporal sampling error and the characteristic length scale.

An estimate of this scale dependent sampling error could be included (along with consideration of the other sources of error, such as those discussed in Chapter 3) in a more comprehensive radar error model to improve the estimation of the total measurement error. A possible application of such an error model could be contributing towards a complete radar rainfall uncertainty model that would enable the generation of representative radar rainfall accumulation ensembles for use with probabilistic quantitative precipitation forecasting and hydrology.

Hypothesis 3 was observed to be true for this dataset. Furthermore, it was observed that observing at lower resolutions also results in an overestimation of the total rainfall accumulation. Rainfall can be overestimated by as much as 26% for 1000 m sampling and by as much as 54% for 2000 m sampling when compared to the high resolution (200 m, 50 s) data. This is important to bear in mind when using data from long ranges where beam spreading is excessive.

In the above analysis, higher resolution radar data than is usually available is used to better approximate ‘true’ rainfall fields. It is, however, important to take into consideration that structure exists at smaller (and larger) scales not resolved by the equipment in this analysis.

2.2 Can Sampling Errors Be Diminished?

Now that sampling errors have been quantified in the previous section, it would be useful to look at ways to minimize their impact.

Again, we shall begin with some hypotheses:

1. The advection based temporal interpolation scheme substantially decreases error introduced by low temporal sampling rates.

2. Sampling error decreases with longer accumulation times.

3. Sampling error is less of a problem when considering spatially averaged rainfall accumulations.

2.2.1 Advection Based Temporal Interpolation

To investigate the effect that the advection interpolation scheme has on the 10 minute accumulation sampling error, the mean error was determined in the same manner as before but without the use of advection interpolation. Instead, the rainfall rates retrieved from each (subsampled) scan were simply multiplied by the sampling interval and these were then summed over all scans in the 10 minute period to calculate the accumulation. The decidedly incorrect physical interpretation of this treatment is to allow the rain to hover in place for the duration of the sampling interval and then instantly translate to a new location in time to be observed by the next radar scan. Figure 2.11 illustrates the difference in a 10 minute rainfall accumulation derived from three radar scans with and without using the advection interpolation scheme. The 'hovering' effect is apparent in the simple addition scheme, which results in physically unrealistic discontinuities and large localized accumulations compared to the smoother accumulation generated with the advection interpolation scheme.

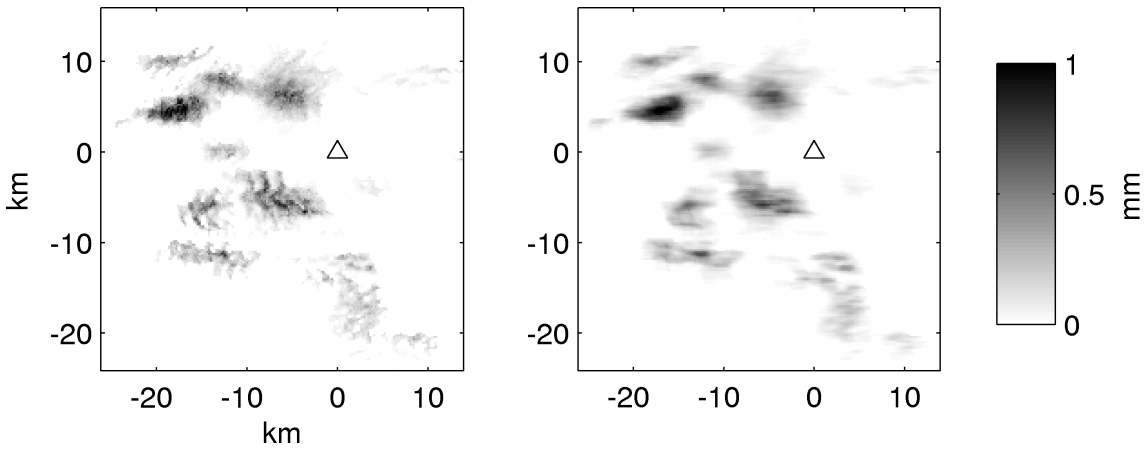

Figure 2.11: 10 min rainfall accumulation maps generated from three radar maps by simple addition (a) and by using advection interpolation (b). The location of the radar is indicated ($\triangle$).

The mean error diagram for the 48 events accumulated without using the advection interpolation scheme is presented in Figure 2.12. Examining this diagram it is obvious that for longer sampling intervals the benefit of using coarser spatial resolutions is much more pronounced than for the interpolated case. This is because, for a given advection speed, precipitation takes longer to traverse the distance represented by the lower resolution pixels. This leads to a reduction of the problem due to the precipitation instantly translating between sampled frames, reducing the large error that comes when comparing raining pixels to pixels absent rainfall.

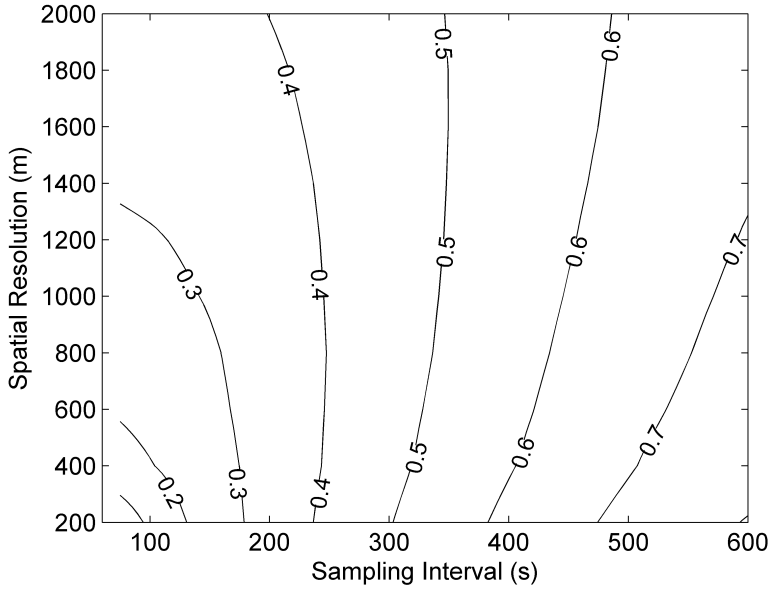

Figure 2.12: Average spatial temporal error diagram for 10 min rainfall accumulations for all 48 significant events, accumulated without using the advection interpolation scheme. Contours are NRMSE.

In contrast to the statistics generated using the advection interpolated scheme, for coarser spatial resolutions it is not beneficial to use longer sampling intervals. Additionally, the sampling interval has a much greater bearing on the NRMS error than the spatial resolution. For 2 km 300 s sampling, the RMS error is around 50% of the mean 10 minute rainfall accumulation. This error is almost twice that of when the advection interpolated scheme is used. This result implies that a significant proportion of the sampling error can be corrected for by using such a scheme. This result was initially

reported by Fabry et al. (1994) and has been acted upon for the reduction of this source of error in several studies (Ciach et al., 1997, Andrieu et al., 1997, Chumchean et al., 2003).

2.2.2 Increasing Accumulation Time

For many uses of rainfall accumulation data the accumulation period of 10 minutes that has been looked at so far is often unnecessarily short. A 1 hour accumulation product is a fairly typical output for radar networks (such as NEXRAD [Klazura and Imy, 1993]).

Figure 2.13 shows mean spatial temporal error diagrams for accumulation times from 10 minutes up to 2 hours. Increasing the accumulation period decreases the sampling error noticeably for all spatial resolution/sampling interval observation pairs. For instance, a 1 hour accumulation time decreases NRMSE for 2 km 300 s sampling from 0.3 down to near 0.2.

Longer accumulation times appear to reduce the influence that temporal resolution has on the NRMSE at any particular spatial resolutions. Comparing the NRMSE curves for 2000 m and 3000 m sampling in Figure 2.13a with those in Figure 2.13e, one notices that the error varies much less with temporal resolution in the latter.

This is shown in another manner in Figure 2.14a as a plot of mean NRMSE with accumulation time for a few specific spatial resolution/sampling interval pairs. The points representing NRMSE from sampling at 2000 m and 300 s converge with those representing 2000 m/600 s sampling (sampling schemes with the same spatial resolution but different temporal resolution) as the accumulation period is increased. This is also evident with 4000 m/150 s and 4000 m/800 s sampling. The same is not as obvious for points which share the same sampling interval but have different spatial resolutions.

An explanation of this result is that low spatial resolution observations—as seen in Section 2.1.6—alter the measured reflectivity distribution, adding a bias. Sampling at low temporal resolution does not introduce this effect. The error from low sampling rates comes from changes in intensity, precipitation area and motion between observations. These effects will be averaged out with long accumulation times as there is some temporal persistence in the statistical characteristics of a storm. Averaging multiple ‘snapshots’ of a storm would therefore tend towards the average case as long as the total accumulation time is shorter than the temporal decorrelation time of the storm’s

statistical form.

It is notable that the sampling error—with an accumulation spatial resolution of 200 m—is not negligible for usual radar operating resolutions (1–2 km, 300–600 s) even when considering two hour accumulation periods. While calculations of sampling errors for coarser accumulation spatial resolutions will be investigated in the subsequent section, the error for accumulations at the highest resolution for this experiment (200 m) have the closest relevance to the process of gauge correction of radar data which will be investigated in Chapter 4.

2.2.3 Decreasing Accumulation Spatial Resolution

The magnitudes of NRMSE seen so far could perhaps be misleading to one interested, not in very high resolution rainfall products, nor with comparison to point measurements but to broader scale areal accumulations. The hydrologist concerned with rainfall input into a catchment for instance. For catchments which are tens of square kilometres or greater in extent, one may think that, due to their aggregating nature, rainfall variation on a 200 m scale may have little impact on catchment outflow. For extreme rainfall, however, the sampling error at such high resolutions may still have an impact as high intensity rainfall is affected more greatly (as seen in Figure 2.10) than low to moderate rainfall intensities. This is the first stage in answering the question stated in Section 1.3 earlier "to what extent does the integrating nature of a catchment reduce the model impact of coarse resolution rainfall data input?".

To examine how coarser scale accumulation would be affected by sampling error, the method given in Section 2.1 was again performed with the added process of spatial averaging of the accumulations before comparison of the original high resolution observations with the downgraded observations. Such a process was also performed by Jordan et al. (2000) who found that spatial averaging was more effective at decreasing temporal sampling error for scattered rainfall than for uniform rainfall but was overall not a very effective way of reducing the error from coarse temporal sampling.

Figure 2.15 gives mean spatial temporal observation resolution error diagrams for accumulation averaging pixel lengths of 200 m (no spatial averaging), 1 km, 2 km, 5 km and 8 km. With accumulation pixel lengths of 2 km, sampling error from observations at 2 km, 300 s sampling decreases to just under 0.2 down from a value of 0.3 with pixel

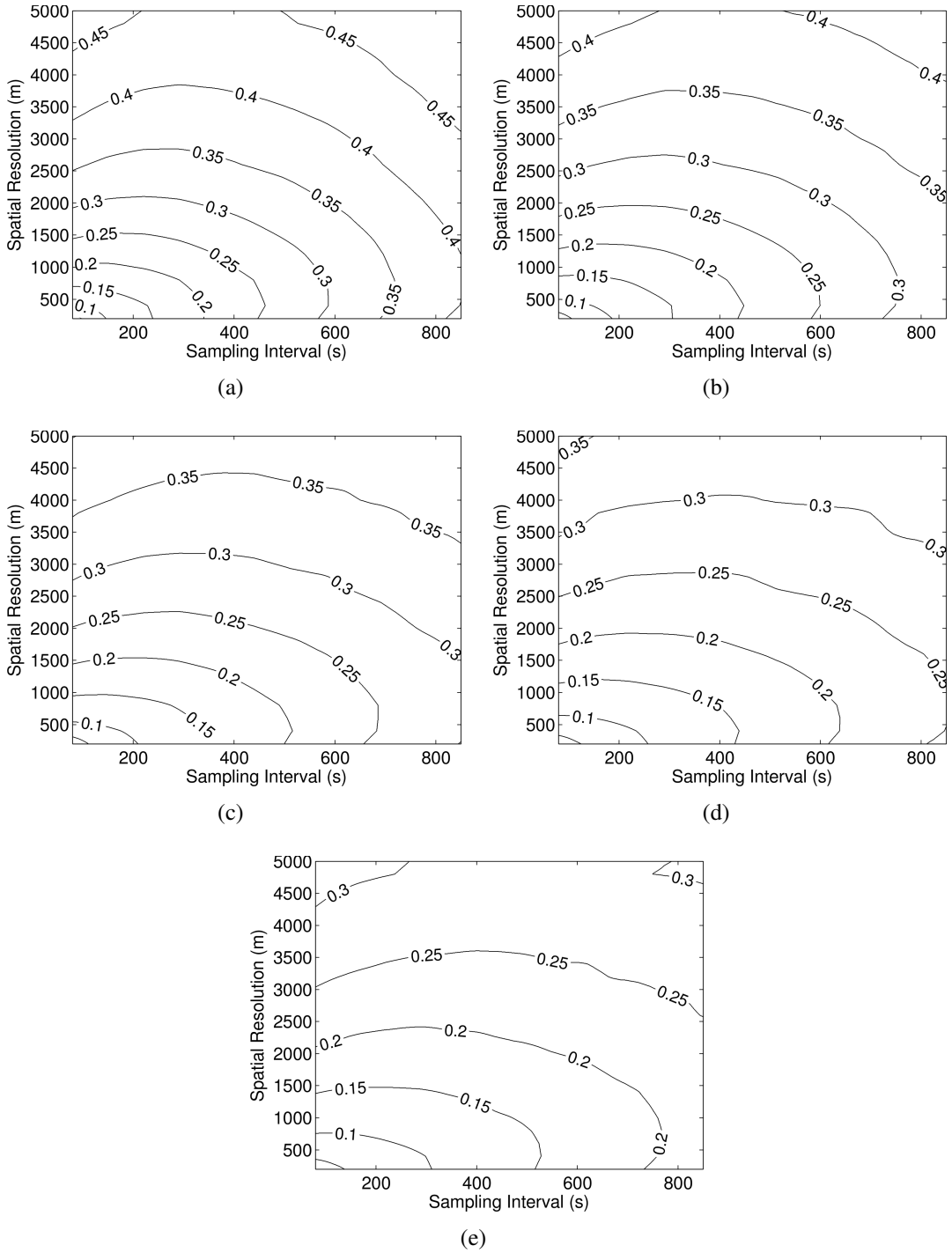

Figure 2.13: Mean NRMSE over the 48 significant events for accumulation times of: (a) 10 minutes, (b) 20 minutes, (c) 30 minutes, (d) 1 hour, (e) 2 hours.

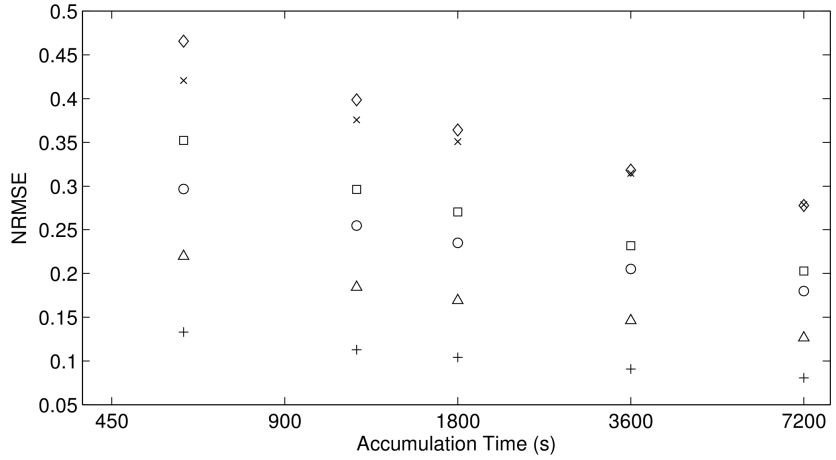

(a)

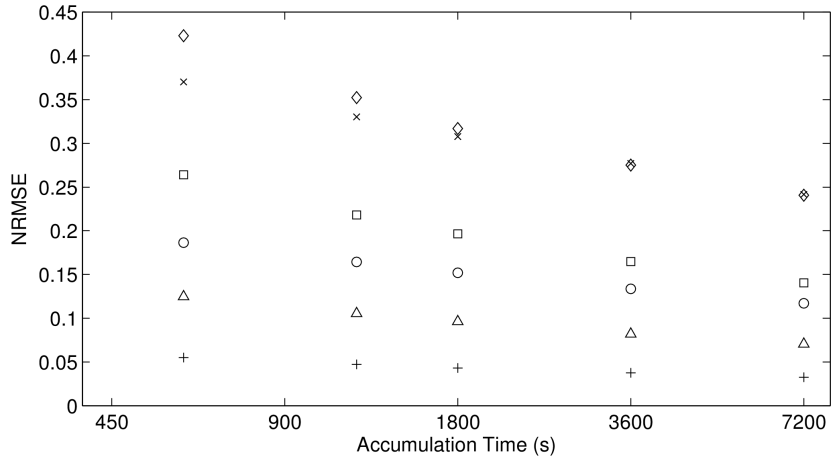

(b)

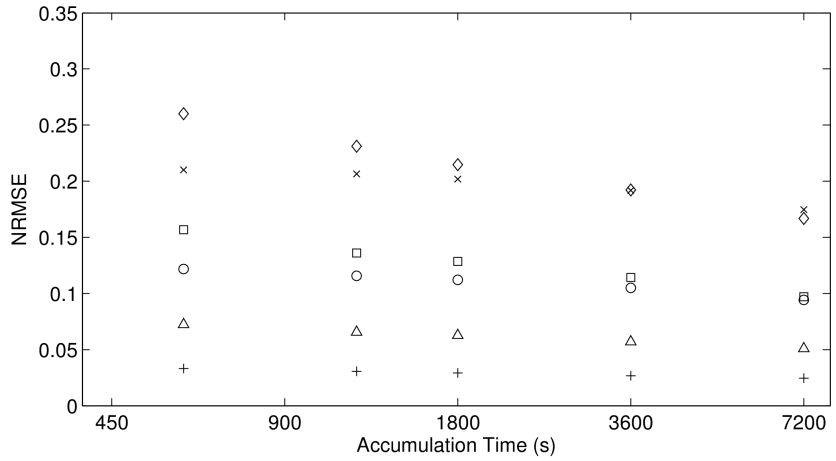

(c)

Figure 2.14: NRMSE error against accumulation time for accumulation spatial resolutions of: (a) 200 m, (b) 2 km, (c) 8 km. Selected spatial and temporal resolutions shown by (+) 500 m, 150 s, (△) 1000 m, 300 s, (○) 2000 m, 300 s, (□) 2000 m, 600 s, (×) 4000 m, 150 s, (◊) 4000 m, 800 s.

lengths of 200 m. This decreases to just over 0.1 at pixel lengths of 8 km.
This near factor three decrease is not equalled by the observation error for 4 km, 600 s sampling which experiences a twofold decrease with 8 km accumulation pixel lengths.

Figure 2.16 shows the sampling error for a selection of spatial resolution/sampling interval observation pairs with increasing accumulation pixel length. From this graph and from Figure 2.15, it is clear that there is no reduction in the dependence of NRMSE with sampling interval as accumulation pixel length is increased, contrary to what was seen with increasing accumulation period. There is, however, a slight convergence of NRMSE for observations that have identical sampling intervals but differing spatial resolutions. This is seen with the 2000 m/300 s and 1000 m/300 s sampling schemes. This convergence is not anywhere near as great as that for those observations with equal spatial resolution but differing sampling interval.

Figure 2.14(a)–(c) show NRMSE with accumulation time for a range of observation resolutions at three different accumulation pixel lengths. It can be noted that for increasing accumulation pixel lengths, increasing accumulation periods provide lesser impact on the NRMSE. The error for 500 m 150 s sampling stays fairly constant just below 0.05 for pixel lengths of 2 km and 8 km. The reduction of dependence on sampling interval with longer accumulation periods is seen at much lower spatial resolutions for accumulation pixel lengths of 2 km and 8 km. The error for 2000 m, 300 s and 2000 m, 600 s sampling is almost exactly the same (at 0.1) with a 7200 s accumulation period and 8 km accumulation pixel length. For such coarse rainfall accumulations, it appears that sampling errors may begin to become secondary to other error sources—with sampling error decreasing below 0.1 for usual radar observing resolutions—and this will be discussed in Chapter 3.

2.2.4 Conclusion

Three ways to decrease the impact of sampling errors have been investigated in this section. In support of hypothesis 1, it was found that the advection based temporal interpolation decreases NRMSE by around a factor of two. This clearly demonstrates the requirement for such an interpolation technique when generating rainfall accumulation products from remote sensed observations.

It was evident that sampling error decreases with longer accumulation times pro-

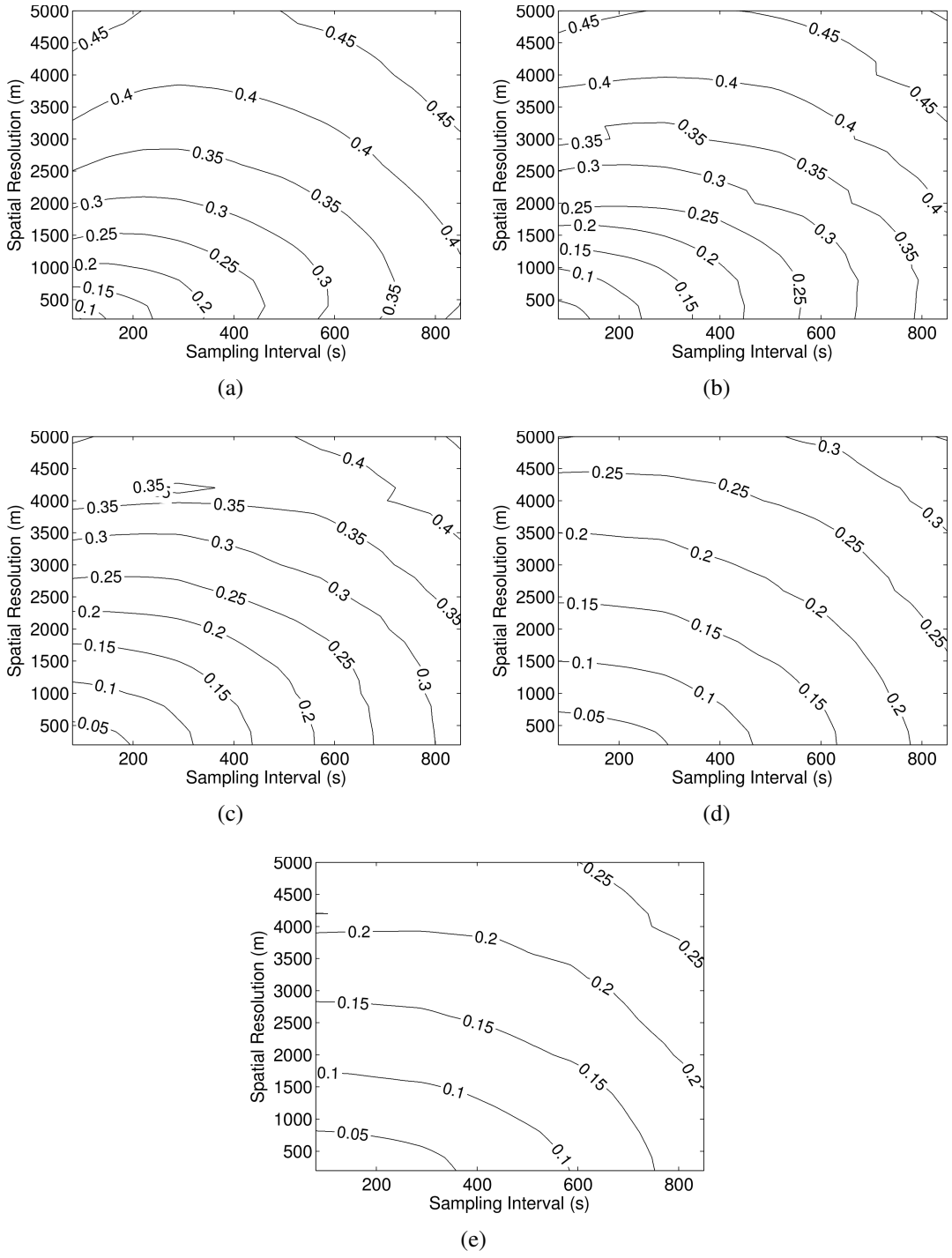

Figure 2.15: Mean NRMSE over the 48 significant events for 600 s accumulations which have been spatially averaged to: (a) 0.2 km, (b) 1 km, (c) 2 km, (d) 5 km, (e) 8 km.

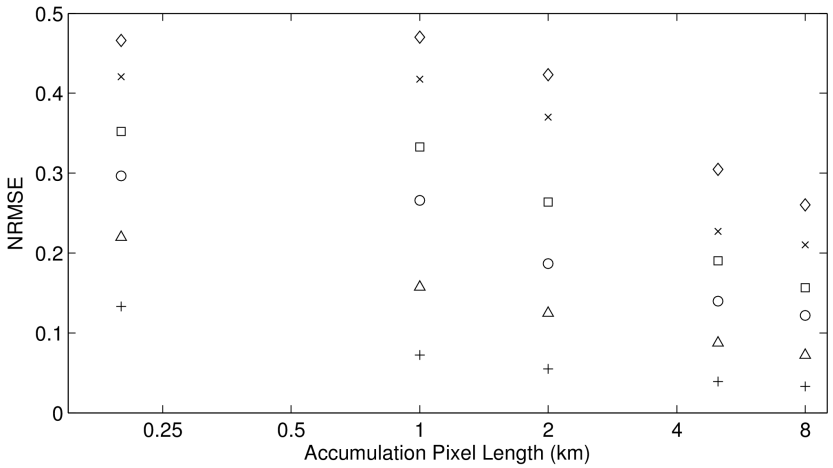

Figure 2.16: NRMSE error against accumulation spatial resolution for a 600 s accumulation period. Selected spatial and temporal resolutions shown by (+) 500 m, 150 s, (△) 1000 m, 300 s, (○) 2000 m, 300 s, (□) 2000 m, 600 s, (×) 4000 m, 150 s, (◊) 4000 m, 800 s.

viding strong evidence for hypothesis 2. It appears that temporal sampling error is decreased more so than spatial sampling error using such a method.

It was also evident that sampling error decreases when spatial averaging is applied to the output rainfall accumulation. For example, a factor three decrease is observed for 2 km/300 s sampling when spatially averaging to 8 km pixels. These results provide strong evidence for hypothesis 3.

2.3 Discussion

We have discussed here the nature of the problem relating to precipitation observation scale and have come a little closer to answering the question posed in Chapter 1.

Sampling errors have been quantified and it has been demonstrated that it is possible to estimate sampling error using only low resolution observations. Such a relationship will at least allow identification of when and where an observed rainfall accumulation should be treated with some suspicion.

From the results obtained in this chapter, along with the logical arguments from Chapter 1, it is evident that certain applications of rainfall data are more susceptible

to error introduced from low resolution measurement. Correction of areal data using point measurements is likely the most severe case, as applying spatial averaging to the observed rainfall accumulation is not an appropriate method of error reduction for such an application. As such, the variation in radar-gauge bias from sampling error will be investigated in Chapter 4.

Hydrological applications are also likely to be susceptible in some cases. It was observed that spatial and temporal integration of the rainfall accumulation diminished sampling errors and such a process could be said to occur when rain falls into and is transported through a catchment. However, this integration process was not observed to completely eliminate sampling error. It is dependent upon the catchment as to how much of an impact sampling error would have on catchment outflow. The catchments most significantly affected would likely be small and/or urban catchments, especially when extreme rainfall is involved.

The problems associated with failing to account for precipitation movement between radar scans when formulating a rainfall accumulation product was revisited. When using a simple non-advecting accumulation scheme, the observed sampling errors were demonstrated to be greater than twice the magnitude of those observed when an advection interpolation scheme was implemented. This has important implications for small scale (urban) hydrology where runoff and infiltration are sensitive to localized rainfall accumulation depth.

It is important to put the magnitude of sampling error measured here into context with other sources of error to determine the significance of its impact. In this regard, the error sources for radar estimation of rainfall will be discussed in the following chapter.

Chapter 3

Radar Error Sources

This chapter seeks to explain the errors associated with radar observation of precipitation, the effects that these errors have on end user rainfall products and also how these errors can and should be mitigated. This will allow the results relating to resolution sampling error to be placed into a wider context.

3.1 What Are the Sources of Radar Uncertainty?

Many sources of radar error have already been mentioned in Chapter 1 of this thesis, most particularly sampling error, which was given an extensive investigation in Chapter 2. The other error sources mentioned were unknown vertical profiles of reflectivity (VPRs), unknown rain drop size distributions, the error due to the random distribution of scatterers in the beam volume, ground clutter, beam blockage and attenuation. Sources that were not mentioned include: calibration error, clear air echoes (insects, birds, etc.), background noise, anomalous propagation, wind drift, departure from Rayleigh scattering and digital quantization error (relating to the bit depth of the digitizer or the file in which the observation is stored).

3.1.1 The Vertical Profile of Reflectivity

Many researchers (e.g. Zawadzki, 1984, Joss and Waldvogel, 1990, Collier, 2002) consider the variation of the VPR—combined with the necessarily increasing beam height

with range—to be the most significant source of error associated with radar rainfall estimation. As discussed in Section 1.1.2, there is a trade off between using low elevation scan angles, which reduce the contribution of VPR variation to radar error (hereafter referred to as VPR error), and the occurrence of ground clutter (a problem at shorter ranges) and beam blockage (which is a problem at all ranges past a blocking object). One must also make a trade off between the number of elevation scan angles, which would reveal greater detail of the VPR, and the temporal resolution of the observations. It is not necessary to repeat the more in depth look at these trade offs and compromises that were discussed earlier, we shall instead focus on the types of weather systems in which this error has the greatest impact on radar rainfall measurements and the measures which can be taken to reduce such an impact.

Overshooting rainfall altogether must be the most drastic realization of VPR error, in which a radar's beam propagates above underlying precipitation and thus fails to observe it. This results in what may be interpreted as a false negative observation of surface precipitation. Such overshooting occurs at a range dependent upon the lowest usable beam angle (that is not affected by ground clutter or beam blockage) and the height to which precipitation extends. Shallow precipitation, therefore, can only be observed at short range, while deep convective systems are often observable out to long ranges.

The type of precipitation systems that are more likely to be 'overshot' are shallow convective systems (which often, but not always, consist of low to moderate rainfall intensities) and some stratiform systems, usually those which are less intense and particularly those occurring on cold days when the melting layer is near the ground or is not present at all (considering snowfall).

While low to moderate intensity rainfall from transient shallow convective systems may not contribute too much to overall rainfall accumulations or to flash flooding, rainfall from stratiform systems generally persists for much longer durations and over much greater areas. This means that stratiform systems *do* contribute greatly to overall accumulations and cannot, therefore, be ignored without consequence. There is, however, little which can be done solely using radar data to correct for beam overshooting. Either the radar network density is to be increased in areas where such shallow precipitation contributes significantly to rainfall accumulations or additional information from rain

gauge or satellite could be used to detect the occurrence of these false negative observations and provide the precipitation measurements themselves. A Rainsat (Bellon et al., 1980) like algorithm (in which a relationship between satellite observations and radar rainfall is first established and then extended outside of the radar domain to improve rainfall detection from satellite data alone) could be used on the satellite data to increase the quality of its quantitative precipitation estimates.

False positive observations relating to the VPR, which are just as drastic as the false negatives from beam overshooting, can also occur. Precipitation aloft which does not fall to the ground (virga) occurs either when the air mass underneath a precipitating cloud has a low humidity, leading to evaporation as the precipitation descends, or when updrafts are sufficiently strong so as to prevent the precipitation from falling (often seen with snow). As with beam overshooting, false positive observations from virga cannot be accounted for solely with radar and require surface precipitation measurements to be detected and corrected.

We arrive now at the less dramatic (being absent of divide by zero possibilities) but still potentially serious form of VPR error, where an observation is made that is a convolution of the radar's beam with the particular vertical reflectivity profile at the location we are interested in observing. Knowing what that profile is, along with knowledge of the radar beam's radiation profile, allows a multiplication factor (or additive constant, if expressed in dBZ) to be obtained that converts the radar measurement aloft to an estimate of the surface precipitation.

It is important to state here that there is significant random fluctuation (in space and time) about the local mean VPR. Furthermore, even if the VPR is known precisely at every point in the radar observed domain, one would still not be able to make a perfect VPR correction as the hydrometeors aloft are affected by turbulence and stochastic growth and decay processes as they fall towards the ground. This means that, although a proportion of the systematic bias due to the VPR uncertainty issues can be corrected for, a substantial random error due to these processes will remain.

For stratiform rainfall, the VPR is on average similar to that in Figure 3.1. This form is often broken down into three parts; reflectivity remains constant from the surface up to some point several hundred metres below the melting layer where reflectivity peaks (this peak is known as the 'bright band') and then falls off linearly (in dBZ, exponentially

in Z) with height above the melting layer. The bright band can account for rainfall overestimates that are 3–5 times 'ground truth' rainfall.

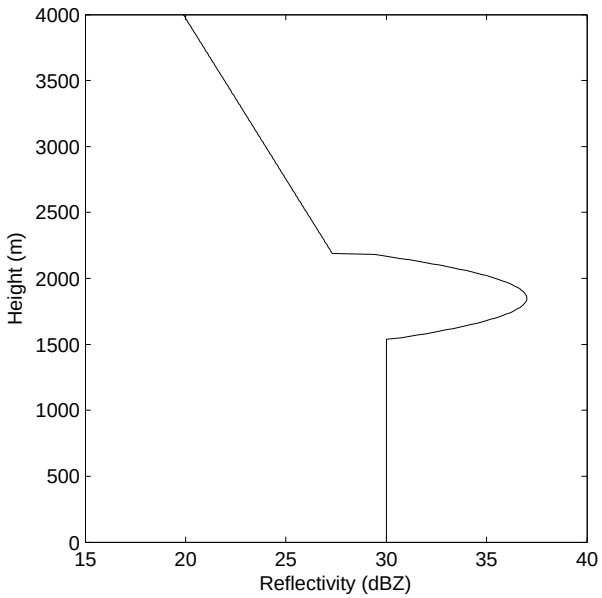

Figure 3.1: Representation of the average vertical profile of reflectivity for stratiform rainfall.

The bright band has been extensively studied over the history of radar (Austin and Bemis, 1950, Stewart et al., 1984, Willis and Heymsfield, 1989, Fabry and Zawadzki, 1995) and has been found to be caused by the melting of the larger snow crystals (which grow by aggregation) as they enter the melting layer (at the 0 °C isotherm) combined with the difference in fall speed between snow crystals and rain drops. Snow crystals can attain greater sizes than rain drops as the latter cannot sustain diameters larger than 5–6 mm without breaking apart as they descend (Gunn and Kinzer, 1949). Although frozen ice crystals make much weaker targets than liquid rain drops due to a much lower complex index of refraction for ice (0.18 compared to 0.93 for liquid water), as they enter the melting layer the ice crystals' outer layer necessarily melts first to give the crystals a liquid 'skin' so that to the radar they appear as large water drops (having a complex index of refraction much closer to that of water). These partially melted drops benefit from the D^6 term in Equation 3.8 to provide larger reflectivities than can be achieved with liquid drops. Once completely melted, the large drops break apart and

speed up which leads to a reduction of the drop density—ice crystals typically reach terminal velocities of 0.5–3 m/s compared to speeds of 4–9 m/s for rain drops (Locatelli and Hobbs, 1974, Gunn and Kinzer, 1949). These two processes combine to reduce the reflectivity of the rainfall below the bright band.

Bright band 'contamination' refers to the occurrence of overestimation of rainfall intensity caused by the radar beam intercepting the bright band zone of stratiform precipitation. This contamination is much more pronounced at near ranges (when the zero degree isotherm is low or when higher elevation angles are used) as beam spreading diminishes the effect of the bright band due to averaging out the VPR.

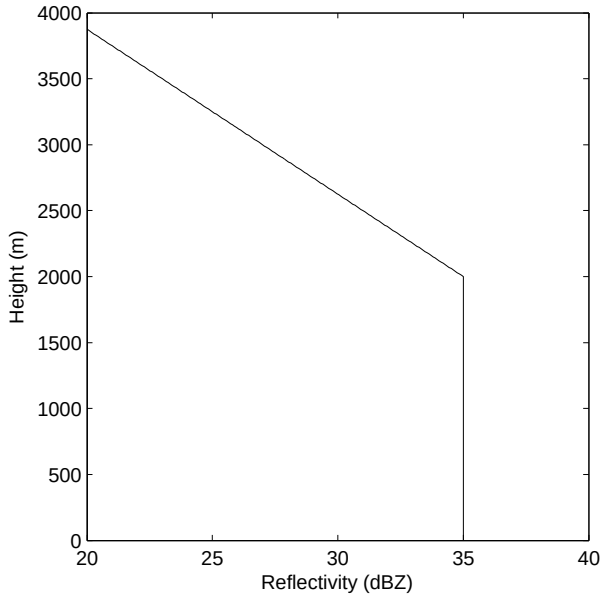

Figure 3.2: Representation of the average vertical profile of reflectivity for convective rainfall.

The average VPR form of convective rainfall shown in Figure 3.2 gives a simpler picture than that for stratiform rainfall with reflectivity remaining constant up to the melting layer, above which reflectivity decreases linearly (in dBZ) with height. This simpler picture is, however, somewhat misleading as the VPR of convective storms varies greatly between storms (see Figures 3.3 and 3.4) and Figure 3.2 is merely representative of the average case.

Convective rainfall involves much stronger updrafts than for stratiform rainfall which

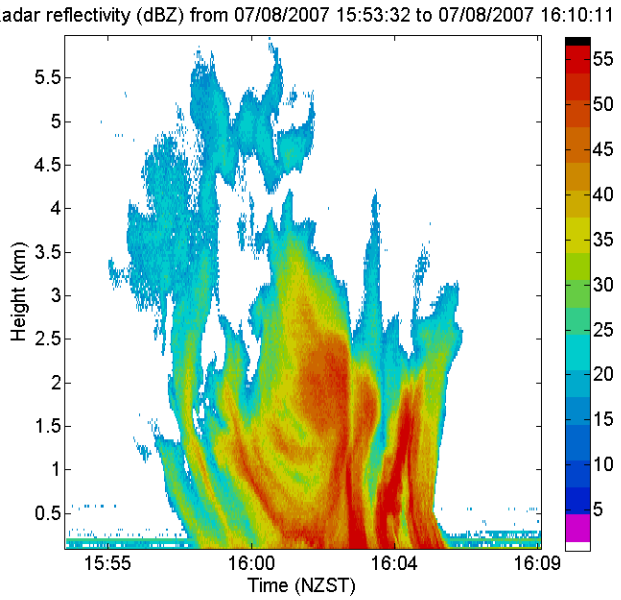

Figure 3.3: A HTI (height time indicator) plot of a convective rainfall event on 07/08/2007.

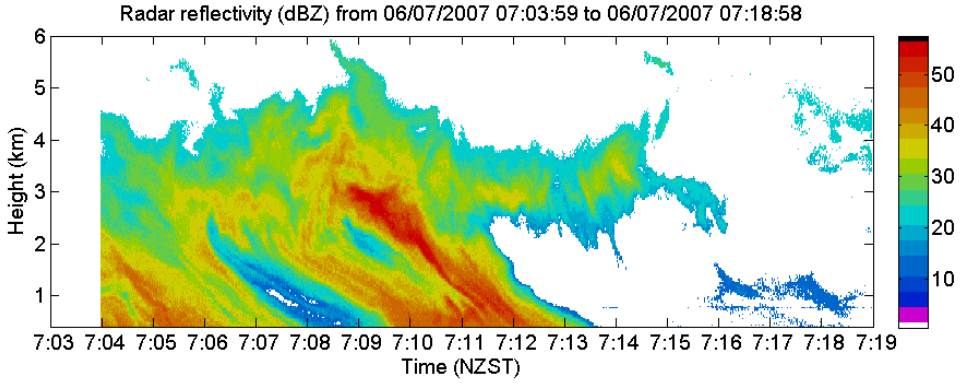

Figure 3.4: A HTI (height time indicator) plot of a convective rainfall event on 06/07/2007.

allows large solid and liquid hydrometeors to be held aloft to grow by coalescence and riming. Once large enough that the updraft no longer sustains their descent, these hydrometeors fall, sweeping up other smaller hydrometeors on the way. A bright band is not visible as the updraft prevents the layered form exhibited by stratiform rainfall from being established. Large (low density) aggregate snow crystals also do not form in convective rainfall.

Correction Methods

There are several routes one can go down to reduce the impact of VPR errors on quantitative precipitation estimation (QPE). Preventative measures can be taken when first selecting the radar site; by making sure to avoid sites subjected to beam blockage and excessive ground clutter at low elevation angles (allowing these angles to be viable for observation), VPR error can be minimized. Correction methods that are used to mitigate existing VPR error can be divided into two camps, those which seek to observe or model the VPR and apply a correction based on the predicted beam sampling height and spread and those which merely apply a bias based on range or 'ground truth' measurements from gauges.

Those of the first camp include single radar correction methods, which use two or more beam elevations to establish a picture of the VPR either at each pixel or on average for the entire radar domain. Such methods become less effective at increasing range as beam spreading reduces the resolution at which the VPR can be observed which in turn decreases the accuracy of the VPR correction.

Smith (1986) described a dual elevation scan correction method, based on one by Harrold and Kitchingman (1975), which used the ratio of reflectivities from the two elevation scans to determine the VPR at each pixel (removing the assumption of homogeneous rainfall intensity that would be necessary if only one elevation scan were used). An improved method was developed by Andrieu and Creutin (1995) using an inverse method approach.

For operational use Germann and Joss (2002) suggest that a mesoscale correction should be applied—rather than attempting to correct every pixel in each scan separately—in which the average profile from within around 50 km from the radar is calculated and averaged in time relative to the surrounding precipitation systems' temporal scales

(shorter time averaging for the more quickly fluctuating convective systems, longer for stratiform systems).

Berne et al. (2004a) describes a dual radar method whereby an X-band radar determines the VPR that is then used to correct an S-band radar PPI.

Also included in this camp are those methods which predict the VPR using climatological average forms. For instance, Bellon et al. (2005) describes a method in which historical VPRs which match present conditions are altered so that bright band height is consistent with temperature measurements. They compare this method to a method based on the average VPR observed from multiple elevation scans and find the latter to be more effective at minimizing error.

Gauge correction methods will be discussed in Chapter 4.

3.1.2 Errors from Fluctuating Radar Signals

As referred to in Chapter 1, when observing precipitation with a radar, the randomly varying distribution of scatterers in the beam volume causes the returned radar signal to be incoherent and exhibit a random fluctuation. From Marshall (1953), the distribution of the returned instantaneous radar intensity is

$$P(A^2)dA^2 = \frac{1}{\overline{A^2}} e^{-A^2/\overline{A^2}} dA^2 \tag{3.1}$$

where $\overline{A^2}$ is the mean intensity. In log form this is expressed as

$$P(\log A^2)d\log A^2 = \frac{1}{M\overline{A^2}} \exp\left(\frac{\log A^2}{M} - \frac{1}{\overline{A^2}} e^{\log A^2/M}\right) d\log A^2 \tag{3.2}$$

where $1/M = \log_e 10 = 2.30259$. The standard deviation is $\pi(\log e)/\sqrt{6} = 0.557$.

It is required to average several independent pulses together to acquire a meaningful observation. The probability distribution function for k pulses averaged in intensity (J_k) is also given in Marshall (1953).

$$P(J_k)dJ_k = \frac{k^k}{(\overline{A^2})^k (k-1)!} J_k^{k-1} e^{-kJ_k/\overline{A^2}} dJ_k \tag{3.3}$$

The standard deviation of this distribution varies as $\sigma = \overline{A^2}/\sqrt{k}$

While it is not possible to find an analytic expression for the average of k measurements of log(intensity), based on a numerical analysis, Marshall (1953) found that the probability distribution of the average of k pulses in log(intensity) tends towards that of equation 3.3 for large k. The standard deviation can then be written as

$$\sigma \approx \frac{5.6}{\sqrt{k}} \tag{3.4}$$

The need for multiple pulses to be averaged to minimize this error must be balanced with the radar's PRF and desired temporal sampling rate. A question that could well be asked here is "What is the optimum balance between the number of samples, k, and the temporal sampling rate (for a certain radar PRF) so that radar error is minimized?". To ascertain this, the variation described by Equation 3.4 will have to be put into the same form as the sampling error in Chapter 2. This will allow a comparison between the two error sources to be made.

This was performed as follows. Noise—numerically generated from the distribution of k measurements of $\log(intensity)$— was added to the individual radar scans of the 48 significant events from Chapter 2 over a range of k values. These scans were then accumulated (using advection interpolation) into 10 minute periods and compared to the noiseless accumulations to obtain NRMSE. This was performed 10 times for each accumulation.

Figure 3.5 shows the average NRMSE over the 48 significant events. For a typical value of k (k = 32), NRMSE is approximately 0.06. Doubling the temporal sampling rate would require k = 16 which would increase the error to just over 0.08. From Figure 2.2, it is apparent that for 1000 m/300 s sampling, little benefit would be gained in doing this. For 500 m/300 s sampling on the other hand, there would be a benefit. There is likely little need to quadruple the sampling rate, unless the sampling rate is greater than 500–600 s and high spatial resolution measurements are being made.

3.1.3 Z-R relationship

The relationship between radar reflectivity and rainfall rate was first accurately quantified by Marshall et al. (1947). They found the general relationship to be of the form $Z = aR^b$ and found the values of a and b to be on average 190 and 1.72 respectively.

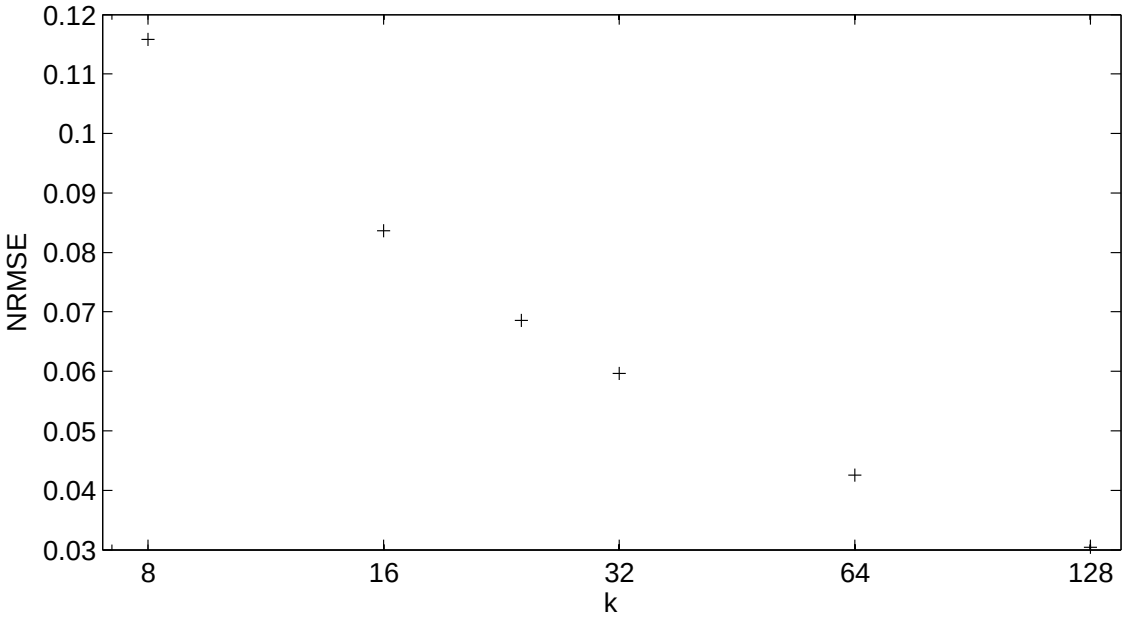

Figure 3.5: Average NRMSE resulting from error due to the random distribution of scatterers in the beam volume against the number of radar pulses averaged (k) for the 48 significant events.

These values were later refined to give the familiar equation of

$$Z = 200R^{1.6} \tag{3.5}$$

The variation in the mean values of a and b—and in the random error associated with these values—between different precipitation events and even during the same event (varying in time and in space) has often been blamed for the sometimes major discrepancies between observed reflectivity Z and the observed rainfall rate R.

To further discuss this topic it would be of use to understand where the Z-R relationship comes from. We shall start with the radar equation from Probert-Jones (1962) which takes the following form

$$P_r = \frac{\pi^3 c}{1024 \ln 2} \left(\frac{P_t \tau G^2 \theta \phi}{\lambda^2} \right) \left(\frac{|K|^2 Z}{r^2} \right) \tag{3.6}$$

This equation gives an expression for the received signal power (P_r) as a function of the radar parameters (P_t, τ, G, θ, ϕ and λ) and the target characteristics (K, Z, and r). The radar parameter P_t is transmitted power, τ is pulse length, G is antenna gain, θ and ϕ are the horizontal and vertical half power beam width respectively and λ is the transmitter wavelength. Relating to the target, $|K|^2$ is complex index of refraction, r is the range of the target from the radar and Z is defined as

$$Z = \sum_{i=1}^{N} D_i^6 \tag{3.7}$$

$$= \int N(D) D^6 \, dD \tag{3.8}$$

where $N(D)$ is the drop size distribution so that $N(D)dD$ is the number of particles with diameter D between D and $D + dD$ in a unit volume. Z has units of mm^6 m^{-3}.

As the radar parameters are constant, equation 3.6 can be simplified to

$$P_r = \frac{C' |K|^2 Z}{r^2} \tag{3.9}$$

This equation is further simplified with the assumption that $|K|$ remains constant. This is valid if all targets in the sampling volume are either liquid rain drops or ice particles for example.

$$P_r = \frac{CZ}{r^2} \tag{3.10}$$

Z can be converted into a rainfall rate using the drop distribution given by Marshall and Palmer (1948):

$$N(D) = N_0 e^{-\Lambda D} \tag{3.11}$$

Where Marshall and Palmer (1948) give values for N_0 and Λ as follows:

$$\Lambda = 4.1 R^{-0.21} \text{ mm}^{-1} \tag{3.12}$$

$$N_0 = 8000 \text{ m}^{-3} \text{ mm}^{-1} \tag{3.13}$$

where R is the rainfall rate (in mm hr^{-1}).
Z can be written

$$Z = N_0 \int e^{-\Lambda D} D^6 dD \tag{3.14}$$

Which upon integration becomes

$$Z = \frac{720 N_0}{\Lambda^7} \tag{3.15}$$

Using the above values for Λ and N_0 gives

$$Z = 296 R^{1.47} \tag{3.16}$$

which is a Z-R relationship of the form $Z = aR^b$ with a of 296 and b of 1.47.

We see that the Marshall and Palmer distribution for raindrop diameter is assumed in this derivation. The parameters of this distribution determine the parameters of the Z-R relationship. The raindrop size distribution must be known in order to convert radar reflectivity to rainfall rate. As it is not possible to measure this size distribution with a radar which operates with a single wavelength and polarization, assumptions must be made about the size distribution, leading to an error being introduced into the rainfall estimate.

That the parameters a and b in the Z-R relationship often vary significantly between and within rainfall events was noted early on in the history of weather radar—for instance Atlas (1990) states that more than a dozen Z-R relationships had been put forward by 1953—and much research has been focused on this since (eg. Twomey, 1953, Battan, 1973, Atlas et al., 1999). There is evidence that at minimum, separating radar

observed precipitation into snow, stratiform rainfall and convective rainfall and using particular a and b parameters for each precipitation type improves on precipitation estimates that use only one one specific combination of these values for all precipitation types (Austin, 1987).

While dual-polarization radars have been put forward as a solution to this problem, they often do not get far in achieving this goal. This is because the dual polarization products (Z_{DR} and K_{DP}) are often too noisy to be used operationally (Collier, 2002). Furthermore, implementing dual polarization in a radar increases the complexity of calibration and maintenance considerably (Delrieu et al., 2009).

Dual-polarization radars rely on the fact that large raindrops become deformed and flatten (become oblate) as they fall and thus return different reflectivities to pulses polarized horizontally and vertically. Where this becomes unstuck is that the majority of raindrops are very close to spherical, it is only drops above ~ 3 mm which deform. Additionally, the drops which do deform oscillate as they fall (from oblate to prolate and vice versa) making the mean shape appear more spherical (Brandes et al., 2002).

It is common that equation 3.5 is used to convert radar reflectivity to rainfall rate for all observed precipitation. This would obviously lead to a disparity between the actual rainfall rate and the radar estimated rainfall rate. It is difficult to assess the magnitude of this disparity, comparing the radar estimate to rain gauges adds the complications of (predominantly) VPR error and sampling error.

Disdrometers can be used to measure the size distribution directly, so that the appropriate Z-R relationship for the storm can be formulated. Such devices also suffer sampling problems, it takes a certain length of time for enough hydrometeors to be observed so that an accurate drop size distribution can be obtained. During this time one would have to assume that the distribution itself did not alter. Even if the exact distribution could be measured instantaneously at a certain point, it is questionable as to how representative it would be of the distribution over entire radar beam volume, which is also likely a significant distance from the ground.

3.1.4 Ground Clutter

Radar echoes returned from ground targets are termed ‘ground clutter’. The radar does not have to be pointed directly at the ground for ground clutter to be observed. This

is because a radar's radiated beam pattern is not shaped as a perfect cone, side-lobes are present at angles greater than the beam width with power on the order of 30–40 dB below the central maximum. Although there is much less power in the side-lobes than in the central beam, hills, trees and houses make good targets compared to precipitation, providing substantial measured returns. Ground clutter is usually of greatest impact at near ranges where the beam is low to the ground. Multiple elevation scan regimes mentioned in Chapter 1 (regarding temporal resolution) allow avoidance of clutter close to the radar by using high elevations while preventing beam overshooting at long range by using low elevations.

One would think that ground clutter could simply be measured in the absence of precipitation to produce a 'clutter map' and that this map could then be subtracted from the measured (precipitation plus clutter) field to determine the radar return from precipitation alone. If ground clutter intensity remained constant then this would be feasible, however, this is not the case. When ground targets become wet their target cross section is altered, meaning that during precipitation the measured dry clutter map no longer represents the clutter intensity correctly so that it is not possible to separate the clutter return from the precipitation return. Additionally, during times of anomalous propagation, the portion of the radar beam making contact with the clutter source may not be the same, leading to an increase or decrease of clutter reflectivity (or even appearance of new clutter or complete disappearance of usual clutter).

Clutter can be minimized by utilizing Doppler radar. As clutter (although not sea clutter) is caused by stationary targets, using a Doppler radar can suppress the clutter signal by filtering out targets with zero (or near-zero) velocity.

Instead of trying to subtract clutter maps from radar images, one can use such a map to mask clutter locations so that they do not falsely contribute to rainfall accumulations. To estimate reflectivity values in these masked out regions, values from higher clutter free elevations can be used. Somewhat more advanced methods involve interpolation from surrounding clutter free locations in 2d or 3d (Wesson and Pegram, 2004).

To overcome the problems that occur when relying on historic average clutter maps in instances of anomalous propagation, methods can be used to detect ground clutter automatically at much shorter time scales (Rico-Ramirez and Cluckie, 2008). Nowcasting methods—whereby rainfall from an earlier time at a clutter free pixel could be trans-

lated in its direction of motion to replace a ground clutter contaminated pixel—could also be used.

3.1.5 Attenuation

The microwave radiation emitted from a weather radar is attenuated as it passes through cloud/fog, rainfall, snow and hail as well as through the air itself. This attenuation is usually only of significance at shorter wavelengths (less than ~ 10 cm) (Keeler and Serafin, 2008) due to the nature of Rayleigh scattering.

Of the sources of attenuation, precipitation is the most significant. For example at microwave wavelengths of 3.2 cm (X-band) attenuation of 0.56 dB km^{-1} occurs through rainfall of 25 mm h^{-1}. The highly variable nature of precipitation also adds a great deal of uncertainty to the estimation of attenuation magnitude. The attenuation through cloud or fog with visibility of 90 m at a 3.2 cm wavelength is only 0.04 dB km^{-1}, an order of magnitude less than that from 25 mm h^{-1} rainfall.

The attenuation from the atmosphere (from oxygen and water vapour, specifically) is accurately known (1.5 dB per 100 km at C-band) and remains fairly constant, varying only somewhat with water vapour content. It is trivial, therefore, to correct for (Joss and Waldvogel, 1990).

The attenuation caused by a wet radome may also be significant. Hudlow et al. (1979) states that this attenuation can be up to 5 dB at 5 cm wavelengths. Germann (1999) reported possible two-way attenuation of ~ 5.4 dB at moderate rainfall intensities at C-band.

Theoretical relationships for the attenuation of microwave radiation through air, cloud/fog and precipitation were discovered by the Rydes during the Second World War (Ryde and Ryde, 1944, Ryde, 1946). Total attenuation in dB can be approximately expressed (from Keeler and Serafin, 2008) as

$$K_r = \int_0^{r_0} K\,[R(r)]^{\alpha}\,dr \tag{3.17}$$

where $R(r)$ is the rainfall rate along the path r, r_0 is the length of the propagation path (in km), K is a constant which depends on frequency and temperature and α is a constant dependent on frequency. The attenuation cross section depends on temperature due to the variability of the dielectric properties of water with temperature.

Attenuation correction methods have been proposed whereby attenuation due to rainfall is calculated using the measured reflectivity along a path from the radar (Hildebrand, 1978, Hitschfeld and Bordan, 1954). Such techniques are noted, however, to be unstable with respect to uncertainty in radar calibration (Hitschfeld and Bordan, 1954, Delrieu et al., 1999, Berne and Uijlenhoet, 2006). Limits on the magnitude of path integrated attenuation have, therefore, been proposed, in the range of 5–10 dB (Delrieu et al., 1999, Joss and Waldvogel, 1990). Correction is also obviously impossible for more drastic attenuation where no echo is received from behind intercepting severe precipitation.

3.1.6 Beam Blockage

Beam blockage occurs when a radar's beam is blocked either fully or partially by an object such as a tree, a building or a hill/mountain. Although attempts are usually made to avoid beam blockage when initially siting a radar, it is often inevitable, especially in mountainous areas. Blocking objects have a much greater impact the closer they are to the radar as the angular view obscured is larger following $\theta \approx rx$ (for small angles) where r is the range to blocking object and x is the blocking objects horizontal extent normal to the radar beam. Figure 3.6 shows an example of beam blocking (predominantly by hills and mountains) experienced by a radar sited in the North Island of New Zealand.

Blocking can only be corrected if it is not absolute (absolute meaning no signal is returned from the blocked region) or if the completely blocked area is relatively small. Andrieu et al. (1997) describe a correction method utilizing a digital terrain model to determine the fraction of the radar beam that is occluded by terrain. A correction factor can then be obtained that is applied to reflectivity measurements at all ranges past the obstruction (or until another obstruction is encountered). The method is susceptible to anomalous propagation and radar pointing error. If the beam path differs from what is expected (either by uncertainty in the dish elevation angle or by unusual propagation of the radar radiation through the atmosphere) then the occluded beam fraction and thus the correction factor will be miscalculated. Correction of completely blocked areas can be made either by interpolation neighbouring blockage free azimuth or elevation angles or by advection of echoes (nowcasting) into the blocked region.

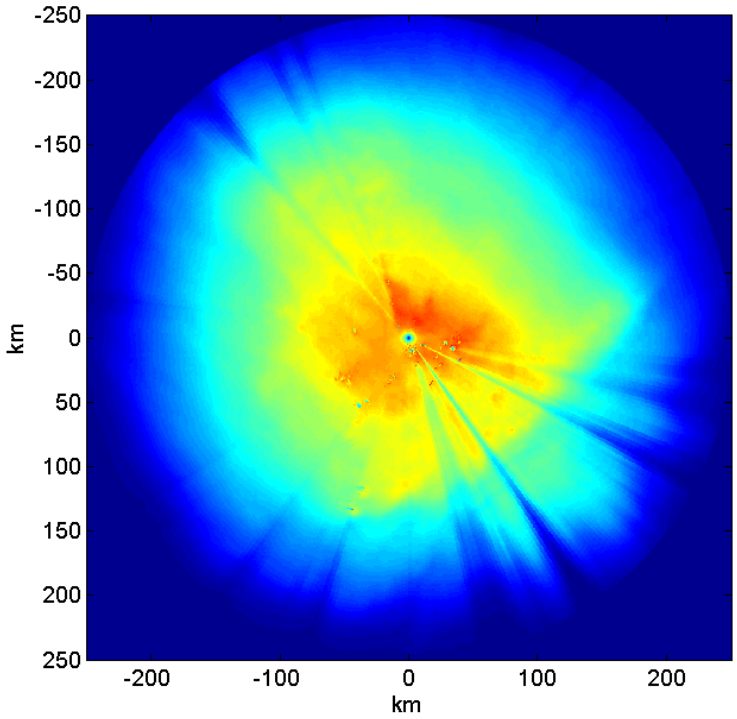

Figure 3.6: Radar accumulation depicting beam blocking for the Bay of Plenty radar in the North Island of New Zealand.

3.1.7 Anomalous Propagation

On a flat Earth without an atmosphere, a radar's beam height (h) would increase linearly with range (r) dependent upon the radar dish's elevation angle (ϕ) using simple trigonometry:

$$h = r \sin \phi \tag{3.18}$$

When considering a spheroidal Earth, the curvature of the Earth must also be taken into account. As range increases, the Earth 'curves away' below the beam, leading to the requirement of an addition term in the equation. Additionally, we must consider the changes of refractive index with altitude. The refractive index in air is given by

$$n = 1 + a\frac{P}{T} + b\frac{e}{T^2} \tag{3.19}$$

where P is pressure, T is temperature and e is water vapour pressure and a and b are constants.

In the atmosphere, n can vary from the order 1.0005 at the surface down to 1 in free space as pressure and temperature as well as vapour pressure usually decrease with increasing altitude. This change in refractive index with altitude leads to a bending downwards of the radar beam with range (following Snell's law). It works out that this effect is approximately the same as if the Earth were considered to be 4/3 the size of the actual Earth with the radar beam following a straight path. This leads to the following equation for beam height with range:

$$h = \sqrt{\left(r^2 + \left(R_e + h_r\right)^2 + 2r\left(R_e + h_r\right)\sin\phi - R_e\right)} \tag{3.20}$$

This approximation assumes a standard atmosphere with temperature decreasing with height at a certain rate. If this rate (termed the lapse rate) is greater than average, under refraction occurs and the beam is located higher than what is predicted in Equation 3.20. If this rate is lower than average or even increases with height (a temperature inversion), the beam will be lower than what is predicted. Variation of the beam propagation from the standard model is termed anomalous propagation or 'anaprop'. More extreme cases of anaprop, typically occurring when strong thin inversions exist at low altitude, lead to atmospheric ducting, where the beam is trapped inside a 'duct' staying at a low altitude for a significant range (Patterson, 2008).

It is not really possible to correct for anomalous propagation, however it can be possible to predict its occurrence so that inferences from the data can be made appropriately.

3.1.8 Other Error Sources

Calibration Error

To convert the received power measured by a radar to radar reflectivity Z (Equation 3.6), a calibration must be made. This is primarily because the parameters relating to the dish radiation pattern (dish gain and 3dB beam width) as well as other parameters, such as waveguide losses, are difficult to determine exactly with theory. A calibration must also be made to find received radar power from the voltage output of a radar's receiver. This calibration can often change over time, the transmitter also does not supply constant power pulses over its lifetime.

Calibration is usually performed using a standard reflecting target, such as a sphere covered in metal foil. The radar cross section for such targets being easily calculated from theory. Other methods include calibration against measured rainfall rates or calibration by the sun. A poorly calibrated radar will possess a systematic error in the measured reflectivity.

Non-precipitation Targets (insects birds, etc.)

Not all echoes observed by a weather radar correspond to weather targets. Ignoring ground (and sea) clutter already mentioned, echoes are commonly observed from insects, birds and aeroplanes. Such echoes can often resemble precipitation leading to false positive detection of rainfall. In the early days of radar meteorology, such 'angel' echoes were a mystery and led to much research into their cause. Return from gradients of refractive index in the atmosphere was considered a possible cause before it was finally realized that swarms of insects or flocks of birds were responsible. It can often be difficult to automatically remove such echoes, although, except in extreme cases, they would not have significant impact on rainfall accumulations.

Receiver Noise

The noise in a radar's receiver combined with external sources of noise such as from thermal radiation from the Earth or from the Sun impacts the signal to noise ratio of a radar (Keeler, 1990). This determines the weakest signal detectable by the radar. This noise does not usually contribute greatly to the total radar error for the majority of precipitation (ie. it is only for very weak precipitation or that at long range—thus at high altitude—that receiver noise becomes significant). Usually the dominant noise source when measuring precipitation is that from the fluctuating radar echo due to the random distribution of scatterers in the beam volume described earlier.

Wind Drift

Radar necessarily observes precipitation at a certain height above the ground. If precipitation always fell directly downwards, this would be less of a problem. However, in the presence of wind, hydrometeors experience what is termed wind drift. This refers to the phenomenon whereby hydrometeors are transported horizontally by the wind while they fall leading to a disagreement between measurements at the ground and those made aloft. The amount of drift depends on wind speed and hydrometeor size and type. Large raindrops (and to a much greater extent, hailstones) fall much faster than small raindrops and snow and so experience less of a drift. For beam altitudes of 4 km, raindrops can experience drifts of 10 km or more and snow can experience drifts of over 40 km (Gunn and Marshall, 1955). Rainfall drift can often be ignored in radar to gauge comparisons even though it can be a substantial source of error in such a comparison. Lack and Fox (2007) found this error to be substantial, especially when comparing high spatial resolution radar data to gauges.

Correction methods must have knowledge of the 3D wind speeds from the radar volume down to the ground at each radar pixel as well as hydrometeor fall speed at each radar pixel. Typically, precipitation motion is determined using Doppler measurements and a relationship between reflectivity/rainfall rate and fall speed gives an average fall speed for all drops in the pixel.

Departure from Rayleigh Scattering

The Z-R relationship is based on Rayleigh scattering, which applies to scattering of radiation by particles with $\pi\frac{D}{\lambda} < 0.22$ where D is the particle's diameter and λ is the incident radiation's wavelength. For particles larger than this, the Mie scattering solution must be applied. For S-band radars with wavelengths of ~10 cm, this is not of much concern as there are very few hydrometeors with diameters greater than 7 mm, however, this becomes of increasing concern when considering C-band radars (particles greater than ~4 mm) and of much greater concern considering X-band radars (particles greater than ~ 2.1 mm).

Bit Error

There is a noise component added to the reflectivity measurement by digital quantization. This occurs in the ADC (which typically have resolutions of 8–16 bits) after the logarithmic amplifier as well as when range corrected reflectivity values are saved to disk (as 8 or 16 bit unsigned integers). To explain, consider an ADC with n bit resolution. The total number of digital levels that an analogue signal can be converted to is given by 2^n. A digital level of a, would therefore be assigned to analogue signals in the following range

$$\left(\frac{a*V}{2^n} - \frac{1}{2}\frac{V}{2^n}, \frac{a*V}{2^n} + \frac{1}{2}\frac{V}{2^n}\right) \tag{3.21}$$

where V is the voltage range of the analogue signal. Thus an error is introduced with approximately uniform distribution (when typical analogue voltages are much greater than $\frac{1}{2^n}$) of mean zero and standard deviation of $\frac{1}{\sqrt{12}}\frac{1}{2^n}$. For a logarithmic receiver with a range of 90 dB, sampling with an 8 bit ADC would introduce a bit error of $\frac{1}{12}\frac{1}{2^8}$ = 0.1 dB, a 12 bit ADC would reduce this to only 0.006 dB. Generally this noise source is eclipsed by the other errors mentioned.

3.2 Discussion

Now that most of the sources of uncertainty (both from systematic errors and random errors) in rainfall observation by radar have been described individually, we shall now discuss how they contribute to radar error as a whole.

Ground clutter and beam blocking can both provide very significant contributions to the uncertainty in radar rainfall estimation. However, these errors are usually predictable. In the absence of anomalous propagation, they will always occur in the same place and will not vary between different rainfall events. Both error sources are potentially preventable (by choosing a sensible site for the radar) and are possibly partially correctable (for less severe cases). If not preventable or correctable they must be considered inevitable (for instance, beam blocking by a mountain range) and must be accepted as a limitation of the measurement device.

Calibration errors, potentially considerable, are quite easily correctable and therefore should not be a major contributor to overall radar rainfall uncertainty.

The error from receiver noise, bit error, non-precipitating targets and the departure from Rayleigh scattering similarly would not be significant contributors to uncertainty in a radar rainfall accumulation as they are eclipsed by the other error sources.

The sources of error that are the most significant contributors to overall rainfall uncertainty—for the case where the radar has a direct clutter free view of the sampling volume—are VPR error, sampling error, attenuation, Z-R error, signal fluctuation from distributed scatterers and wind drift. VPR error is likely the most significant of these for most rainfall systems. While the systematic error is partially correctable in non extreme cases (i.e. beam overshooting is not occurring), it is not possible to completely correct for, leaving a potentially substantial error in addition to the random error component.

Attenuation is serious only for shorter wavelength radars (< 5 cm) when intense rainfall is present or in the case of hail (where all weather radars will suffer to varying extents). Correction can be made to a limited extent, but for serious cases, the radar's range will just be limited in the direction of the attenuating precipitation.

VPR error, sampling error, Z-R error, signal fluctuation and error from wind drift (all contributing a random error component with some also including potentially correctable systematic errors) will all be included in any comparison of radar observed rainfall with gauge measurements. If gauges are to be used to provide corrections for Z-R error and VPR error, errors will be introduced into this process by wind drift and sampling error, potentially very large errors (with divide by zero possibilities). It is, therefore, difficult to ascertain the individual contributions of residual VPR errors (after a radar or climatologically based correction has been applied), sampling error and Z-R error.

The bias between a rain gauge measurement and a radar measurement will be from a combination of all of these errors. It should also not be forgotten that rain gauges themselves exhibit uncertainty in their measurements of rainfall.

To get an idea of the contribution that sampling error provides to the radar/gauge disparity, Chapter 4 will investigate the magnitude of this disparity solely through the use of high resolution radar data. This will avoid the introduction of VPR error and Z-R error. This magnitude can then be compared with the total error magnitude so that the individual contribution by sampling error can be estimated.

Chapter 4

Radar Sampling Error — Consequences for Gauge Correction

4.1 Introduction to Gauge Correction

As discussed in Chapter 1, the rain gauge is the device that comes closest to giving an absolute measure of rainfall at the surface. As such, rain gauge observations are often used to correct or calibrate radar rainfall measurements (Brandes, 1975, Collier et al., 1983, Andrieu, 2002, Borga et al., 2002). This is usually performed by determining the bias between gauge observations and the radar observations above the respective gauge sites. Bias is usually calculated at each gauge site as follows (e.g. Seo and Breidenbach, 2002):

$$b_i = \frac{R_{r_i}}{R_{g_i}} \tag{4.1}$$

where R_{r_i} is the radar estimated rainfall over the i^{th} gauge site and R_{g_i} is the i^{th} gauge accumulated rainfall.

The log of this bias is often used instead of the bias itself (eg. Collier, 1986) due to the biases being approximately log normally distributed (Smith, 1990). The mean bias represents systematic error between radar and gauge (due to radar calibration issues, Z-R uncertainties, etc.) and the standard deviation represents the random error (Collier, 1986).

Mean field bias is also used for this comparison, calculated as

$$b_{mean_i} = \frac{\sum_{i=1}^{N} R_{r_i}}{\sum_{i=1}^{N} R_{g_i}} \tag{4.2}$$

for example, used by Holleman (2007).

The mean field bias is also sometimes calculated as

$$b_{mean_i} = \frac{1}{N} \sum_{i=0}^{N} \frac{\sum_{t=0}^{n} R_{r_i^t}}{\sum_{t=0}^{n} R_{g_i^t}} \tag{4.3}$$

where $R_{r_i^t}$ represents the radar estimated rainfall over the i^{th} gauge site at time t, $R_{g_i^t}$ being similarly defined and n being the total number of accumulation time bins. In this calculation, therefore, bias is first averaged in time at each gauge location and then averaged over all gauges in the domain. The limit n can also be set to unity so that averaging in time is not performed.

The individual bias values calculated using Equation 4.1 are applied to radar pixels neighbouring the gauge location using a method of interpolation. The simplest such method being nearest neighbour interpolation; the radar pixels would be corrected using the bias from the nearest radar/gauge pair following

$$R_{c_i} = \frac{R_{r_i}}{b_{nn_i}} \tag{4.4}$$

where R_{c_i} is the i^{th} corrected radar pixel and b_{nn_i} is the i^{th} nearest neighbour interpolated bias. The equation is the same for the mean field method if b_{mean} is substituted for b_{nn_i}.

More involved interpolation methods include inverse distance weighting, kriging or cokriging (Krajewski, 1987) and Kalman filtering techniques (e.g. Chumchean et al., 2006). Some researchers have found that simple methods perform just as effectively as the more complex. For instance, Collier (1986) states that simple nearest neighbour interpolation is likely as satisfactory as using complex methods, with resulting errors using the nearest gauge being similar to those from multiple regression procedures using many gauges.

Regarding the mean field method, Cole and Moore (2008) compared a mean field method of the form from Equation 4.3 to a spatially varying method whereby gauge bias was mapped to the radar grid by way of multiquadric surface fitting. They found that although the mean field method resulted in a reduction of error compared to uncorrected radar data, it was not as effective as the spatially varying method.

Gauge bias is calculated for a particular accumulation time T. This correction process is usually performed with T being on the order of an hour or more (e.g. Anagnostou and Krajewski, 1999, Borga et al., 2000, Seo and Breidenbach, 2002). Considering the impact that radar sampling error has on this process, even a one hour accumulation may be too short (as suggested in Chapter 2) although following weather radar's goal of quantitative rainfall measurement, one would expect radar data to agree with gauge accumulations at least over very long time scales ($T \approx$ months).

The use of bias correction has been much debated by researchers. Joss and Waldvogel (1990) emphasize that all radar systematic errors should be removed before attempting such a correction. This includes VPR error, beam blockage, ground clutter and attenuation. Smith (1990) states that there is "general agreement that comparisons with gages should be made routinely, as a check on the radar performance, and that appropriate adjustments should be made if a radar bias is clearly indicated" and adds that a spatially varying adjustment remains controversial. Joss and Waldvogel (1990) further state that spatially varying bias correction is "unsatisfactory" as it fails to take into account error from unrepresentative sampling.

It has been found that gauge adjustment does not consistently improve QPE, it can sometimes do just the opposite (Smith, 1990, Collier et al., 1983). Collier (2002) agrees that systematic radar errors should first be removed and states that "The appropriateness of subsequent rain-gauge adjustment of the radar estimates to mitigate residual errors remains uncertain". He does, however, point out that improvement can be made with time integrated bias correction, especially in mountainous terrain, citing Joss and Lee (1995).

In terms of the random error fluctuation in the bias, Collier (1986) found values of around $\sigma(F) = 0.4$ (where $\sigma(F)$ is the standard deviation of $\log_{10} b$) at distances of up to ~80 km for frontal rain with one hour accumulations from an S-band radar (with a 2° beam width) and values of $\sigma(F) = 0.3$–0.6 (increasing with distance) for convective rainfall. Collier et al. (1983) observed an average value of $\sigma(F)$ to be 0.31 for all rain types with a radar calibrated by statistical methods (i.e. very long duration mean gauge calibration) and around 0.24 after bias correction with a scheme which separates the radar/gauge bias values into orographic domains. Le Bouar et al. (2001) found $\sigma^2(F) \cong 0.2$ for 30 minute accumulation times using a new rain profiling algorithm

(ZPHI) and $\sigma^2(F) \cong 0.37$ using a classical rainfall estimate. Holleman (2007) found the full width at half maximum of the distribution of F for three hourly mean bias corrections to be 0.4.

Being a process likely to be sensitive to sampling error (as in indicated in Chapter 2) it would be a good idea to investigate this sensitivity here. The primary question that is asked here is "what effect does fine scale (below conventional radar resolution) variability in the precipitation field have on point measurement correction of radar (areal) measurements?".

The comparison of point measurements of a rainfall field to spatially averaged measurements of that field (the point-area problem) has been looked at using geostatistical methods by several researchers. For example, Wang and Wolff (2010) assessed the relative magnitude of the area-point error with respect to the error between TRMM radar observations and a network of rain gauges using the EVSM method of Ciach and Krajewski (1999). Such methods rely on a range of assumptions about the nature of the rainfall field: no correlation between radar and gauge errors, second order stationarity of the rainfall field and an exponential form of the rainfall field's correlation function (often determined from gauge network data). The method proposed below does not rely upon these assumptions. It also looks at the sampling error for a range of spatial and temporal resolutions. The downside to the method is that there are scales of variability—in both time and space—finer than that which the high resolution radar can detect. This means that one can only determine a lower bound to the estimated sampling error.

Another question could also be posed in this Chapter, "can gauge correction, in light of the impact of sampling errors, be used to determine changes in the Z-R relationship during or between storms or should it only be used over longer time periods?".

To come closer to answering these two questions, the high resolution radar dataset described in Section 2.1 will be subsampled (for a variety of grid patterns and 'gauge' densities) to represent point measurements and then degraded in resolution to represent observations from a typical lower resolution radar (in the same manner as described in Section 2.1). The downgraded data will then be corrected by the 'point' data (using nearest neighbour and mean field correction schemes) and the impact on error calculated.

Some hypotheses can be made at this stage:

1. The variability in radar/gauge bias (as measured by the standard deviation of F) increases for decreasing spatial and temporal resolutions.

2. The variability in radar/gauge bias from sampling error is sufficiently large so as to make gauge correction ineffective at reducing radar error for small accumulation times.

3. The variability in radar/gauge bias caused by sampling error diminishes with longer accumulation times, so that past a certain accumulation length (dependent upon the storm and the observation resolution) bias correction becomes beneficial.

4. The variability in radar/gauge bias will be greater for more variable (less uniform) rainfall events.

4.2 Method

The method is initially very similar to that in Section 2.1 but instead of comparing the simulated low resolution data to the high resolution data on a pixel by pixel basis for all non zero pixels, the high resolution pixels are subsampled to represent a simulated 'gauge' network. Obviously there is a scale disparity between the high resolution dataset, placed on a 200 m by 200 m grid ($40\,000$ m^2), and that of a rain gauge with a standard diameter of 20 cm (0.03 m^2). Indeed, this disparity is three orders of magnitude in linear dimensions and six orders of magnitude in area. What is possible to say is that the sampling error impact would be at minimum as large as that will which be seen in this experiment.

4.2.1 Gauge Network Patterns

The radar data is limited to a domain of 40 km by 40 km (leading to 200 by 200 pixels at 200 m resolution) as the minimum clutter free beam elevation is 6° and the radar's minimum detectable reflectivity at this range is approximately 23 dBZ. Three different gauge patterns are assessed: regular grid, triangular grid and random. The random pattern is not completely random, gauges closer than 40% of the specified gauge spacing

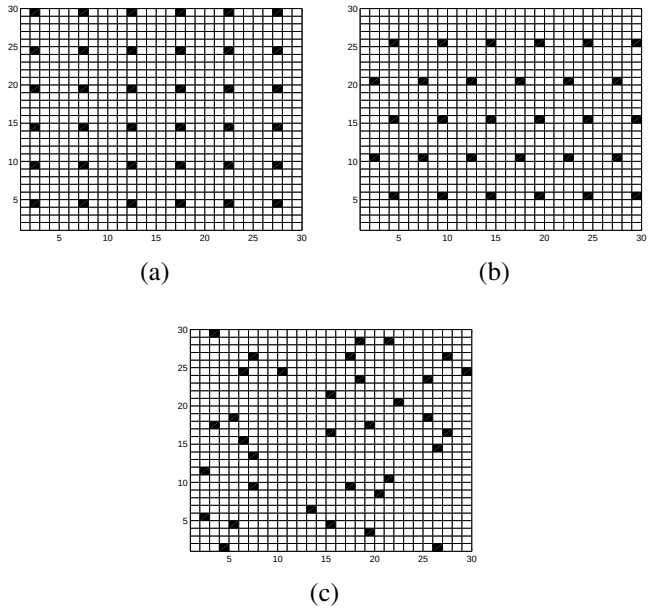

Figure 4.1: Simulated 'gauge' patterns: (a) regular grid, (b) triangular grid, (c) random grid.

are not allowed to occur. This is done to mimic a real gauge network where it would be highly unlikely that two gauges be placed in the immediate vicinity of one another. The chosen gauge spacings vary from 2 km to 20 km. For the random pattern, the number of gauges is the same as that for a regular grid with a given grid spacing.

Each grid pattern and gauge spacing combination is generated five times (by shifting the grid up and down and side to side by a random number of pixels for the regular and triangular grid and by generating a new random selection for the random pattern) so that the average impact of the schemes is measured. Figure 4.1 shows a possible realization of the grid patterns (not to the same scale as is used in the analysis).

4.2.2 Gauge Correction

Once downgraded rainfall accumulations are generated from the high resolution dataset, the original high resolution data are subsampled using the grid patterns to obtain simulated gauge accumulations. Biases are then calculated for pixels where both downgraded resolution radar and simulated gauge observed rainfall accumulations corresponding to

an average rainfall rate of 1 mm/hr or higher. Biases are calculated as follows:

$$b_i = \frac{R_{L_i}}{R_{H_i}} \tag{4.5}$$

in the same manner as Equation 4.1 but here b_i is the bias at simulated gauge i, R_{L_i} is the downgraded resolution accumulation and R_{H_i} is the high resolution accumulation at gauge location i. The bias values are then interpolated onto the radar grid using a nearest neighbour approach so that a 'correction' can be made for each radar pixel using Equation 4.4. After this correction is made, the 'corrected' radar accumulations are compared to the uncorrected downgraded resolution accumulations (i.e. the uncorrected accumulations created from downgraded radar images) in the same manner as in Section 2.1: the comparison metric being the mean RMSE normalized by the mean non-zero rainfall in each radar image. Comparing the corrected accumulations to the downgraded resolution accumulations—rather than to high resolution accumulations—separates the error that is added by applying sampling error contaminated bias corrections from the sampling error itself.

4.3 Results

Figure 4.2 gives the standard deviation of log biases (for all 'gauge'/radar pairs over all accumulations in a particular event) averaged over all events for accumulation periods from 600–7200 s.

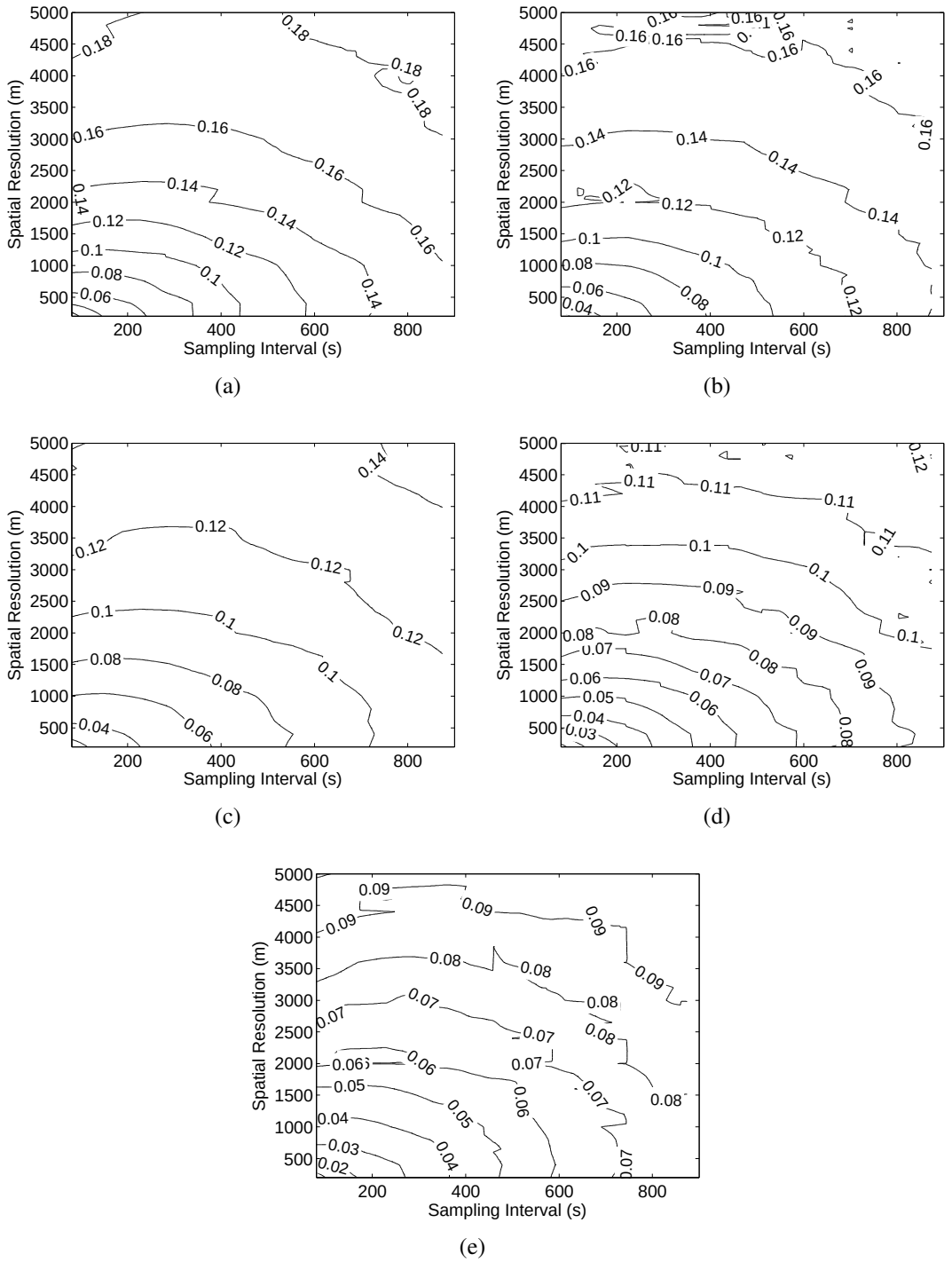

Figure 4.2: Average of $\sigma(F)$ over the 48 significant events for accumulation times of: (a) 10 minutes, (b) 15 minutes, (c) 30 minutes, (d) 1 hour, (e) 2 hours.

As was the case with the mean spatial temporal resolution error diagrams in Chapter 2, the impact of temporal resolution—in this case on $\sigma(F)$, the standard deviation of F—is diminished when sampling at lower spatial resolutions. Additionally, $\sigma(F)$ decreases with increasing accumulation time, for two hour accumulations $\sigma(F)$ is half or less than $\sigma(F)$ for 600 s accumulations.

The mean of F appears to decrease somewhat with increasing accumulation time and increase with decreasing spatial resolutions. The mean of b varies in the same manner, being around 1.04 and 1.06 for 1 km/300 s sampling and 2 km/300 s sampling respectively with one hour accumulations. The mean of b is also observed to decrease with decreasing temporal sampling rate, especially at lower spatial resolutions. This effect is more pronounced at longer accumulation times. It appears that the positive bias introduced by spatial sampling error is balanced by a negative influence on the bias from the temporal sampling error. Bias does just drop below 1 for 200 m sampling when sampling period increases beyond 400 s. This may be related to the limited domain size of the radar observations, meaning rainfall outside of the domain is not included in the advection interpolation.

For one hour accumulations at 2000 m/600 s sampling (similar to the sampling characteristics of the radar used in the analysis of Collier et al. 1983), $\sigma(F)$ is observed to be ~0.09. This represents a significant portion of the average random error, which was estimated to be 0.31 by Collier et al. (1983). A one sigma variation in bias would therefore be approximately $0.81 < b < 1.23$, assuming the mean to be zero.

One should bear in mind that the variability in F here is a lower limit due to the still large difference in scale between the high resolution radar data used to simulate the 'gauges' used in this comparison (~200 m/50–70 s) and that of real gauges (0.2 m/time for 1 tip). The value from Collier et al. (1983) was also calculated without first applying any VPR correction to the radar data before biases were calculated, only a long term gauge based correction was applied. Therefore, this value includes not only variability of VPR with space and time over the course of a single event, but also that variability of VPR between events. Variation in the VPR during an event is included to a certain extent in the orographic domain gauge correction scheme in Collier et al. (1983), where a value of $\sigma(F) = 0.24$ was observed. Some allowance for the variation of the Z-R relationship in space and time would also be made by such a method.

Figure 4.3 shows the relationship between $\sigma(F)$ at two different resolutions (2000 m/600 s and 1000 m/300 s) and the mean decorrelation length of an event for one hour accumulations for 37 of the 48 events. The remaining 11 events did not have a sufficient number of radar/gauge pairs at a one hour accumulation time for $\sigma(F)$ to be accurately determined.

The variability in F generally trends downwards with increasing mean decorrelation length for both sampling regimes. There are, however, events with a low mean decorrelation length that also exhibit a low $\sigma(F)$. From Figure 4.3 it appears that there are two separate modes in which $\sigma(F)$ relates to mean decorrelation length, one in which $\sigma(F)$ decreases linearly in relation to the logarithm of the mean decorrelation length and one in which it remains fairly constant. This indicates the influence of another variable or variables. Alternatively, it may be that there are not sufficient data points for such a relationship to be discerned.

To look at the variability in bias with longer accumulation times, the mean of $\sigma(F)$ was calculated over all accumulation periods (that contained rainfall) varying in duration from six hours to two weeks. This is somewhat different to how the mean was taken for the results above (and displayed in Figure 4.2), in which $\sigma(F)$ is calculated for all bias values in a single event and then averaged over all events (so that an event lasting twice as long as another event contributes the same weighting as the shorter event in the final average).

The results of the long duration $\sigma(F)$ calculation are shown in Figure 4.4. It is apparent that the variation in bias does not seem to reduce with increasing accumulation times from six hours to two weeks. It even appears to increase slightly. This is somewhat due to the fact that two weeks of rainfall accumulation does not have 14 times the duration of rainfall as a single day's accumulation; much of the time it is not raining.

The average maximum (and minimum) bias (b) was found to be equal to 1.54 (0.68) for 2000 m/600 s sampling and 1.32 (0.79) for 1000 m/300 s sampling with one hour accumulations.

4.3.1 Case Studies

We look again at cases C1 and C2 from Section 2.1 to observe how $\sigma(F)$ varies with different events. To refresh our memories, C1 is a predominantly stratiform event with

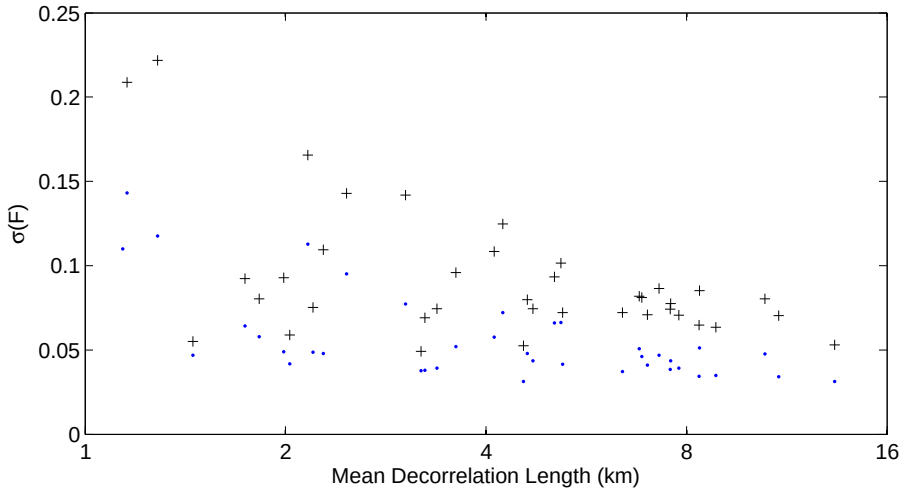

Figure 4.3: $\sigma(F)$ for 1 hour accumulations over each event (for 37 of the 48 significant events which had a sufficient number of radar/'gauge' comparisons) against that event's mean decorrelation length, for 2000 m/600 s sampling (+) and 1000 m/300 s sampling (.).

characteristic length scale ~9 km and C2 is a predominantly convective event with characteristic length scale ~2.5 km.

Figures 4.5 and 4.6 show the variation of $\sigma(F)$ with spatial and temporal resolution for 1 hour accumulations over event C1 and C2 respectively. As we would expect from results in Section 2.1, $\sigma(F)$ is much greater for C2 than for C1, being 2–3 times the magnitude depending on spatial/temporal resolution.

The shape of the contours in these diagrams also looks very similar to those in the NRMSE diagrams (Figures 2.5 and 2.7). This is evident with the reduction in sensitivity to spatial resolution at long sampling times (as well as temporal resolution at low spatial resolution) in C1 and to temporal resolution at low spatial resolutions in C2. Regarding C2, this indicates how the variability in radar/gauge bias from spatial averaging dominates over that from any evolution in the rainfall pattern that occurs in periods of up to ~15 minutes. In C1, there is a slight dominance of temporal resolution on the resulting variation in bias, which indicates that the impact of low spatial resolution sampling is fairly low (as we would expect for stratiform rainfall) but evolution in the precipitating system is of greater significance.

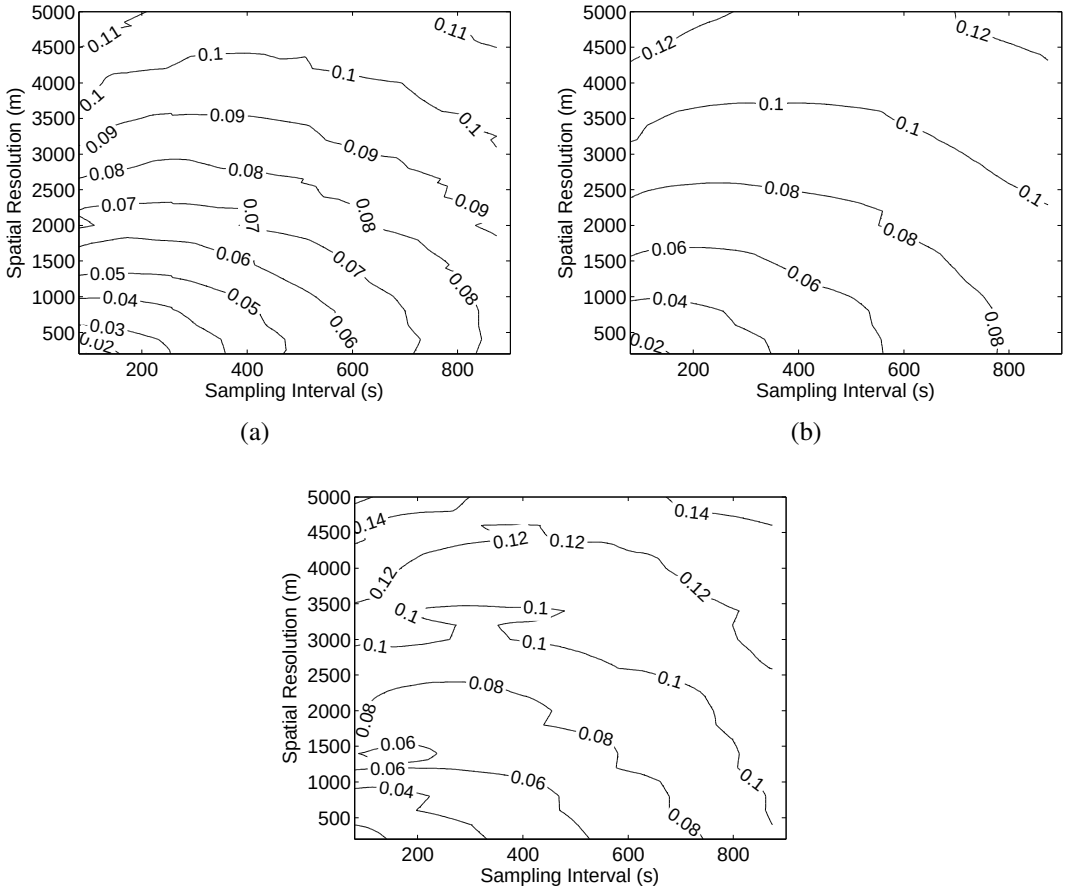

Figure 4.4: Average $\sigma(F)$ over all periods of duration: (a) 6 hours, (b) 2 days, (c) 2 weeks, where rainfall was present. Note that this average is not first taken over each event as in Figure 4.2.

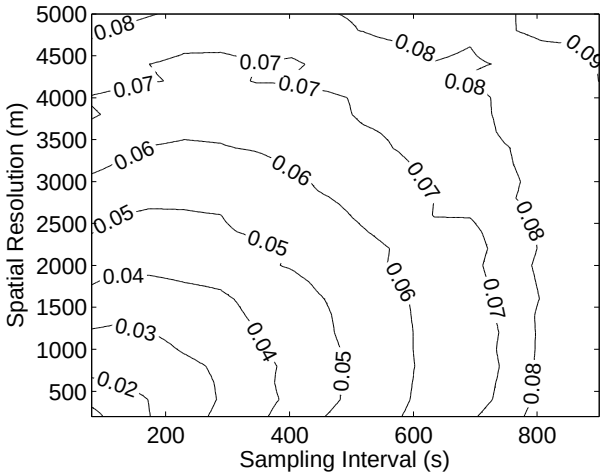

Figure 4.5: $\sigma(F)$ for 1 hour accumulations over event C1.

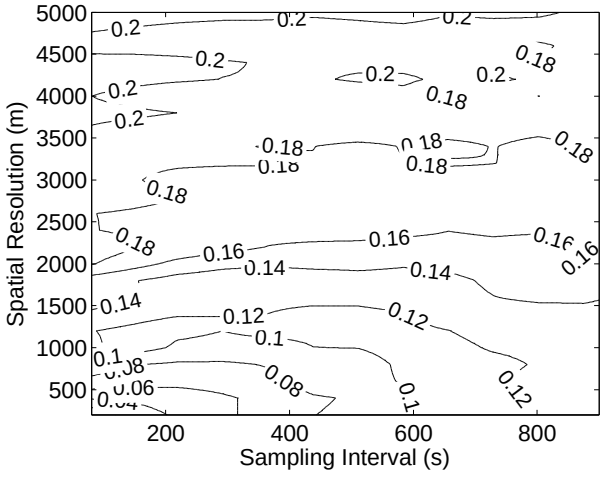

Figure 4.6: $\sigma(F)$ for 1 hour accumulations over event C2.

4.3.2 Mean Field Correction

We earlier discovered that the mean bias increases with decreasing spatial resolution of observation. Additionally, the variation of F was characterized on an individual gauge basis. We wish to assess here how estimates of the mean field bias (as calculated by Equation 4.2) vary in practice with a differing density of gauges. This would determine the error one would expect from applying a mean field bias correction (this error will be denoted σ_{MFB}). Figure 4.7 shows σ_{MFB} for four different 'gauge' spacings.

We might expect σ_{MFB} to decrease following the usual formula for standard error:

$$\sigma_{\mathrm{MFB}} = \frac{\sigma(b)}{\sqrt{n}} \tag{4.6}$$

as the mean field bias from Equation 4.2 is very closely related to the mean bias. However, this formula assumes independent observations. If this were the case we would expect σ_{MFB} to be reduced by a factor of 10 when decreasing the gauge spacing from 20 km to 2 km (a factor 100 increase in the number of gauges). In fact, we see only a halving of σ_{MFB}, indicating that the assumption of independence is not met. This is expected as rainfall fields exhibit spatial correlation (Vieux (2004) gives a discussion of this).

Temporal resolution has slightly less of an impact on σ_{MFB} than spatial resolution. This is more pronounced at coarser spatial resolutions. This seems to be fairly invariant with gauge spacing.

The relationship of σ_{MFB} with accumulation time is shown in Figure 4.8 for sampling of 2000 m/600 s and 1000 m/300 s at three different gauge spacings. We see that σ_{MFB} reduces linearly with the logarithm of accumulation time from 10 minutes to 2 hours. The variation of error with gauge spacing diminishes with increasing accumulation time. This implies that an increase in the density of gauges for long accumulation time calibration is not of great benefit, at least regarding the reduction of sampling errors. For sampling other variability in the radar/gauge bias field (due to Z-R variability or orographic effects), having a higher density of gauges would presumably be of benefit.

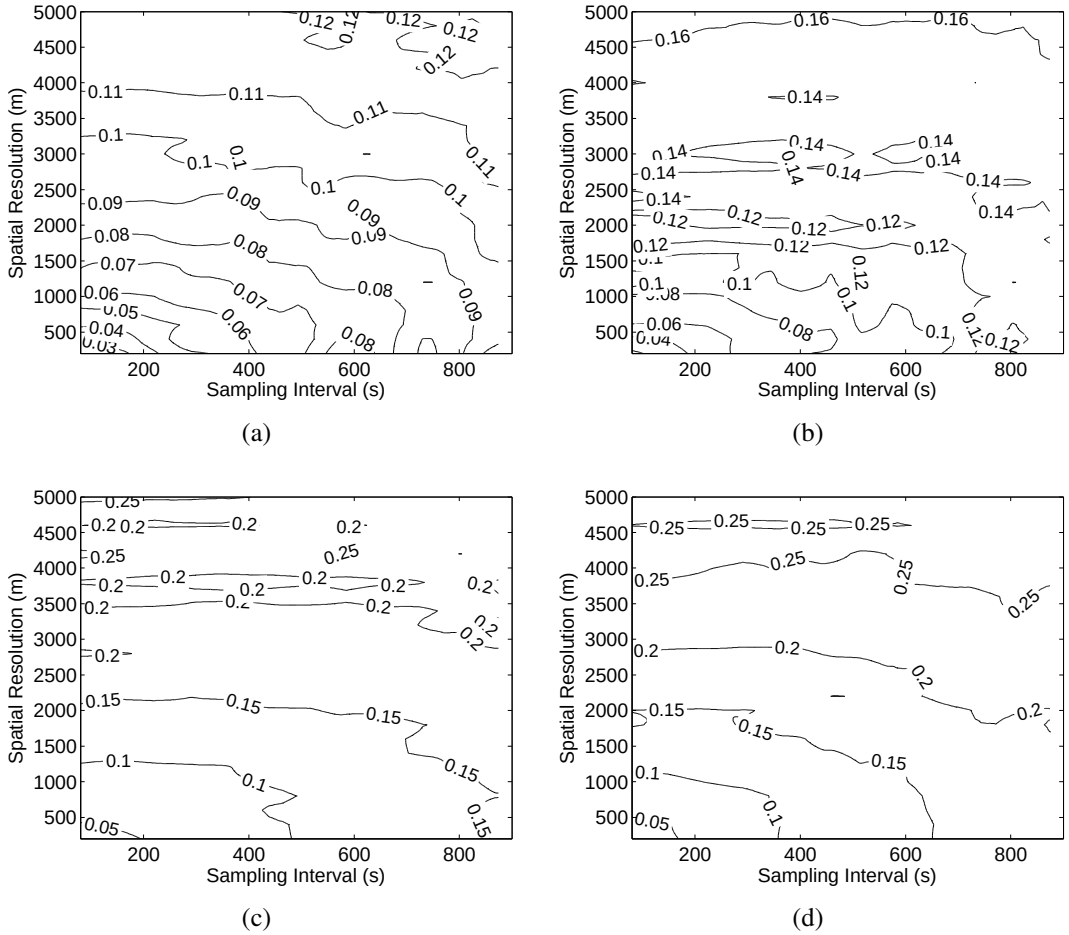

Figure 4.7: σ_{MFB} for an accumulation period of one hour with simulated gauge spacings of: (a) 2 km, (b) 5 km, (c) 10 km, (d) 20 km.

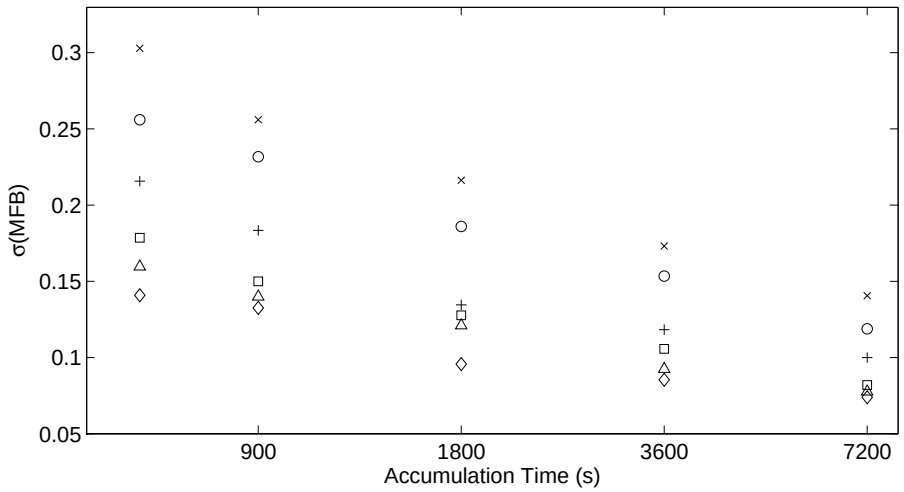

Figure 4.8: Relationship of σ_{MFB} with accumulation time. + (◊) is 5 km spacing ○ (△) is 10 km spacing and × (□) is 20 km spacing with 2000 m/600 s (1000 m/300 s) sampling.

4.3.3 Nearest Neighbour Bias Correction

Figure 4.9 show the average NRMSE from between 'gauge corrected' and uncorrected degraded resolution accumulations over all of the events for 2 km gauge spacing with a regular grid. Errors were only calculated if the nearest gauge recorded a rainfall rate over 1 mm hr^{-1}. NRMSE appears to be of a similar magnitude to the sampling error NRMSE from Figure 2.13.

NRMSE from 'gauge correcting' with low resolution observations is slightly less sensitive to temporal resolution than sampling error alone, however. These results indicate that gauge correction should not be used for accumulation periods of under one hour unless high spatial resolution observations are used to generate these bias correction factors or large deviations in the Z-R relationship or the VPR from the long term average are occurring. NRMSE even for 1000 m/300 s sampling is ~0.20 with 10 minute accumulations. This is a strong argument against the usage of gauge correction to adjust for Z-R variability within a precipitating system. Any attempt to achieve this should be made through precipitation type identification using radar (eg. identifying convective activity and applying a convective Z-R for that area) or potentially through the usage of disdrometers. As spatial resolution is higher close to the radar, gauge correction is

somewhat more appropriate in this region.

Figures 4.11 show the NRMSE for events C1 and C2 with 1 hour accumulations with gauge spacing of 2 km. For C1, there is a more equal sensitivity to spatial and temporal resolution than for the average case. Additionally, the NRMSE is lower than for the average. C2, on the other hand has a much greater error, over double the average case. Even for the one hour accumulation period looked at here, at spatial resolutions over 1 km, error is at 0.3 and at resolutions over 2 km the error is 0.50, 50% of the magnitude of the average rainfall rate in that event. This quantifies the assumptions many would hold on the unreliability of gauge correction in convective conditions. Corrections could, however, be justified for stratiform events for accumulation periods greater than an hour, especially at short ranges where spatial resolutions are higher.

There appears to be a decrease in the mean NRMS error from applying a nearest neighbour bias correction when fewer gauges are used for the correction (i.e. a longer grid spacing is used). However, this is likely related to the rainfall threshold over which biases are applied. If no bias was applied, the 'corrected' field in that location is identical to the 'uncorrected' field. The variation of NRMSE between accumulation periods also appears to stay the same when varying gauge density. There is also no appreciable difference between the NRMSE from the differing gauge sampling patterns. A difference may, however, be observed if a longer dataset were to be used along with a greater number of gauge network realization for each pattern.

4.4 Discussion

Two questions were asked in this chapter:

- What effect does fine scale (below conventional radar resolution) variability in the precipitation field have on point measurement correction of radar (areal) measurements?

- Can gauge correction, in light of the impact of sampling errors, be used to determine changes in the Z-R relationship during or between storms or should it only be used over longer time periods?

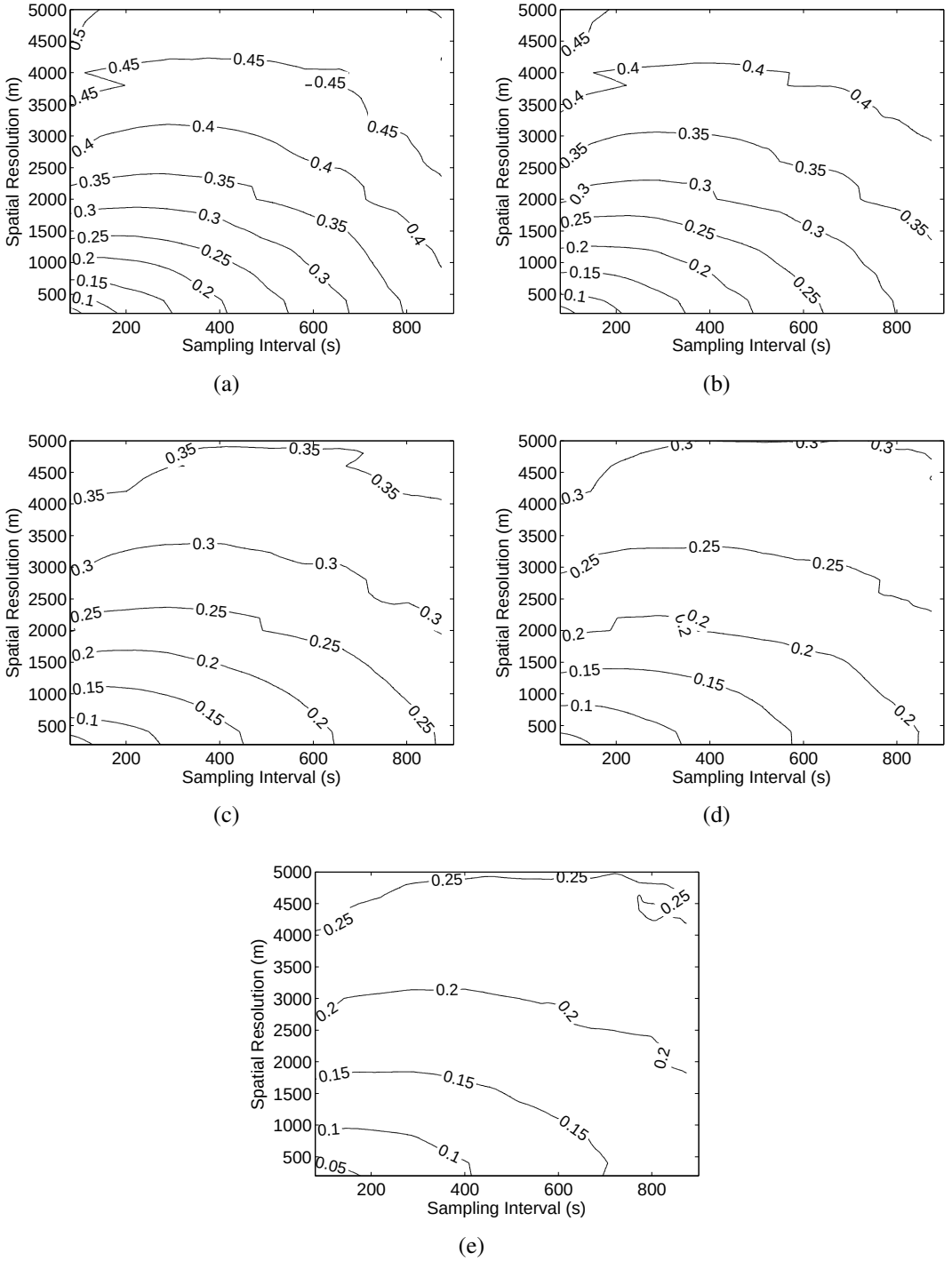

Figure 4.9: Mean NRMSE between 'gauge corrected' downgraded resolution accumulations and non-corrected downgraded resolution accumulations for 2 km grid spacing over all accumulations of period: (a) 10 minutes, (b) 15 minutes, (c) 30 minutes, (d) 1 hour, (e) 2 hours.

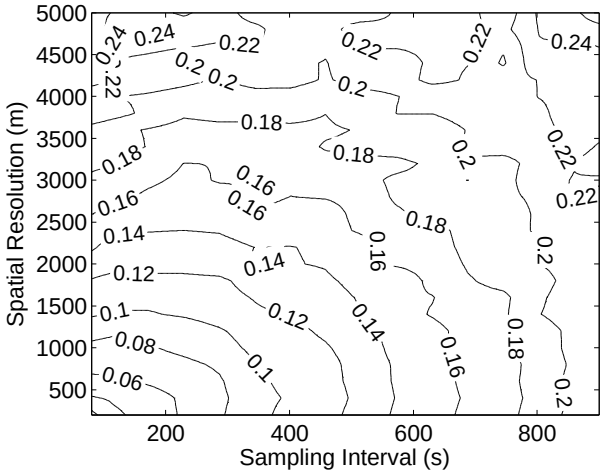

Figure 4.10: Mean NRMSE for near neighbour 'gauge correction' scheme with 1 hour accumulations for event C1.

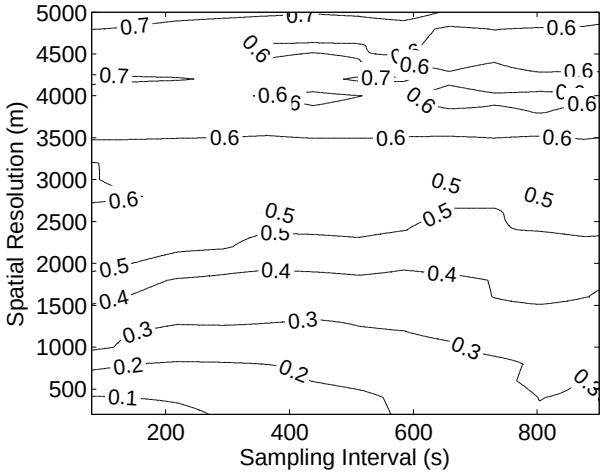

Figure 4.11: Mean NRMSE for nearest neighbour 'gauge correction' scheme with 1 hour accumulations for event C2.

These two questions were investigated by subsampling high resolution radar data to simulate a rain gauge network and determining the radar/'gauge' bias between this 'gauge' network and downgraded resolution radar data.

It was found that the variability in the radar/gauge bias, as measured by $\sigma(F)$, increases for decreasing spatial and temporal radar resolutions. For one hour accumulations at 2 km/600 s sampling $\sigma(F)$ is observed to be ~0.09, giving a one sigma range for the bias (b) of 0.81 to 1.23. This represents around a third of the total variability in radar/gauge bias observed by Collier et al. (1983) ($\sigma(F) = 0.24$). These results support hypothesis 1.

The variability in F, and consequently b, was observed to decrease with increasing accumulation times, as was expected. Additionally, $\sigma(F)$ was found to decrease for rainfall events with longer mean decorrelation lengths. However, there seemed to be two modes for this relationship, one as just described and one in which $\sigma(F)$ remains constant with mean decorrelation length. This provides evidence against the universality of hypothesis 4 (i.e. it is very unlikely to be true for all cases).

A systematic change to the observed bias was also found. The mean bias was found to increase with decreasing spatial resolution, reaching around 1.06 for 2 km/300 s sampling for one hour accumulation periods. This increase is diminished for longer accumulation times. Additionally, for longer temporal resolutions, a reduction in mean bias was observed, partially offsetting the increase from low spatial resolution sampling.

The results discussed above provide the first clue in answering the first question listed above. We know that sampling error adds a quite substantial variability to the observed radar/gauge bias as well as a systematic bias to the bias values. Further information to answer this question is provided by the results from the simple nearest neighbour correction, which solely 'corrected' for the biases introduced by sampling error.

These results indicated that bias correction with conventional radar resolutions produces NRMSE (measured by comparison of bias corrected degraded resolution accumulations to uncorrected degraded resolution accumulations) of a very similar magnitude to that observed for sampling error alone (comparing degraded resolution accumulations to high resolution accumulations). This error decreases with increasing accumulation length, but is still substantial for 1 hour accumulations.

The results also allow us to give some answers to the second question listed above. For short accumulation periods, e.g. 10 minutes, it is likely that any variation that occurs in the Z-R relationship (variation in space and time in an event)—which is not relatively easy to correct with radar alone (e.g. stratiform/convective/snow discrimination)—would not be large enough to exceed the error that any gauge based correction would introduce due to sampling issues. As such, unless high resolution radar data is used, it would not be appropriate to correct for Z-R changes in a storm using a rain gauge based correction procedure. A possible exception to this statement is for very uniform rainfall, where sampling errors are minimal.

This statement does not rule out the use of such techniques for long term calibration of a radar. We saw in this chapter that the error generally decreases with accumulation time. It would be prudent, however, to exclude small scale rainfall from such a procedure as well as using only radar rainfall data from near ranges. This would be to avoid the introduced bias that low resolution spatial sampling has on the radar to gauge comparison.

The results obtained in this chapter could also be used to develop a procedure whereby gauge correction could be applied over a shorter time scale in a more appropriate manner. One would first diagnose the expected radar/gauge variation by looking at the above charts and selecting the values for $\sigma(F)$ depending upon the sampling resolution and accumulation time. If observed radar/gauge biases were consistently outside of two sigma confidence intervals, gauge correction would be applied. Rainfall systems with very short decorrelation lengths would be excluded from a correction.

Chapter 5

Radar and Hydrology

5.1 What Does Radar Offer to Hydrology?

Rainfall runoff is the primary source of flooding for many catchments. Rainfall observations, therefore, are of principal importance when modelling such catchments. The traditional source of rainfall data for hydrological use is the rain gauge. Usually a sparse network of gauges which are either averaged in some manner over the catchment (for a lumped model) or interpolated using a method such as nearest neighbour, inverse distance weighting or kriging etc. (for a distributed model) so as to be ingested into a rainfall runoff model.

Because rainfall is highly variable in space and time, the density of gauges in a network is of great significance to that network's ability to adequately measure rainfall over a catchment. Some guidelines to gauge density have been recommended, for example, the U.S Army Corps of Engineers recommends that the number of gauges in a catchment should be at least

$$N_g = A^{0.33} \tag{5.1}$$

where A is catchment area in square miles (Vieux, 2004). Using this formula, an area of 10 km^2 would require at least two gauges, giving a density of 5 km^2/gauge. For an area of 100 km^2, three gauges are recommended giving a gauge density of 33.3 km^2/gauge.

Even these recommendations, which are likely fairly lenient (especially with respect to convective rainfall), are often not met in operational gauge networks. For example, the Waipapa catchment that will be described later in this chapter has an area of

~140 km^2. According to Equation 5.1, at least four gauges should be located within this catchment. In actuality, only a single gauge is located here. Additionally, this single gauge is co-located with the river gauge at the catchment outlet. The reasons for this being cost and accessibility as much of the catchment is forested.

A radar addresses the problems associated with measuring a spatially distributed quantity with sparse point observations by observing precipitation over a large domain at spatial resolutions normally infeasible for a gauge network (Austin and Austin, 1974) all in real-time and from a single instrument location. Joss and Waldvogel (1990) lists these reasons as the most important advantages of radar for precipitation measurement.

Aside from getting a better estimate of the average rainfall over a catchment (due to its inherently volumetric sampling procedure being more suited to make areal observations and greater sampling density), radar also provides measurements of rainfall variability in space and time which is particularly relevant for urban and mountainous catchments (Delrieu et al., 2009). Radar is also best suited for general study on the structure of precipitation systems, a topic long studied in the field (Joss and Waldvogel, 1990).

Nowcasting is also a benefit of radar, this is again particularly relevant for urban and mountainous catchments with short catchment response times (Andrieu et al., 1997). Smith (1990) suggests that for flood forecasting only a semi-quantitative knowledge that a lot of rain will fall in a short period of time in a catchment is required. This is beneficial as a nowcast's skill primarily degrades with lead time due to changes in rainfall intensity and spatial distribution rather than changes in storm velocity (Bellon and Austin, 1984), so that valuable lead time can be added to flash flood forecasting chains.

Although radar solves many problems it also adds many problems as we have looked at in earlier Chapters. Regarding hydrology, Duncan et al. (1993) comes to the conclusion that whether or not radar or rain gauge networks are the most accurate for rainfall estimation, low density rain gauges simply cannot be used accurately to estimate hydrograph parameters. They further suggest that a radar in combination with a moderately dense gauge network is the best solution. Hildebrand et al. (1979) shows that radars add little to high density (> 1 per 100 km^2) gauge networks for hydrology but do add benefits for low gauge densities in some climates.

5.2 A Brief History

Although many rainfall runoff models were formulated in the early 20th Century—many based on the unit hydrograph method introduced by Sherman (1932), for example: Bernard (1935), Hoyt (1936), Clark (1945), Dooge (1959) or on time-area methods, for example, Ross (1921), Richards (1944)—it wasn't until the widespread access to digital computers in the 1970s that predictive hydrological models became feasible (Birks et al., 1991). Shultz (1968) describes an early computer based hydrological model. These models initially ran with rain gauge inputs.

Recognition of the sampling issues associated with sparse gauge networks combined with the development of radar networks (that also possessed digital storage and transmission capabilities) in the 70s and 80s led to interest in the usage of radar rainfall as the input to these models (Tilford et al., 2002). An early trial of radar input in hydrological forecasting is found in Anderl et al. (1976). Operational use of radar in hydrological models became more widespread in the 80s and 90s (eg. Haggett and Richards, 1991, Oliveira and Ford, 1991, Georgakakos et al., 1993).

Also in the 90s, there was an increase in the usage of radar as a rainfall input to model urban drainage systems which are more sensitive to the spatial distribution of rainfall than rural river models (Sempere-Torres et al., 1999, Yuan et al., 1999).

5.3 Long-standing Issues

Even though radar has been used to quantitatively observe rainfall since the late 40s/early 50s and has been used as input to hydrological computer models since the 70s, its use is still not widespread amongst hydrologists (Collier, 2002, Emmanuel et al., 2012).

Joss and Waldvogel (1990) lamented that the comment made by Wilson and Brandes (1979) that "both confusion and misunderstanding exist in the inherent ability of radar to measure rainfall, about factors that contribute to errors, and about the importance of careful calibration and signal processing" was still true 11 years later.

Twelve years after that statement, Tilford et al. (2002) states that "before the engineering community will accept the use of radar rainfall information, the reliability and accuracy of these measurements need to be unequivocally demonstrated" and that the application of weather radar to urban hydrology "is still in its infancy".

In the same year, Collier (2002) stated "It is now over 40 years since digital weather-radar data became available in significant quantities, and yet, while there has been considerable improvement in the quality of these data, flood forecasters remain reluctant to use them directly as input to river-catchment models".

Closer to the present day, Collier (2009) stated "the unpredictable nature of radar errors continues to discourage many operational hydrologists from using radar data quantitatively as input to models. The tendency has been to wait for all errors to be removed".

Joss and Waldvogel (1990) puts the reason behind these comments as being the vast variation in both meteorological phenomena and the application of the precipitation data. They further add that the VPR is often not corrected for which leads to underestimation in most cases, being most serious in mountainous catchments. Agreeing with Zawadzki (1984) they do not believe Z-R uncertainty to be the dominant source of error.

Emmanuel et al. (2012), evaluating the new French radar product which includes a comprehensive VPR correction scheme still finds a range dependent bias and concludes that radar are "not yet reliable enough for direct use as autonomous rainfall measurement devices in quantitative applications within the field of urban hydrology". Although the fact that their findings are that "radar results differ significantly from gauges" is not exactly unexpected even if radar were to provide perfect rainfall measurement.

Berne and Krajewski (2013) add (in addition to much of what has been said above) that part of the reason for the low adoption rate of radar data for use in hydrology is that the majority of hydrologists are just much more used to working with rain gauge data. This, combined with the added complexity of handling and archiving the much greater amount of data associated with radar observations makes the use of radar rainfall data a fairly daunting task. At the end of their review on the use of radar in hydrology, they provide an answer to the question posed by their article's title by stating that radar for hydrology is both an unfulfilled promise as well as possessing unrecognized potential.

Collier (2002) suggests that as no rainfall observation technique will ever reach perfection, the data assimilation schemes of the models should be designed to deal with error prone measurement rather than for hydrologists to wait for a rainfall observation utopia that will never come.

The first step in this process is to create a comprehensive model of radar error in-

cluding VPR variability and sampling error. Much research has focused on aspects of radar errors although few have created such combined models. Hydrological models would then be run as ensembles (as they already often are varying other model inputs) by applying a stochastic rainfall error term.

It is hoped that the findings of this thesis will aid in the construction and validation of such models in relation to sampling error.

5.4 Hydrological models

Hydrological models come in several flavours. There are models which are distributed, where catchments are divided into a grid with model processes (eg. rainfall input, infiltration, overland flow, etc.) being calculated at each grid square, models which are lumped, where processes are calculated for the catchment as a whole and models which are a mix between the two; semi-distributed where some of the processes are distributed and others are lumped or the spatial distribution of some parameters are included in the model.

Lumped models can be broken down to conceptual, physically based and black box models. Lumped conceptual models first take the mean rainfall input and calculate the rainfall excess by some form of infiltration calculation (such as constant rate with initial loss or exponentially decreasing rate). A transform is then applied to the rainfall excess (which applies some delay and smoothing in time), usually using a unit hydrograph method, to estimate the catchment discharge. Parameters for the rainfall excess calculation and transform are chosen based on a calibration, whereby many rainfall events (preferably several years worth) are fed into the hydrological model and the model is run over a range of model parameter values. A minimization process is then performed between the model output and the measured catchment outflow to select the appropriate model parameters. This calibration process can fall over for extreme events that may not have been in the calibration data set. The process also assumes uniformity in precipitation over the (sub)catchments so that timing of the flood peak as well as peak flow and total volume (due to variation in the distribution of soil saturation) can be highly variable even after calibration.

Physically based lumped models are similar to conceptual models except they use

more physically based equations for infiltration (such as the Green and Ampt method or the Smith Parlange method) and would incorporate evapotranspiration processes for multiple event simulation. These models also require calibration due to the simplification of the physical processes that occur in the catchment. This calibration sometimes requires these physical parameters to be forced into unphysical values for a fit to occur. It is questionable, therefore, how physical such models actually are.

Black box models are purely statistical models which are trained with previously observed rainfall data and catchment discharge. The term black box stems from the lack of any physical or conceptual preconceived relationship between the input data (rainfall and possibly other parameters for evapotranspiration, etc.) and the measured catchment discharge. Black box models usually consist of autoregressive models or artificial neural network models which are trained on a preferably long data set from a gauged catchment in order to make future predictions. Such models have been used with some success (Shamseldin, 1997, Sajikumar and Thandaveswara, 1999).

Distributed physically based models try to model all catchment processes using the physical laws which govern them. For instance, 2D precipitation is utilized, the transport of water over and often through the soil is explicitly modelled and channel flow is explicitly modelled. While this is more scientific than the conceptual and black box lumped described above, calibration is still a necessity. This is due to the lack of knowledge of all of the required parameters at the resolution of the grid over the entire domain. While some of these parameters are easier to come by than others, for example land use (which can be determined from aerial/satellite observation) and—to a certain degree of accuracy and resolution—topography, others, such as soil parameters, can only be determined at point locations (usually spaced very far apart).

Additionally, because of the great number of parameters, it is difficult to determine which possible calibration is the sensible one. Delrieu et al. (2009) question the usefulness of distributed models due to this overparameterization problem as well as for problems with model validation. Because of these reasons, along with the complexity of such models, the difficulty of setting up the models for a catchment, the computational cost of running the models and the fact that they do not perform significantly better than much simpler models, distributed models are not yet widespread in an operational context (O'Conner, 2006).

Semi-distributed models allow the use of distributed 2D rainfall input and often include information from the catchment topography, but have much simpler water transport processes. An example of such a model is the Topmodel (Beven et al., 1995).

5.5 Model Description

The model that was chosen to explore the impact of sampling error on rainfall runoff modelling in this and the next chapter is Gridded Surface Subsurface Hydrologic Analysis (GSSHA [Downer and Ogden, 2004]). GSSHA is a physics based, distributed model based on the CASC2D model. GSSHA models 2D overland flow, 1D infiltration, 1D stream flow, 2D ground water as well as sediment transport. A distributed model was chosen so as to fully analyze the impact of the spatial and temporal variability of precipitation and how this is altered by sampling.

For the research presented here, GSSHA is run in episodic mode using initial soil moisture maps that were output from a long term simulation of the 2009 Mangakino dataset described in Section 2.1.1 at different stages in the simulation (so as to obtain different antecedent moisture conditions). A continuous model run was not used as it was thought to be unnecessarily processor intensive considering we are only interested in looking at rainfall runoff processes. It is these processes that are likely to be more substantially affected by the resolution of rainfall observation. Ground water was also not simulated for this reason.

The processes simulated include 1D channel flow and 2D overland flow, which use a two-step explicit finite volume scheme (for details see the GSSHA manual [Downer et al., 2008]), as well as infiltration, which is modelled using the Green and Ampt equation:

$$f(t) = K_{ga}\left[\frac{\psi_f(\theta_s - \theta_i)}{F} + 1\right] \tag{5.2}$$

where $f(t)$ is the infiltration rate (cm hr^{-1}) at time t, ψ_f is the wetting front suction head (in cm), K_{ga} is the Green and Ampt hydraulic conductivity (cm hr^{-1}), which is half the saturated hydraulic conductivity, θ_s and θ_i are the saturated and initial moisture content and F is the total amount of infiltration (in cm) (Green and Ampt, 1911).

For the long term simulation that was run over the entire Mangakino radar dataset to

obtain distributed initial moisture maps, evapotranspiration was also modelled using the Penman-Monteith equation (Penman, 1953, Monteith, 1965) and the Green and Ampt with Redistribution (GAR) method (Ogden and Saghafian, 1997) was used to simulate the infiltration process (as simple Green and Ampt infiltration is not appropriate for continuous simulations).

5.6 Catchment Description

The catchment that will be used for the following rainfall runoff studies is the Waipapa River catchment, a 122 km^2 rural catchment in the central region of the North Island of New Zealand. The catchment, along with stream network is depicted in Figure 5.1. The Waipapa River is a tributary for the Waikato River, the longest river in New Zealand on which nine hydroelectric power stations operate.

The land use in the catchment consists of pasture for dairy farming, native forest and plantation pine forest in varying states of growth. As we are interested in the impact of rainfall variability rather than the impact of variability of land use and soil parameters, uniform values will be used for these parameters. Interception by vegetation is not considered.

Obviously there could be some relationship between precipitation observation resolution and land use/soil variability. To assess this, areas of the catchment (either 20% or 50% of the total catchment area) will be made impervious in the model (a crude simulation of urbanization). Overland flow Manning numbers are also reduced in these areas. The impervious areas are generated using a gaussian smoothed random field thresholded to provide the required percentage coverage of the catchment. Two different averaging lengths were used to provide a highly variable coverage and a more uniform but patchy coverage. Surface conditions are listed in Table 5.1.

The topographic information required to describe the catchment was obtained from the SRTM (Shuttle Radar Topography Mission) dataset, a 3 arc second resolution over New Zealand in WGS84 datum. Vertical error is less than 16 m. This elevation data was projected onto a 75×75 m NZTM (New Zealand Transverse Mercator) grid using GRASS (Geographic Resources Analysis Support System) GIS. The catchment and stream network were delineated from the elevation data using r.watershed in GRASS.

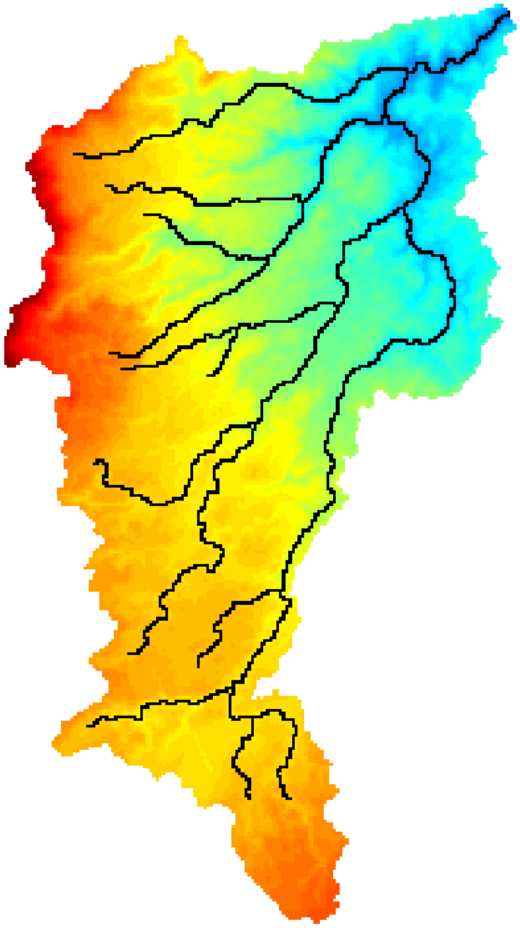

Figure 5.1: Waipapa catchment including stream network. Colour indicates elevation (with red being higher elevation, blue being lower elevation).

Table 5.1: Surface conditions used for the hydrological modelling in Chapter 5 and 6

Surface Condition	Initial Moisture (% of Saturated Condition)	Impervious Area (% of Catchment Area)	Impervious Area Character
1	59	0	n/a
2	81	0	n/a
3	81	20	concentrated
4	81	20	scattered
5	81	50	concentrated
6	81	50	scattered

For use in GSSHA, 'digital dams' (artificial blockages to flow caused by inaccuracies in the elevation data) were removed using the program CleanDam followed by a manual procedure.

Soil parameters used for the Green-Ampt infiltration scheme were selected from the values for the 'sandy clay loam' soil type given in the GSSHA manual. Saturated hydraulic conductivity was selected using a manual 'calibration' procedure. This procedure involved ensuring that modelled peak flows were a similar order of magnitude to flows that are actually experience in the catchment by comparing to stream flow observations. The same process was used to determine the Manning's N values used for overland flow and for the stream network.

5.7 Case Studies

Five of the most hydrologically significant events from the 2009 Mangakino dataset will be examined in the following hydrological analyses. They will be described in this section. Figure 5.2 shows the catchment averaged rainfall accumulations along with model output hydrographs produced with high resolution 5 minute distributed rainfall input.

Event 1 covers the 23 hour period from 23:15 on the 7th to 22:15 on the 8th of July 2009. The event begins with around 3 hours of moderate intensity stratiform rainfall with some embedded higher intensity structure. This period accounts for around 6 mm

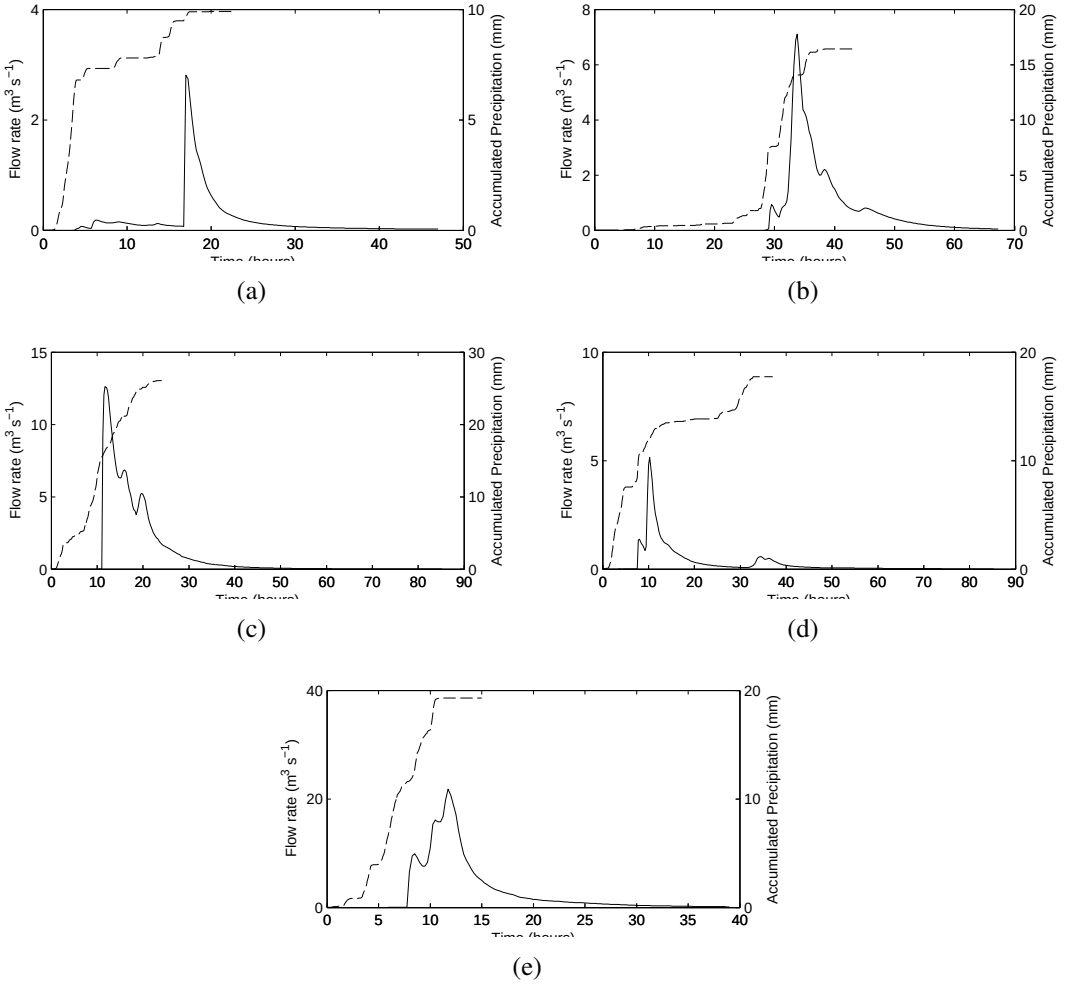

Figure 5.2: Hydrographs (solid line) for model runs with distributed rainfall input and with surface condition 2 along with catchment average precipitation accumulation (dashed line) for events: (a) 1, (b) 2, (c) 3, (d) 4 and (e) 5.

of catchment averaged rainfall which covers the whole catchment for the duration. Although this period represents the majority of the rainfall in this event, from Figure 5.2a we see there is very little resulting runoff as the rainfall intensities did not exceed the infiltration rate.

This period is followed by some low to moderate intensity patchy rainfall until some intense convective cells (with reflectivities exceeding 50 dBZ) pass over the catchment near the catchment outlet. These cells provide only ~2 mm of catchment averaged rainfall as they fall on only a fraction of the catchment, however, the high intensities present lead to significant runoff, with the flood peak for this event at just under 3 m^3 s^{-1}.

Event 2 begins at 07:45 on 31/07/2009 and lasts until 03:00 on 02/08/2009. The event begins with light to moderate intensity small scale (< 1–5 km) rain cells and collections of cells. These provide little to catchment averaged precipitation or runoff. The situation changes at approximately 07:00 on 01/08/2008 when moderate to high intensity stratiform rainfall with embedded convection passes over the catchment in several waves. While this rainfall covers most of the catchment, the intensity varies quite considerably in space. Over 15 mm of rainfall falls and a flood peak of ~7 m^3 s^{-1} results.

Event 3 occurs from 24/09/2009 05:30 until 25/09/2009 05:40. The event begins with some light to moderate intensity stratiform rainfall which covers the catchment and contributes around 4 mm of catchment average precipitation. This is followed by a several hour period of moderate intensity widespread stratiform rainfall interspersed with patchy stratiform which provides the remaining 20 mm plus to the rainfall accumulation and a flood peak of > 12 m^3 s^{-1}.

Event 4 is really the latter part of event 3 but consists of very different rainfall so it was decided to investigate it as a separate event. It spans the duration from 25/09/2009 05:50 until 26/09/2009 19:00. The event consists of spatially varied moderate to intense convective rainfall occasionally embedded in stratiform rainfall. A flood peak of 5 m^3 s^{-1} results.

Event 5 occurs from 05:00–20:00 on 28/09/2009. This events consists of some high intensity convective rainfall along with, at times, moderate intensity stratiform rainfall. Rainfall intensity can be highly variable in space. A flood peak of ~20 m^3 s^{-1} is seen from the model.

5.8 Lumped vs Distributed Rainfall

To assess the impact that spatial/temporal variability of rainfall has on the model response for this catchment, we shall first compare lumped rainfall input (where the high resolution radar data has been averaged over the catchment) with distributed rainfall input.

Table 5.2 gives the peak flow for each event for each of the six surface conditions for both a distributed and a lumped rainfall input. The bias, B is calculated simply as

$$B = \frac{F_L}{F_D} \tag{5.3}$$

where F_L and F_D are the peak flow resulting from lumped rainfall input and distributed rainfall input respectively.

The greatest disparity between predicted peak flows run with lumped rainfall inputs and those run with distributed rainfall inputs is seen with surface condition 1, especially for events 1 and 4. No catchment outflow occurs at all for event 1 with this surface condition. This result is not surprising as the runoff from the distributed input run is mostly caused by intense convective cells near the catchment outlet, once averaged over the entire catchment, this rainfall rate is not sufficient to exceed the infiltration rate. Even for surface condition 2, where initial moisture is at 81%, there is still no runoff during the convective rainfall period of event 1.

The reason that running the model with surface condition 1 results in a more biased peak flow, is because of the lower initial moisture content used. This results in a greater infiltration rate threshold which must be exceeded by rainfall before runoff occurs. The infiltration rate threshold creates a non-linear response to rainfall which is enhanced with lower initial moisture conditions.

Figure 5.3 shows output hydrographs for the five case study events with lumped and distributed rainfall inputs for surface conditions 1 and 2. These hydrographs illustrate what is seen in the tables. It is clear to see that lumped rainfall inputs do not provide sufficient information to reproduce the distributed hydrograph shape for surface conditions 1 (for all events) and 2 (for events 1 and 4). If the model were to be calibrated with lumped rainfall inputs, as would be the case in practice when using lumped rainfall input, dramatically different surface conditions would have to be chosen (in GSSHA's case, saturated conductivity would be the primarily varied parameter) to minimize error

with the observed outflow. This calibration would obviously not be consistent between events with differing amounts of rainfall variability (stratiform vs convective for example).

For conditions 3–6, where areas of the catchment are made impervious, the non-linear runoff response is masked somewhat by the much greater volume of water that now runs off without facing infiltration. Biases are much closer to unity for these conditions, but are still generally less than 1. It appears that surface flow routing may be of primary importance to assessing the impact of sampling error on urban hydrology rather than just the variability in runoff. To properly assess this, it is likely that a drainage model should be implemented (which is not possible with GSSHA).

Table 5.2: Comparison of catchment peak discharge rate (in $m^3\ s^{-1}$) for lumped (F_L) and distributed (F_D) rainfall inputs with surface conditions 1–6. B is bias as calculated as F_L/F_D

	Condition 1			Condition 2			Condition 3		
Event	F_L	F_D	B	F_L	F_D	B	F_L	F_D	B
1	0.00	1.32	0.00	0.18	2.94	0.06	8.15	8.31	0.98
2	0.14	2.07	0.07	3.43	7.10	0.48	17.70	26.47	0.67
3	0.56	5.65	0.10	6.40	12.63	0.51	22.35	27.31	0.82
4	0.06	2.55	0.02	0.63	5.17	0.12	10.16	15.07	0.67
5	1.77	13.50	0.13	9.87	21.92	0.45	26.98	50.39	0.54
	Condition 4			Condition 5			Condition 6		
Event	F_L	F_D	B	F_L	F_D	B	F_L	F_D	B
1	5.00	6.67	0.75	29.44	24.89	1.18	19.83	18.15	1.09
2	13.01	21.12	0.62	49.98	57.43	0.87	32.27	44.74	0.72
3	19.78	25.61	0.77	55.55	60.61	0.92	51.29	56.24	0.91
4	5.41	12.68	0.43	24.88	44.04	0.56	16.95	27.91	0.61
5	23.55	47.91	0.49	56.97	74.07	0.77	58.63	68.12	0.86

The total flow volume, from Table 5.3 paints a similar picture to the flow peak results.

Table 5.3: Comparison of catchment discharge volume V (units of 10 000 m^3) for lumped (V_L) and distributed (V_D) rainfall inputs with surface conditions 1–6. B is the bias as calculated as V_L/V_D

	Condition 1			Condition 2			Condition 3		
Event	V_L	V_D	B	V_L	V_D	B	V_L	V_D	B
1	0	1.33	0.00	0.597	3.13	0.19	22.3	24.8	0.90
2	0.53	3.75	0.14	6.23	14.1	0.44	46.5	52.9	0.88
3	1.66	10.2	0.16	13.3	32	0.42	81.2	92.1	0.88
4	0.407	3.85	0.11	1.62	8.73	0.19	43.4	46.4	0.94
5	3.39	17.1	0.20	18.4	38.8	0.47	68.1	80	0.85
	Condition 4			Condition 5			Condition 6		
Event	V_L	V_D	B	V_L	V_D	B	V_L	V_D	B
1	10	14.4	0.69	56.2	54.8	1.03	39.6	45.5	0.87
2	31.7	42.6	0.74	107	108	0.99	90.5	97.7	0.93
3	64.7	80.7	0.80	182	199	0.91	162	177	0.92
4	20.7	32.5	0.64	108	115	0.94	80.3	92.9	0.86
5	59.2	76.9	0.77	139	151	0.92	130	138	0.94

The differences in time to peak between lumped input and distributed input are given in Table 5.4. Although many of these results are meaningless, for instance, event 1 does not produce any flow, meaning that there is no time to peak, there are results where the time to peak is sensible. For events 2,3 and 5, the hydrographs from lumped rainfall input do appear similar to those from distributed rainfall.

Table 5.4: Difference (in minutes) between time of peak discharge for lumped rainfall input and that for distributed rainfall input with surface conditions 1–6

Event	Condition 1	Condition 2	Condition 3	Condition 4	Condition 5	Condition 6
1	302	-361	-679	-678	-12	21
2	363	5	28	-2	26	5
3	137	33	-8	5	61	8
4	513	105	4	10	-211	-229
5	53	11	20	3	-30	-28

5.9 Rainfall Accumulation Period

The impact that precipitation accumulation period has on the model for the five case study events shall be examined here. We may imagine that the impact will be similar to that from averaging the precipitation field in space as seen above; peak rainfall amounts will be smoothed out leading to a reduction in surface runoff and therefore lower peak flows and flow volumes.

Many others have looked at precipitation accumulation period requirements for hydrological modelling, for example Collier and Cluckie (1985) and Cluckie and Owens (1987) looked at using 1 hour accumulations instead of 15 minute accumulations and concluded that “greater degrees of spatial and temporal variation can be tolerated in practical forecasting applications, than would first seem reasonable”. Collier (2009) recommends rainfall updates of 15 minutes or less for flash flood forecasting. Urban flood forecasting has similar requirements due to fast catchment response times, for example Emmanuel et al. (2012) uses ‘urban’ time steps of 5–60 minutes and Berne et al. (2004b) state that 5 minute temporal resolution is required for 1000 ha catchments and

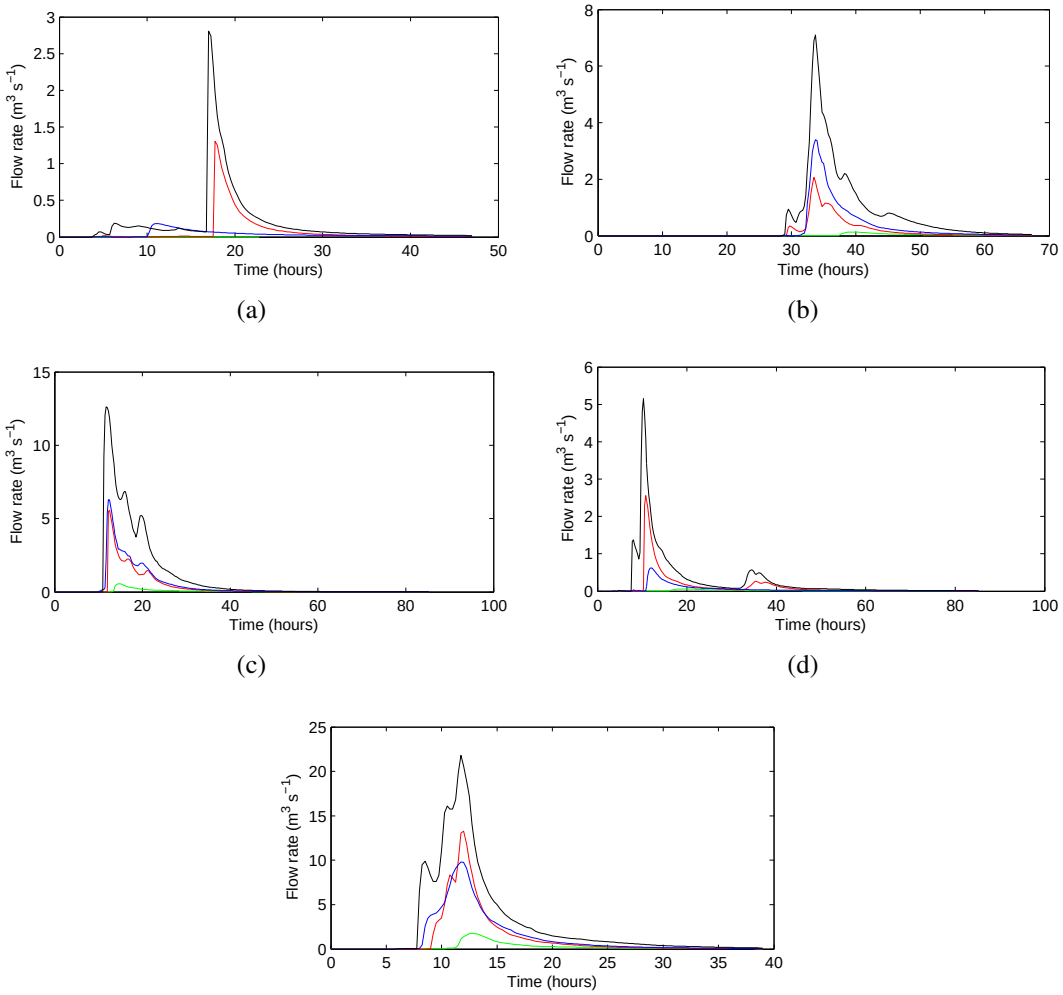

Figure 5.3: Hydrographs for distributed and lumped rainfall inputs for surface conditions 1 (green for lumped, red for distributed rainfall) and 2 (blue for lumped and black for distributed rainfall) for events: (a) 1, (b) 2, (c) 3, (d) 4 and (e) 5.

3 minute resolution is required for 100 ha catchments. Schilling (1991) recommends 1 minute temporal resolution and 1 km spatial resolution for urban hydrology.

GSSHA allows for a minimum period of 1 minute and recommends using periods no longer than 60 minutes. Figures 5.4 and 5.5 show peak flow and flow volume bias (in comparison to output from 2 minute accumulations) respectively for accumulation times ranging from 3–60 minutes over the five case study events and for three different surface conditions. Distributed rainfall input is used.

There is a general decreasing trend in peak flow with increasing accumulation time across all events and surface conditions. There are some events that do see an increase in peak flow over the 2 minute accumulation although a decrease is still seen for further increases in accumulation times.

For surface condition 1, the events that are most affected by long accumulation times are 1 and 4, the same two events that showed the most bias between lumped and distributed rainfall inputs. This indicates that, as may be expected, the temporal integration of using longer accumulation periods has a greater impact on more variable rainfall fields. Even for 10 minute accumulations, reductions in peak flow of 10% and 20% are observed.

Events 3 and 5, on the other hand show much lower variation in peak flow with accumulation time. For event 3, this is to be expected as the rainfall field is fairly uniform. Event 5, however, does include some high intensity convective activity, although this is usually embedded in surrounding larger areas of stratiform rainfall.

Less bias is introduced with increasing accumulation times for surface conditions 2, and the accumulation time has minimal impact for condition 3.

5.10 Discussion

In this Chapter, background information has been provided on the use of radar in hydrology. The model used in this thesis to investigate the impact of rainfall sampling error on hydrology (GSSHA) has been described. Additionally, the test catchment and case studies have been detailed.

It has been shown, by comparison of models run with distributed rainfall input with those run with lumped rainfall input (for the same rainfall fields) that the spatial variabil-

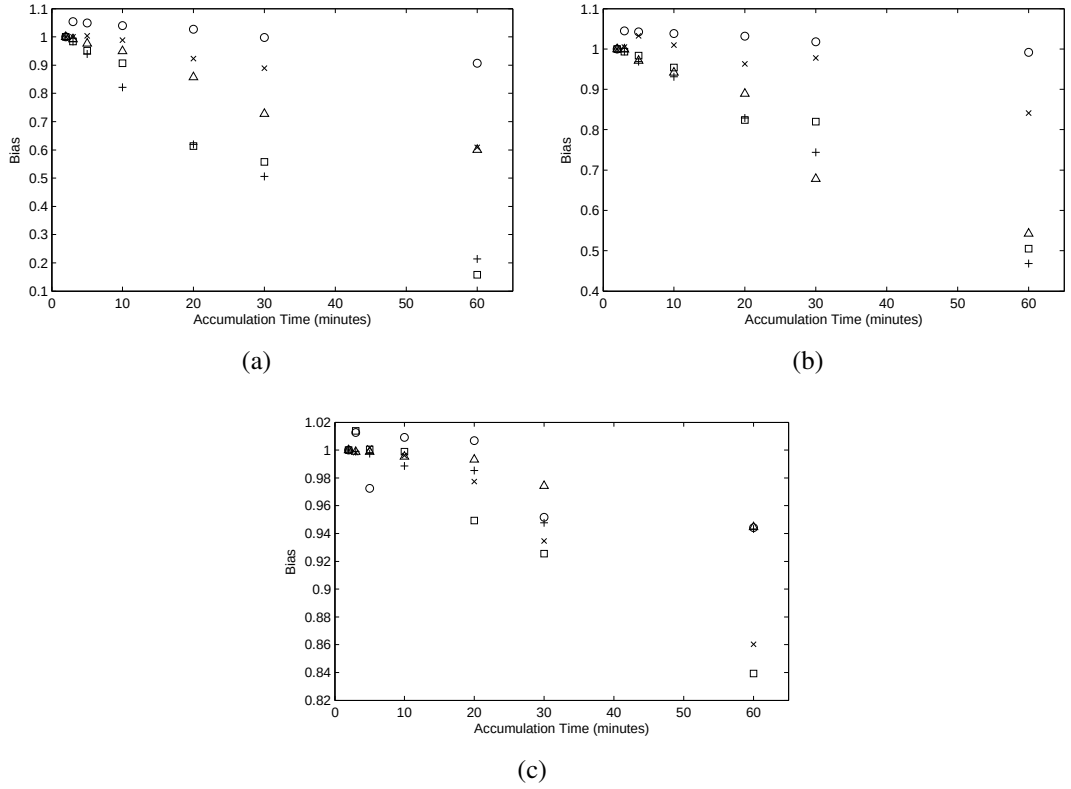

Figure 5.4: Bias in peak flow with precipitation accumulation time relative to peak flow with 2 minute precipitation accumulations for events 1 (+), 2 ($\triangle$), 3 ($\bigcirc$), 4 ($\square$) and 5 ($\times$) for surface conditions: (a) 1, (b) 2 and (c) 3.

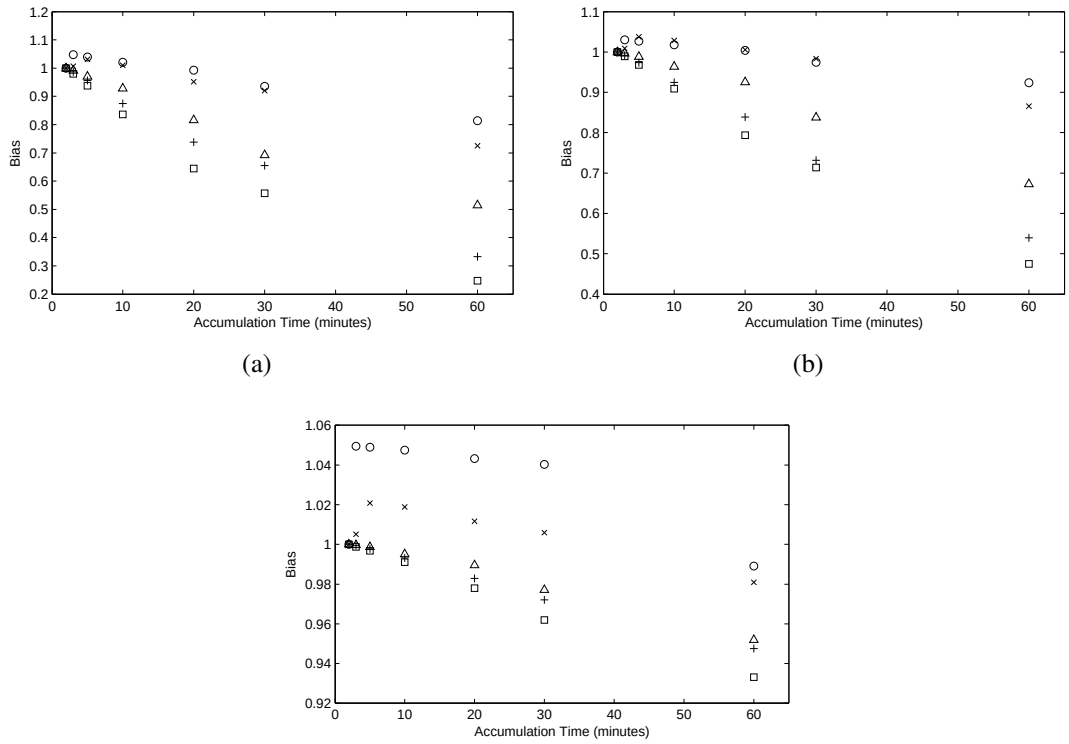

Figure 5.5: Bias in flow volume with precipitation accumulation time relative to volume with 2 minute precipitation accumulations for events 1 (+), 2 (△), 3 (○), 4 (□) and 5 (×) for surface conditions: (a) 1, (b) 2 and (c) 3.

ity of precipitation has a marked effect on this model for this catchment. The difference between the results using the two rainfall inputs is greatest for soil with a low initial moisture content. If a high percentage of the catchment is impermeable, the percentage difference between the peak flow resulting from the two rainfall input schemes is diminished.

The temporal accumulation period has also been examined for this model. The general effect of increasing the temporal accumulation period is a decrease in the total catchment outflow. This is more marked for rainfall events that exhibit more variability in space and time. It has been decided that, based on these results, a 5 minute accumulation period will be used for the analysis in the following chapter. Running the model with an accumulation any shorter than this does not give substantially different results. Additionally, the disk storage requirements for the model run will be decreased and the limit which GSSHA has on the number of accumulation periods in a single rainfall event will not be approached for any of the case study events.

Chapter 6

Impact of Sampling Error on Rainfall Runoff Modelling

In Chapter 2, it was pointed out that only a few studies have looked at the impact of rainfall observation resolution on QPE, this is not the case with respect to rainfall runoff modelling. Many studies have focused on this area, although mostly using fairly standard resolution datasets (eg. Vieux and Farajalla, 1996, Winchell et al., 1998, Koren et al., 1999, Sangati et al., 2009) or synthetic high resolution rainfall datasets. An example of a study which uses a high resolution radar dataset is that of Berne et al. (2004b), where two X-band radars (one vertically pointing and one performing a range height indicator (RHI) scan) were used to examine resolution requirements for urban hydrology.

Although many papers have been published on this topic, the results often contradict one another (Winchell et al., 1998, Sangati et al., 2009). Winchell et al. (1998) suggest a possible reason for this is differences in the rainfall runoff models used in the analyses, especially the choice of infiltration method. They found that infiltration excess methods are much more sensitive to precipitation resolution than saturation excess methods. They also observed that errors are greater when antecedent soil moisture is dry as opposed to wet and that the errors are very storm dependent.

Another reason behind the variability of these studies is the number of case studies used in the analyses. As rainfall is so variable in space and time, the errors that occur when it is sampled are not consistent between events (especially regarding temporal resolution). For example, a consistent bias in rainfall accumulation would not be expected

when decreasing sampling rate. This means that a large number of events should be analysed for any general relationships to be obtained.

To get an idea of the magnitude of sampling errors reported in the literature, we shall discuss some of them here. (Sangati et al., 2009) examined three extreme flood events for a catchment in North Western Italy at a range of spatial scales from 1 to 16 km and with a temporal scale of 10 minutes. They found errors in peak flow of up to 35% for rainfall aggregation of 16 km for subcatchments ranging from 75 to 983 km^2. They also found that variation in the total rainfall volume with aggregation length was minimal until the aggregation length approached the size of the catchment. Additionally, runoff was observed to be be susceptible to the variability of the soil properties, especially with respect to hydraulic conductivity.

Vieux and Farajalla (1996), used the distributed model r.water.fea for a 1200 km^2 catchment to investigate errors from sampling by aggregating WSR-88D level II data onto grids ranging from 0.5 km to 6 km. They found that hydrograph output would become erratic for spatial scales greater than 3.5 km.

Winchell et al. (1998) found that errors from the infiltration excess model were much larger in magnitude than the errors seen in the rainfall input, while for the saturation excess model, errors were much closer to the size of the error in rainfall.

To put the impact of sampling errors on rainfall runoff models in context with the impact of radar errors in general some relevant literature will be discussed below.

Borga (2002) corrected for systematic biases in the radar rainfall estimates by applying a uniform VPR correction, anomalous propagation correction and mean field bias correction using a gauge network. Corrected and non-corrected radar rainfall data were used as input into the probability distributed moisture (PDM) rainfall runoff model (which uses a saturation excess scheme). He observed the IE statistic of simulation efficiency to increase from 0.7 to 0.75 (comparing to observed hydrographs) when using corrected rainfall from a radar scan at 0.5° elevation. Larger increases in IE were observed for higher elevation scans, however, relative to the lowest scan, the rainfall estimates from the higher elevation scans were still quite poor.

Carpenter et al. (2001) looked at the sensitivity of the Hydrologic Research Center Distributed Hydrologic Model to radar rainfall uncertainty using a radar error model of

the form

$$P_e = P_0 10^{\epsilon} \tag{6.1}$$

where P_e is the noisy rainfall, P_0 is the 'true' rainfall and ϵ is a uniformly distributed random variable between -0.2 and 0.2. This added a $\pm 50\%$ error to the rainfall field. Using this noisy field as input to the hydrologic model, they observed a 10–15% uncertainty range in the model hydrograph. A 50% upper-soil-zone parameter error, however, produced a 23–34% uncertainty in the model hydrograph.

Zhu et al. (2013) used a statistical error model based on a Gaussian distribution to assess the impact of radar rainfall errors on three different hydrological models: MIKE SHE (a distributed physically-base model), TOPMODEL (a semi-distributed model) and the unit hydrograph model PRTF. They found that systematic bias in the radar rainfall had the greatest impact on the model simulation. The distributed and semi-distributed models were observed to behave similarly under variations in the introduced systematic bias and random error in the radar field while the unit hydrograph model was the most resistant to these errors.

What is novel about the work presented in the next section is the use of a higher resolution dataset in the analysis. It is also valuable that here we get to put the results from Chapter 2 into perspective with a real-life application of the data.

While the need for a great number of case studies is realized, it is difficult to obtain a high resolution record of such a long duration in a research environment. Conversely, in an operational environment, while a long record is more easily obtainable, high resolution (especially in time) is often not obtainable due to operational constraints (multi elevation angle scan patterns being required, etc.).

6.1 Impact of Sampling Error on Test Catchment

The impact that sampling error can have on a rainfall runoff model will be quantified here using high resolution radar data. It is acknowledged that these results represent only a single catchment, modelled with a particular infiltration process. However, although surface water routing (which has a great influence on peak flow and time to peak) is highly dependent upon the catchment (specifically the catchment's size and steepness),

the total runoff volume is less dependent on the catchment. This means that some more general conclusions could be made for what is a rather widely used infiltration scheme.

Some hypotheses could be made at this time:

1. Variation in catchment outflow with sampling resolution is greater for a less saturated soil. This was seen in Section 5.8 comparing lumped to distributed rainfall, it would be unlikely to be any different here.

2. There is less variation in catchment outflow with sampling resolution when a catchment has a greater fraction of impervious area. Again, this was evident in Section 5.8 and would be expected to be evident in this analysis as well.

3. Error in catchment outflow (in reference to that resulting from the original resolution rainfall accumulation) does not necessarily have the same relationships with spatial and temporal resolution as the error in rainfall considered in Chapter 2. Error in this analysis is not directly related to the error in rainfall accumulation, there are additional layers of complication provided by the infiltration and water routing processes. It would, therefore, not be unexpected that such a difference would be exhibited.

4. Error in catchment outflow due to sampling is lesser in magnitude than that for rainfall accumulation (as in Chapter 2). The integrating nature of a catchment will likely minimize the variation of catchment outflow with sampling resolution.

6.1.1 Method

Five minute rainfall accumulations were generated at a range of spatial and temporal resolutions in the same manner as in Chapter 2. These accumulations were then fed into GSSHA for the Waipapa catchment described in Section 5.6. Error is calculated by a normalized absolute error for peak flow:

$$\epsilon_P = \frac{|P_L - P_H|}{P_H} \tag{6.2}$$

where P_H is peak flow resulting from the high resolution rainfall input and P_L is that resulting from the downgraded resolution rainfall input.

and for total flow volume:

$$\epsilon_V = \frac{|V_L - V_H|}{V_H} \tag{6.3}$$

where V_H is the total flow volume resulting from the high resolution rainfall input and V_L is that resulting from the downgraded resolution rainfall input.

An error in time to peak is also calculated as:

$$\epsilon_\tau = \tau_L - \tau_H \tag{6.4}$$

where τ_H is the time to peak from the high resolution rainfall input and τ_L is that from the downgraded resolution rainfall input.

6.1.2 Results

Figure 6.1 shows spatial/temporal error diagrams for the absolute error in peak flow. The form of these diagrams is much more irregular than that for many of the diagrams in Chapter 2. This appears to indicate weaker relationships between the error metric here and the temporal and spatial resolution of the rainfall input and supports hypothesis 3.

Additionally, the effects that spatial resolution and temporal resolution have on the error for some of the events can substantially offset one another. For example, for event 2, ϵ_P is greater for 1000 m/200 s sampling than it is for 2000 m/800 s sampling; the two error sources cancel each other out to a certain extent. This was not seen to anywhere near the same extent when looking at error in rainfall accumulation itself as was considered in Chapter 2, where error generally increases with increasing spatial and temporal resolution and any decreases observed are usually minimal in comparison.

Magnitudes of ϵ_P vary from around 0.14 to 0.3 for 2 km/5 minute sampling. This is lower than the average normalized error of ~0.3 seen in Chapter 2 for 10 minute rainfall accumulations. This provides evidence in support of hypothesis number 4 (that error in catchment outflow due to sampling is lesser in magnitude than that for rainfall accumulation). It must be noted, however, that this error is highly dependent upon the infiltration and routing processes of the model. For a different catchment and initial moisture values, the result could be very different.

For events 2 and 5, spatial resolution has a greater impact on ϵ_P than temporal resolution. These two events consist of large scale intense rainfall with strong reflectivity

gradients, temporal variability is not as great in these events as it is in the latter stages of event 1 where small convective cells produce the runoff observed here. As such, the spatial smoothing across large intensity gradients dominates over the influence of the missing information between scans. Event 5 has larger ϵ_P values than event 2 as it consists of higher intensity rainfall with stronger reflectivity gradients.

For event 1, there is a similar impact on ϵ_P from spatial and temporal resolution. As just mentioned, the small scale intense cells producing the runoff are grossly distorted when sampled at low spatial resolutions and have fairly quick temporal evolution. Error magnitudes are similar to event 5 and greater than for event 2.

For events 3 and 4, temporal resolution has a greater impact on ϵ_P than spatial resolution. This is especially so for event 3, a stratiform event with fairly uniform rainfall intensity over the catchment. An error is still expected for near uniform rainfall due to the radar averaging process producing a bias in the rainfall accumulation (see Section 2.1.6). ϵ_P does reach high levels for very long sampling periods in event 3, this may be due to temporal variation of the intensity of the widespread rainfall or from the periods during the event with less spatially correlated rainfall.

Error in peak discharge for event 4—consisting of fairly large organized convective activity—is most affected by temporal resolution, although error magnitudes, at least as great as for any other event, are reached with spatial resolution. This is not unexpected, the intense convective activity in this event changes quickly with time and presents very strong intensity gradients.

Figure 6.2 illustrates the variation of the hydrographs with spatial and temporal resolution for each event. These plots indicate that the shape of the hydrograph can vary significantly with rainfall observation resolution. For event 2 this is particularly evident.

There is a drastic change in the hydrograph between 10 minute and 20 minute temporal resolution for event 3. The peak flow halves for only a 5% reduction in total rainfall volume, illustrating the non-linear effect of the runoff process.

The timing of the peak discharge also changes quite noticeably for several events (1,2 and 4).

Figure 6.3 shows the error in total runoff volume with rainfall observation resolution. These spatial/temporal resolution error plots have a similar form to the plots of peak discharge error in Figure 6.1. Error in discharge volume is slightly lower than in peak

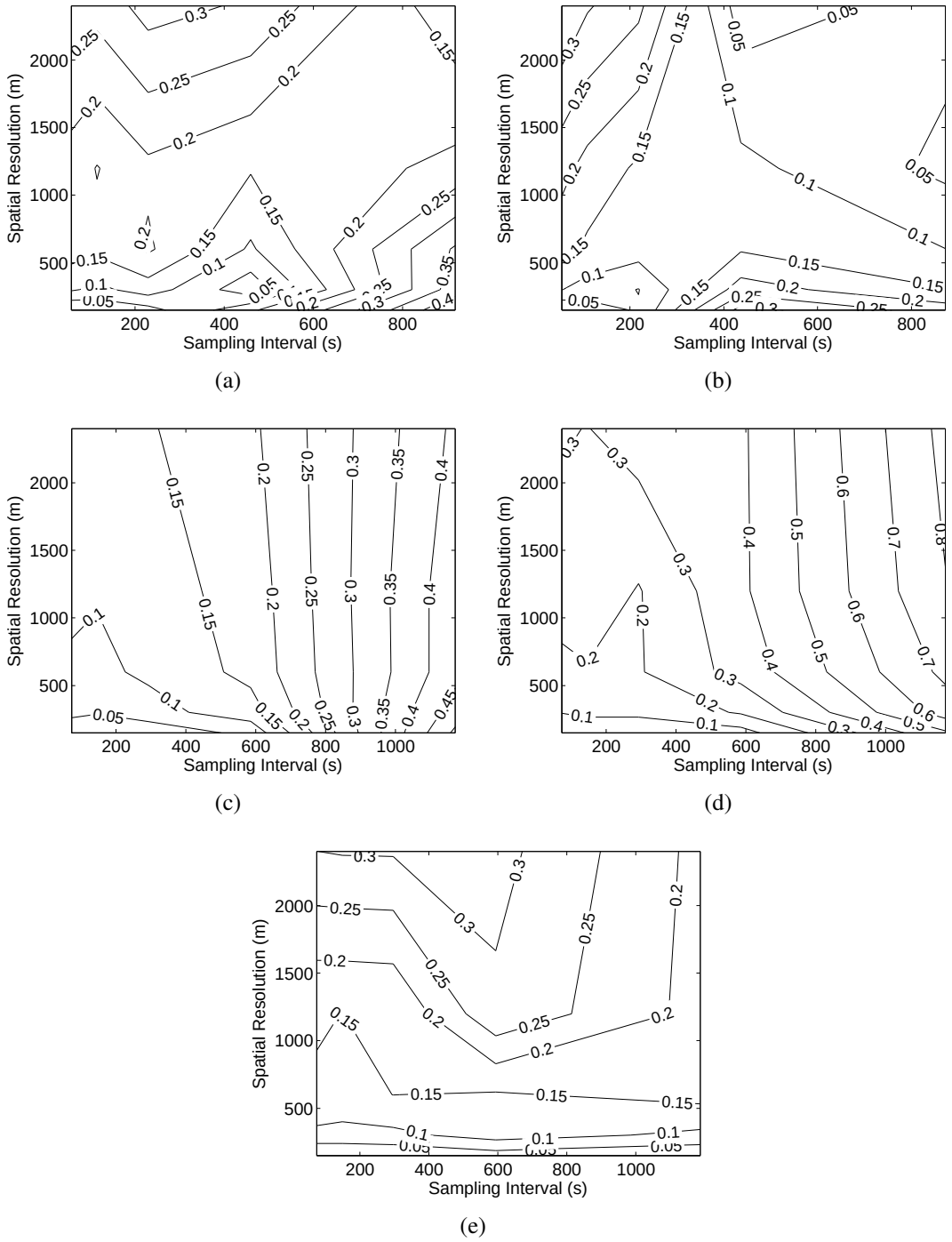

Figure 6.1: Normalized absolute error in peak flow with surface condition 1 for events: (a) 1, (b) 2, (c) 3, (d) 4 and (e) 5.

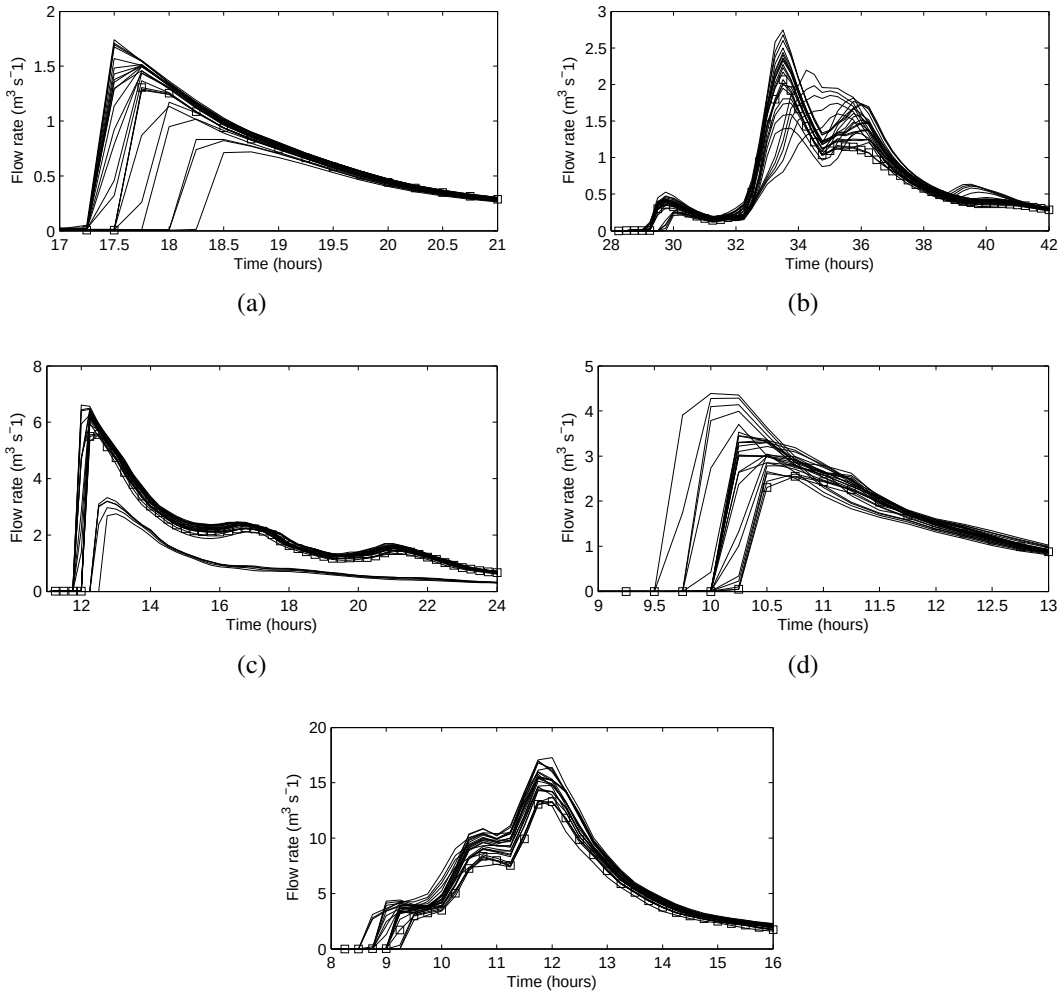

Figure 6.2: Hydrographs showing scale of variation of peak flow with spatial and temporal resolution for events: (a) 1, (b) 2, (c) 3, (d) 4 and (e) 5. The line marked with squares indicates the hydrograph resulting from the original high resolution rainfall accumulation. Run with surface condition 1.

discharge, however. Event 3 shows the greatest difference between ϵ_P and ϵ_V.

Figure 6.4 shows error in peak discharge time (ϵ_T). This error reaches around 10 minutes for 2 km/300 s sampling for several events. For very long sampling periods, the error exceeds 30 minutes for events 2 and 4. With the time to peak for this simulated catchment being around 4 hours, 10 minute and 30 minute variations in the peak time represent an approximate 4% and 12% change in the time to peak respectively. A not insignificant amount.

Variation with Surface Condition

The model was also run with multiple resolution rainfall accumulations using different surface conditions. Figure 6.5 gives the results for ϵ_P with surface condition 2 (no impermeable area but a more saturated soil). For events 1 and 5, the spatial/temporal error plots are almost identical to those generated using surface condition 1 in Figure 6.1. For events 3 and 4, the shape of the diagrams is unchanged, however, the magnitude of ϵ_P has approximately halved. Event 2 shows an increase in error magnitude as well as a change in the form of the spatial/temporal error plot; there is no longer an offsetting effect when both spatial resolution and temporal resolution are coarse.

While the results for events 1,3,4 and 5 do not provide any evidence against hypothesis 1 (that variation in catchment outflow with sampling resolution is greater for a less saturated soil), the results for event 2 do. The situation *is* different from that in section 5.8, in this analysis, spatial averaging is being performed in Z rather than in rainfall rate/accumulation which introduces a bias.

Additionally, it may be the case that the errors arising from decreasing temporal resolution are less diluted/diminished (compared to their impact on rainfall accumulation) by the infiltration process when there is higher soil moisture. It is also worth bearing in mind that such errors do not consistently affect intensity as those from decreasing spatial resolution do but are less predictable in nature. As such, inferences regarding the impact of temporal resolution on runoff modelling should only be made when considering the average over several events.

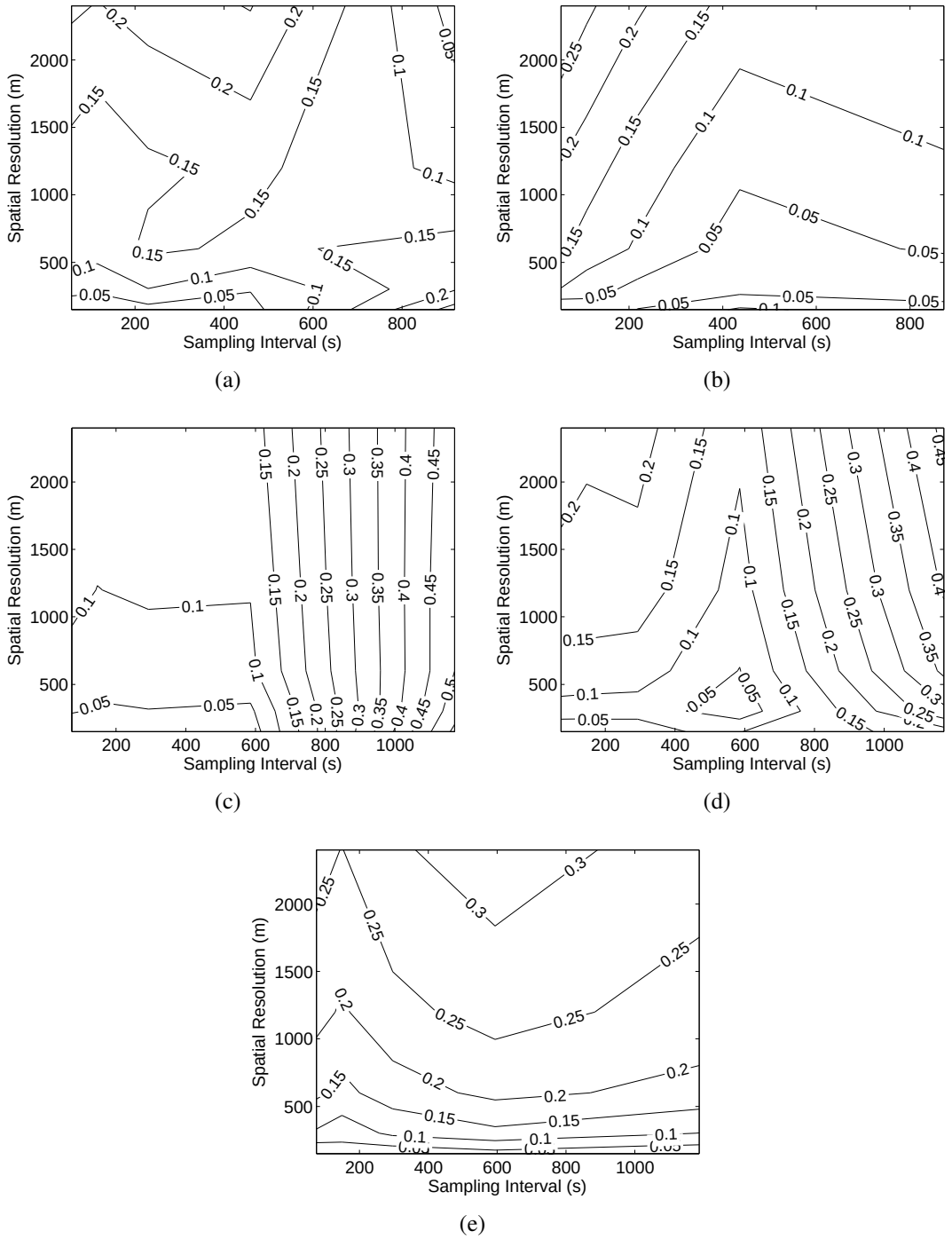

Figure 6.3: Normalized absolute error in total flow volume with surface condition 1 for events: (a) 1, (b) 2, (c) 3, (d) 4 and (e) 5.

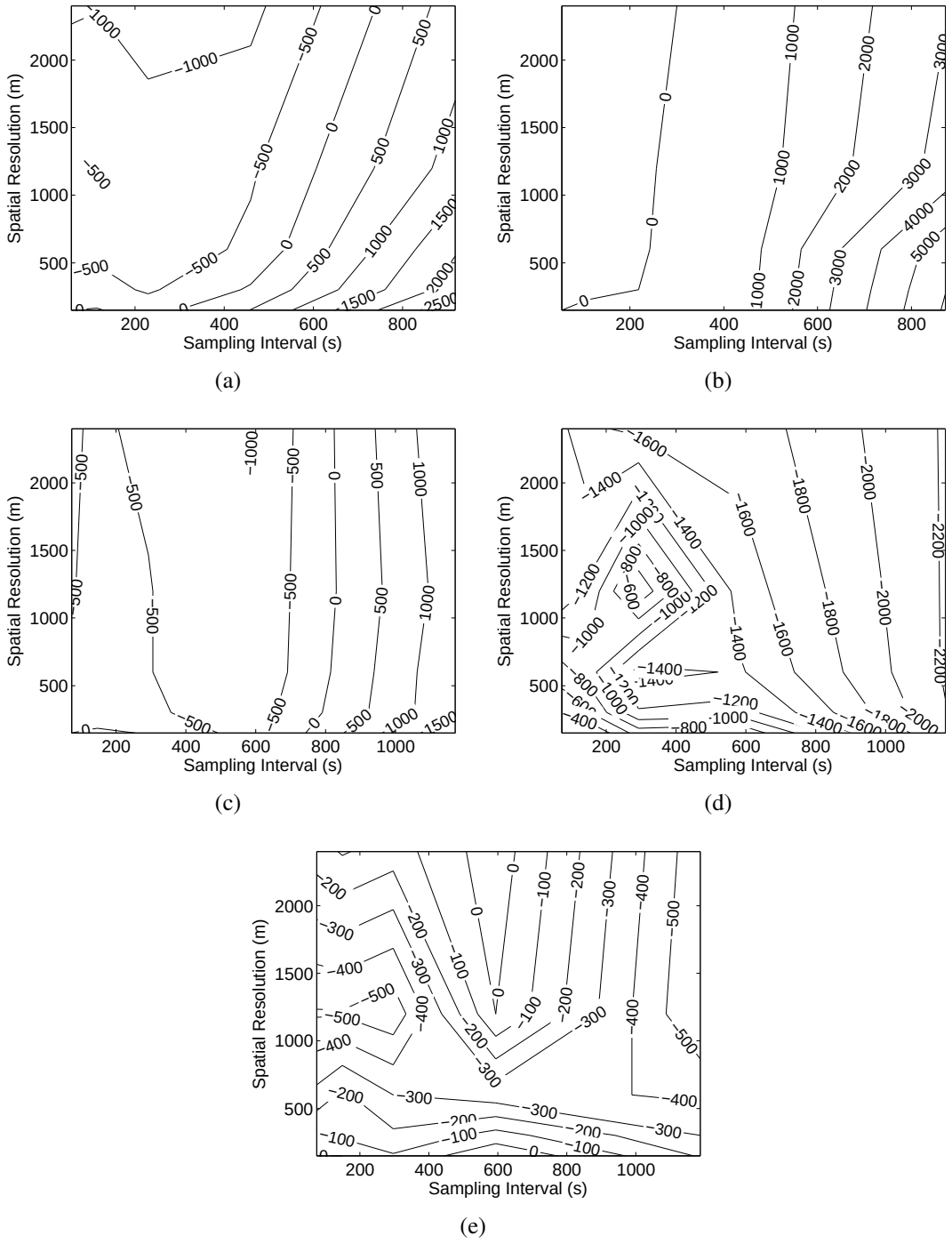

Figure 6.4: Normalized absolute error in total flow timeDiff with surface condition 1 for events: (a) 1, (b) 2, (c) 3, (d) 4 and (e) 5.

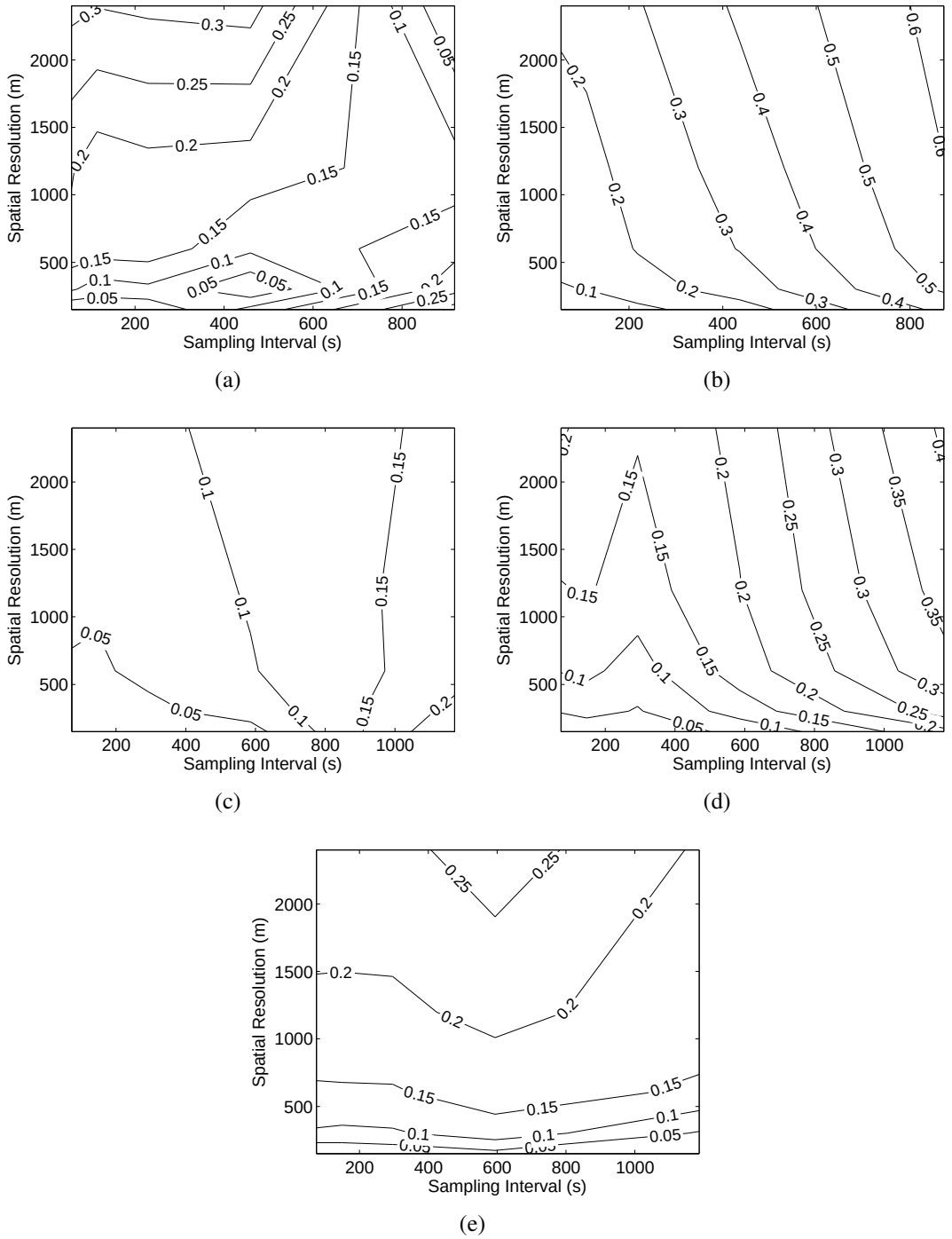

Figure 6.5: Normalized absolute error in total flow peakFlow with surface condition 2 for events: (a) 1, (b) 2, (c) 3, (d) 4 and (e) 5.

The model was also run with surface conditions 4 and 6. For most of the events, ϵ_P is decreased by around a factor of 2 from the magnitudes seen for surface condition 2. The exception to this decrease is seen with event 4, for which ϵ_P remains fairly unchanged from what was seen for surface condition 2 over all spatial/temporal resolutions of rainfall input. Error was again decreased when surface condition 6 was applied for most events. An exception was event 5 where ϵ_P actually increased in magnitude slightly.

These results are generally supportive of hypothesis 2 (that there is less variation in catchment outflow with sampling resolution when a catchment has a greater fraction of impervious area), however, as one finds is usually the case in this field (meaning hydrology as well as meteorology) this is not universally true. For several events the error did not decrease and for one event it did in fact increase when the percentage of impermeable area was increased.

Conclusion

The impact that the spatial and temporal resolution of observation of rainfall has on a rainfall runoff was quantified here for a single catchment with five case study events. Normalized error in peak flow was seen to vary from around 0.14 to 0.3 for 2 km/5 minute sampling. Error in total runoff volume was observed to be very similar (but slightly lesser in magnitude) to that in peak discharge for four out of the five events. Errors in peak time were on average around 10 minutes for most of the events at 2 km/300 s sampling, around 4% of the time to peak for the simulated catchment.

Supporting hypothesis 1, sampling error generally decreased when soil saturation was increased, however, exceptions did occur. Similarly, regarding hypothesis 2, when the percentage of impermeable area in the catchment was increased, for most events (but not all), the error decreased.

Relationships between spatial and temporal sampling resolution and error in peak discharge were quite different from those with rainfall accumulation itself, validating hypothesis 3. The spatial/temporal resolution error plots were much less defined, indicating weaker relationships.

The magnitude of error observed in this analysis was less than for error in rainfall accumulation (validating hypothesis 4), for example, for surface condition 1, at 2 km/300 s sampling, ϵ_P varied from around 0.14 to 0.3 over the five events. In comparison, the av-

erage error in rainfall accumulation over three months of data was ~0.3 (from Figure 2.12). It should be mentioned that the result just mentioned for error in rainfall accumulation was also for 10 minute rainfall accumulations while the rainfall accumulation period used for the runoff modelling presented here was 5 minutes.

6.2 Gauge Correction for Hydrology

It is of interest to assess the effect that the errors from sampling resolution have on gauge correction in the context of a rainfall runoff model. Gauge correction is quite often applied to radar rainfall data for hydrological use (Seo et al., 1999, Steiner et al., 1999, Cole and Moore, 2008).

Applying a multiplicative factor to the rainfall input will directly alter the total rainfall volume in the catchment model. It is likely that this change in rainfall volume will have a greater effect on modelled runoff than a change (due to observation resolution) in the distribution of a fixed volume of rainfall does. Additionally, if the bias introduced by a gauge correction procedure (due to the sampling error when determining the radar/gauge bias) is greater in magnitude than the biases that the procedure is trying to correct for, one would have to question the appropriateness of applying such a correction.

It will also be investigated whether bias correction of the sampling error resulting from coarse spatial resolution can be corrected using such a process. The analysis will be performed using a mean field correction with a 'reasonable' number of gauges for the catchment. The definition of a reasonable number of gauges here will be decided by Equation 5.1.

In this analysis, sampling error has two effects, it produces a fluctuation in the mean field bias between high resolution and degraded resolution fields and it has a direct influence on the runoff process as seen in section 6.1.

Some hypotheses:

1. The change in rainfall volume that occurs from the bias correction procedure produces greater error in the catchment output than the error due to a change in the distribution of rainfall at a fixed rainfall volume.

2. The impact of sampling error is not reduced by the gauge correction scheme. It is likely that the inconsistent nature (in space) of the introduced spatial sampling bias along with the variable nature of the temporal sampling error will result in a 'correction' that actually makes things worse.

6.2.1 Method

One hour rainfall accumulations were made at a range of spatial and temporal resolutions. For 10 realizations of a randomly sited four gauge network inside the Waipapa catchment, the mean field bias between the downgraded resolution accumulations and the high resolution accumulation was calculated as in Equation 4.2. Bias was calculated only where both rainfall values were greater than 0.5 mm. Where none of the simulated gauge sites met this condition, the average bias over the whole event for that gauge network realization was used.

Five minute rainfall accumulations of the downgraded accumulations were then 'corrected' using these bias values. These bias corrected 5 minute accumulations were then input into GSSHA. The error metric used for this analysis is defined as:

$$\mathrm{NRMSE_P} = \frac{\sqrt{\langle (P_C - P_H)^2 \rangle}}{P_H} \tag{6.5}$$

where $\langle ... \rangle$ indicates calculating the mean over the 10 different gauge realizations, P_C is the peak flow resulting from the 'corrected' rainfall accumulation and P_H is the peak flow resulting from the original high resolution rainfall accumulation.

6.2.2 Results

Figure 6.6 shows $NRMSE_P$ for surface condition 1. Error for event 1 has increased compared to the results in Figure 6.1 for all spatial/temporal resolutions. For all other events, error appears to decrease for coarse spatial resolution and low temporal sampling periods. This seems to provide evidence against hypothesis 2 (that the impact of sampling error is not reduced by the gauge correction scheme). On average, mean field bias correction with a four gauge network does decrease the introduced bias from coarse spatial resolution sampling. This correction, however, is overwhelmed if long temporal sampling periods are used.

Although the RMS average error is reduced compared to the previous section's results, for some gauge pattern realizations, error is in fact increased. For example, for 1200 m/200 s sampling for event 2, normalized MAE varied from 0.005 to 0.36, with 2 of the 10 gauge realizations producing higher error than the Section 6.1 results.

These results appear to disagree with hypothesis 1 in general. For event 2, error at 1 km/600 s increases from 0.10 (sampling error only) to 0.60 (gauge correction error plus sampling error), implying the mean gauge correction error is much greater than the sampling error and is in support of hypothesis 1. On the contrary, for events 3,4 and 5 only small increases in error are observed at 1 km/600 s sampling, disagreeing with hypothesis 1. What is observed, however, is that the error from the gauge correction varies considerably with the locations of the gauges in the network. This means that although on average the bias correction error is smaller than the sampling error, it is possible that it will be greater than it.

This analysis was also run for surface condition 2. Figure 6.7 shows the spatial and temporal error plots. As was seen in Section 6.1, error decreases in magnitude for most events in comparison to the results using surface condition 1.

6.2.3 Conclusions

Contrary to what may have been expected in light of previous results in this thesis (especially those of Chapter 4)—and consequently, hypothesis 2 in this section—the bias produced from rainfall observation with coarse spatial resolution was reduced with a four gauge mean field bias correction. This only occurs, however, when spatial resolutions are low and temporal sampling frequency is high. Additionally, the correction is inconsistent, it only performs when taken over the average of all gauge network realizations.

For long temporal sampling rates, error is observed to increase substantially from what was seen in Figure 6.1 for only 2 of the 5 events. For the other events, error does not increase significantly. The error from bias correction does, however, vary quite considerably with gauge placement. For instance, for 1200 m/200 s sampling for event 2, normalized MAE varied from 0.005 to 0.36. Therefore, while for the average case there is disagreement with hypothesis 1, for individual events, applying a bias correction can introduce a larger error than the sampling error.

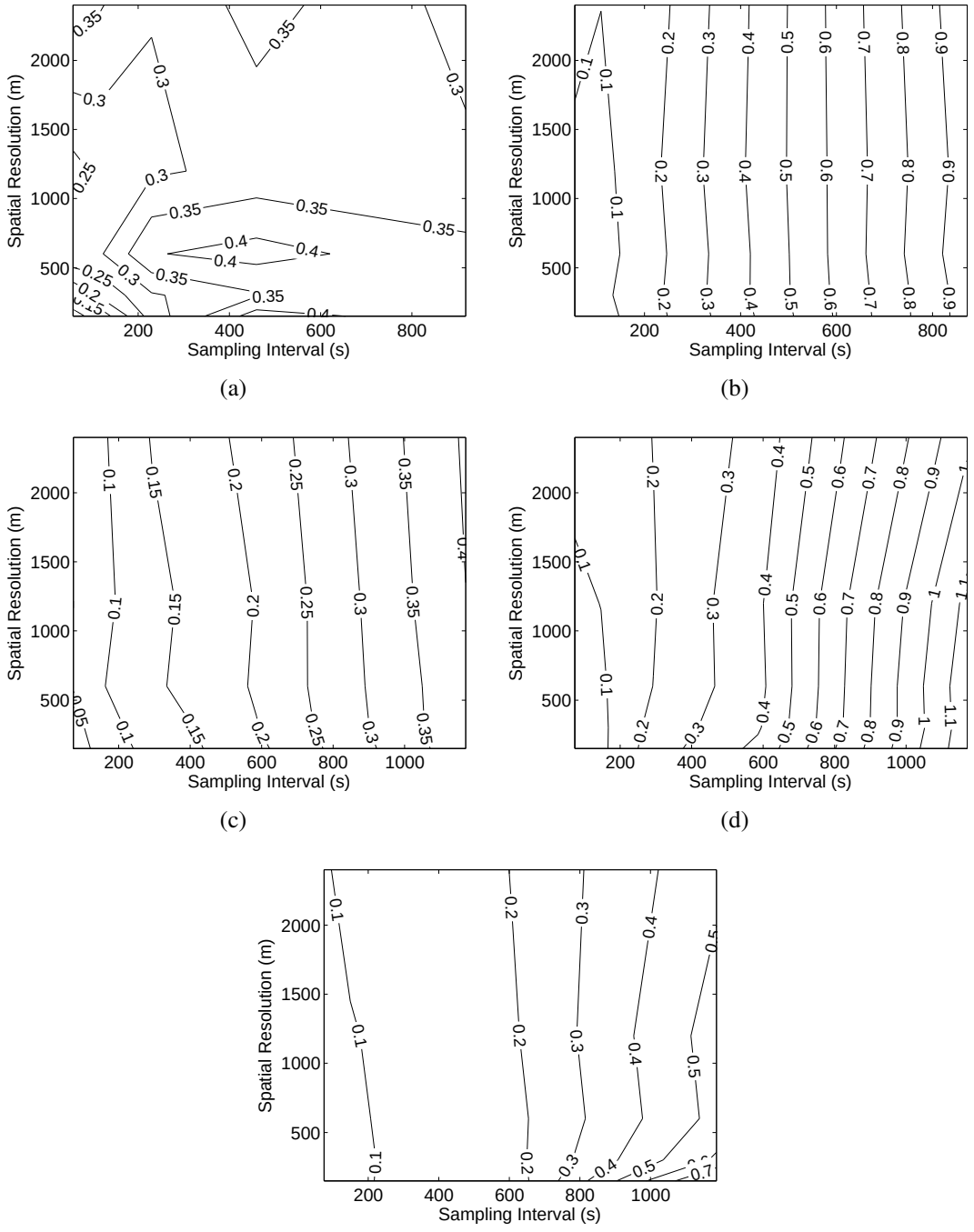

Figure 6.6: Normalized mean absolute error in peak flow with spatial and temporal resolution after 'bias correction' over the 10 'gauge' patterns for events: (a) 1, (b) 2, (c) 3, (d) 4 and (e) 5. Run with surface condition 1.

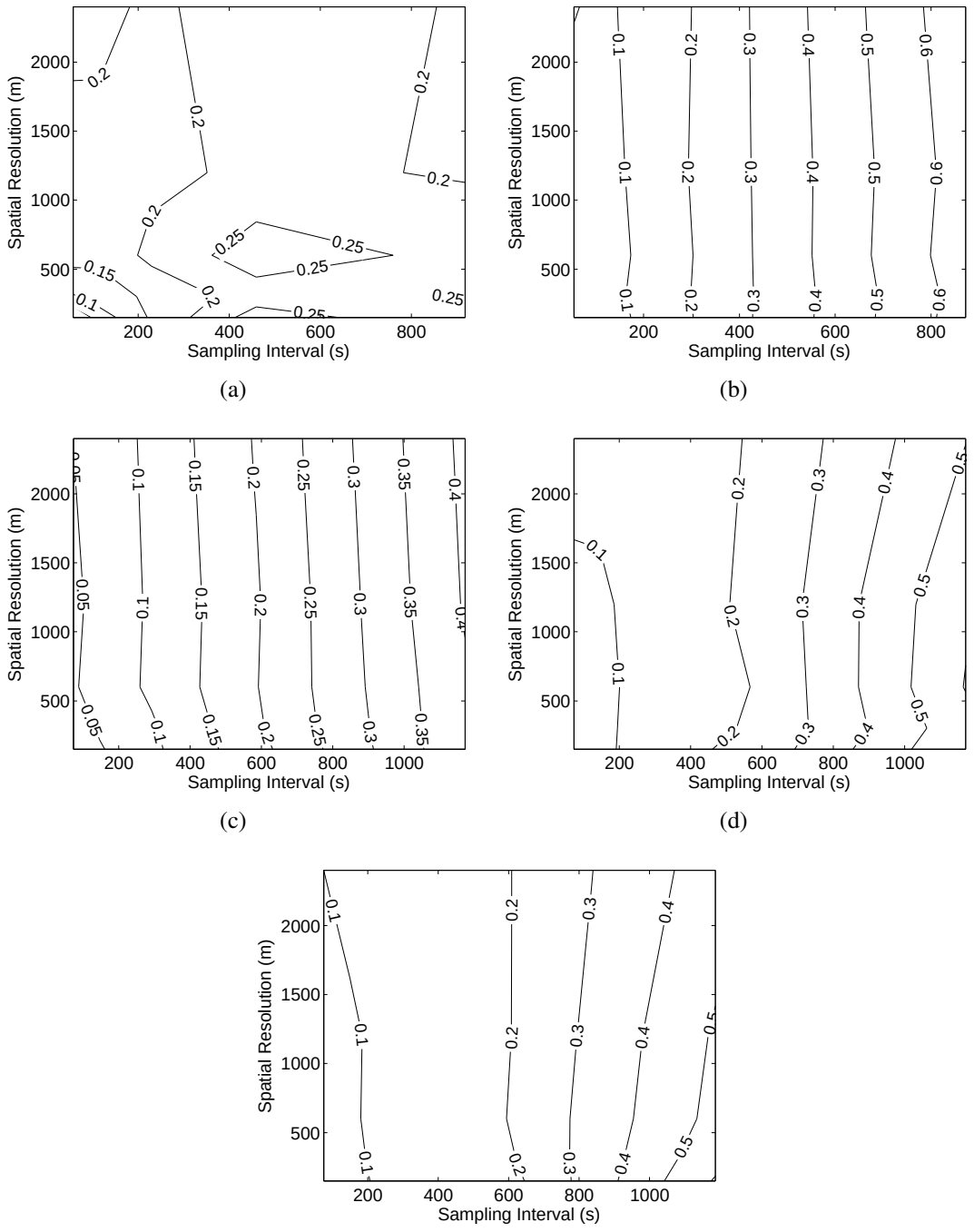

Figure 6.7: Normalized mean absolute error in total flow volume with spatial and temporal resolution after 'bias correction' over the 10 'gauge' patterns for events: (a) 1, (b) 2, (c) 3, (d) 4 and (e) 5.

These results indicate that it is usually appropriate for a mean field bias correction to be applied to the rainfall input to a rainfall runoff model so long as the temporal sampling rate is sufficiently high.

6.3 Discussion

This chapter set out to assess the impact of sampling error on rainfall runoff modelling. Additionally, the appropriateness—in light of sampling error between an areal and a point measurement—of applying a gauge correction to radar observations before being input into runoff models was also assessed.

Observing at lower spatial resolutions provided a positive bias to the total rainfall volume in the model, increasing peak flow levels in general. This positive bias usually, but not always overpowers the reduction in runoff due to spatial smoothing. The error introduced from lower temporal resolutions would sometimes counteract the spatial sampling error, meaning that sometimes for lower spatial and temporal resolution sampling, the error would be less than for higher spatial and temporal resolution sampling. There was no consistent decrease or increase in the peak flow when decreasing the temporal resolution. This would only be the case if advection interpolation were not used when generating the rainfall accumulations. In that situation, rainfall would hover over a location for the duration of the sampling period, saturating the soil beneath, before instantly hopping to another location to do the same. The result would be an overestimation of runoff with increasing sampling period.

The error magnitude was, as predicted, not as great as the error in the QPE. The catchment model does have a damping effect. Error magnitudes were still at not insignificant levels, being comparable with the error in the stream flow measurement process (with a variation of 14–30%). It has, therefore been shown that sampling error should not be ignored completely when running rainfall runoff models.

While a mean field bias correction did appear to reduce some of the bias from spatial sampling errors on average, the results from individual gauge network realizations varied considerably. Again, as in Chapter 4, the recommendation would be that gauge correction only be applied when the difference between the radar and gauge is sufficiently large so as to overcome the errors due to sampling. The above results could be

used as a way to find what this level should be.

Conclusion

The aim of this thesis, as presented in the introduction, was to investigate rainfall sampling error so as to increase our ability to answer a series of questions relating to it. To refresh our memories: What is the magnitude of this [sampling] error? How does it vary with sampling resolution? With rainfall event? What is the impact on the many applications of the data? How much resolution is 'enough' for rainfall measurement? This list of questions was by no means exhaustive, several further questions were asked in the following chapters.

In Chapter 1, it was discussed how the resolution requirements for rainfall observation vary depending on the application as well as on the characteristics of the rainfall system that is to be observed. After describing the sources of rainfall information as well as defining spatial and temporal resolution along with other qualities of rainfall data, several of the most important applications of rainfall data were assessed as to their possible resolution requirements.

From the results of this discussion, particular applications of rainfall data appeared much more likely than others to be impacted by sampling error. These applications involved: all uses of hydrological models where rainfall is the dominant input water source (with regard to rainfall volume estimation and any bias correction), any comparison between an areal measurement and a pointwise measurement (such as radar bias correction by rain gauge or satellite to rain gauge/radar) and short term forecasting (nowcasting), especially of severe weather.

A question regarding hydrological models was asked at this time: "To what extent does the integrating nature of a catchment reduce the model impact of coarse resolution rainfall data input?".

Chapter 2 helped to answer many of our questions regarding sampling error. By de-

grading a high resolution radar dataset's spatial and temporal resolution, the effect that sampling at lower resolutions has on rainfall observation could be assessed by comparison of the degraded data with the original high resolution data. This dataset consisted of 48 events, larger than any related study discovered in the literature.

Performing the analysis in this manner provides an estimate of the lower bound for the sampling error, as the high resolution data is still three orders of magnitude—in spatial length scale—from a rain gauge. It does, however, avoid all of the difficulties that would be encountered if rain gauges were to be used in the comparison instead of the high resolution radar data. This is because all other radar to gauge error sources can be ignored in a radar only study.

Normalized root mean square error due to sampling effects for 10 minute rainfall accumulations was calculated to establish an answer to the questions regarding the magnitude of the sampling error and how it varies with resolution. This error was significant, varying from 17% to 64% of the mean accumulated rainfall for observation resolutions characteristic of operational weather radar networks (2 km and 5 minute sampling).

Sampling error was found to generally increase when rainfall fields were degraded in spatial and temporal resolution. However, for low spatial resolutions, a decrease in sampling error is often seen when longer sampling intervals are used. These results confirmed previous studies performed on much shorter datasets.

The magnitude of sampling error, as well as how it changes with spatial and temporal observation resolution was seen to vary quite considerably between different types of rainfall events (e.g. stratiform or convective rainfall). It was found that spatial sampling error could be predicted—to a certain degree of accuracy ($R^2 = 0.82$)—from knowledge of a rainfall event's characteristic length scale and intensity. As these properties are obtainable from low resolution measurements, the potential magnitude of spatial sampling error can be predicted. This relationship showed that an increase in spatial length scale resulted in a decrease in the sampling error and an increase in the rainfall intensity resulted in an increase in sampling error. This relationship applied only for spatial sampling error, no such relationship was found between temporal sampling error and the characteristic length scale.

Several methods for diminishing the effects of sampling error were assessed. Interpolation between scans using an advection based technique was found to decrease error

by around a factor of two, confirming the results of previous studies. Integration of rainfall accumulations in space and time demonstrated the expected reduction in sampling error. For one hour accumulation times with 2 km/300 s sampling, however, error was still fairly substantial, with an observed NRMSE of 0.2 averaged over all events.

In Chapter 3, all significant sources of radar rainfall uncertainty were detailed. It was explained that it is difficult to assess the relative contribution that sampling error provides to the overall radar rainfall uncertainty as the magnitude of some error sources (predominantly VPR error and Z-R uncertainty) are difficult to determine. A method was proposed to determine a lower bound to the possible relative contribution of sampling error by assessing the variation in radar/gauge bias with radar resolution with the use of a radar only technique (so as to avoid the introduction of other sources of radar uncertainty).

This chapter also looked at the balance between the number of pulses averaged per radar bin and temporal resolution. It was discovered that if a radar is observing with high spatial resolution but with low temporal resolution, it would be of benefit to decrease the number of averaged pulses. If both spatial and temporal resolution were low, however, a benefit would not be gained.

Chapter 4 looked at the suitability of applying gauge corrections to radar data in light of sampling errors. There were two questions looked at here "What effect does fine scale (below conventional radar resolution) variability in the precipitation field have on point measurement correction of radar (areal) measurements?" and "Can gauge correction, in light of the impact of sampling errors, be used to determine changes in the Z-R relationship during or between storms or should it only be used over longer time periods?".

These two questions were investigated by subsampling high resolution radar data to simulate a rain gauge network and determining the radar/'gauge' bias between this 'gauge' network and downgraded resolution radar data.

To answer the first question, it was found that the variability in the radar/gauge bias, as measured by $\sigma(F)$, increases for decreasing spatial and temporal radar resolutions. For one hour accumulations at 2 km/600 s sampling, $\sigma(F)$ is observed to be ~0.09, giving a one sigma range for the bias (b) of 0.81 to 1.23. A systematic change to the observed bias was also found, increasing with decreasing spatial resolution, approaching

1.06 for 2 km/300 s sampling for one hour accumulation periods.

Using this method it was also established that sampling error at 2 km/600 s sampling provides around a third of the total variability in radar/gauge bias, with this being a lower limit due to the still large disparity between the length scale of the high resolution data and that of a rain gauge.

By applying a simple nearest neighbour gauge correction scheme—with the correction based on the difference between the high resolution pixel, representing a gauge, and degraded resolution radar data—it was established that the error resulting from such a scheme was of a similar magnitude again to the impact of sampling error itself (comparing degraded resolution data to high resolution data).

To answer the second question of this chapter, the accumulation period for the gauge bias analysis was varied to assess the magnitude of error at each time scale. As was expected, $\sigma(F)$ decreases with increasing accumulation period. It was concluded that, for short accumulation periods, e.g. 10 minutes, it is likely that any variation that occurs in the Z-R relationship (variation in space and time in an event)—which is not relatively easy to correct with radar alone (e.g. stratiform/convective/snow discrimination)—would not be large enough to exceed the error that any gauge based correction would introduce due to sampling issues. As such, unless high resolution radar data is used, it would not be appropriate to correct for Z-R changes in a storm using a rain gauge based correction procedure. A possible exception to this statement is for very uniform rainfall, where sampling errors are minimal.

The results obtained in this chapter could also be used to develop a procedure whereby gauge correction could be applied over a shorter time scale in a more appropriate manner. One would first diagnose the expected radar/gauge variation by looking at the above charts and selecting the values for $\sigma(F)$ depending upon the sampling resolution and accumulation time. If observed radar/gauge biases were consistently outside of two sigma confidence intervals, gauge correction would be applied. Rainfall systems with very short decorrelation lengths would be excluded from a correction.

Chapter 5 discussed the use of radar in hydrology along with the problems that are encountered with its use. The hydrological model, GSSHA, was introduced here as a means to assess the question “To what extent does the integrating nature of a catchment reduce the model impact of coarse resolution rainfall data input?”. The test catchment

and rainfall case studies that were used with the model were also described.

Keeping all model calibration parameters equal, it was observed that there were major differences between model outflow with lumped rainfall input and that with distributed rainfall input. This difference was greater for less saturated soil. This indicates that the model is quite sensitive to the 2D variation of precipitation intensity across the catchment.

Chapter 6 then set out to answer the aforementioned question directly. By running GSSHA using high resolution radar degraded in resolution to a range of spatial and temporal scales, the impact of low resolution sampling could be assessed.

The catchment model was observed to have a damping effect on the magnitude of sampling error. Although error magnitudes were still at sufficiently worrying levels for conventional radar resolutions (variation of 14–30% in peak flow). It has therefore been shown that sampling error should not be ignored when running rainfall runoff models.

It was discovered that observing at lower spatial resolutions provided a positive bias to the total rainfall volume in the model, increasing peak flow levels in general. The error introduced from lower temporal resolutions would sometimes counteract the spatial sampling error, meaning that sometimes for lower spatial and temporal resolution sampling, the error would be less than for higher spatial and temporal resolution sampling.

The impact that a mean field bias (calculated in the presence of sampling error) would have on a rainfall runoff model was also looked at in the chapter. Although it did appear that a mean field bias correction did reduce some of the bias from spatial sampling errors on average, the results from individual gauge network realizations varied considerably. It was concluded that gauge correction only be applied when the difference between the radar and gauge is sufficiently large so as to overcome the errors due to sampling.

At the end of this thesis it is believed that we now have a greater understanding of sampling error and therefore the resolution requirements for rainfall observation. An answer to the question “How much resolution is ‘enough’ for rainfall measurement?” is now much more enlightened. We have now detailed how it depends upon the application of the rainfall data, the characteristics of the rainfall system being measured and on the instrument which performs the measurement.

The original contributions to knowledge that this thesis has made shall be detailed in

the following paragraph. The approach to estimating the spatial and temporal sampling errors in radar measurements originally put forward by Fabry et al. (1994) was here re-examined using a three month high resolution radar dataset. All previous investigations in this manner were limited to one to three case studies. The larger number of cases analyzed allowed for inferences to be made into the resolution error characteristics of different types of events. A quantitative relationship between a specific function of spatial autocorrelation and rainfall intensity at low resolutions and the spatial sampling error one could expect at that resolution has been discovered. In addition, the error from spatial and temporal sampling was put into context with the total expected radar/rainfall error by using the high resolution radar data to simulate rain gauge networks, something that has not been looked at using the Fabry et al. (1994) technique. The technique was also extended to look at how radar sampling errors affect rainfall runoff models.

References

AMS. Weather analysis and forecasting. *Bulletin - American Meteorological Society*, 88, 2007.

E. N. Anagnostou and W. F. Krajewski. Real-time radar rainfall estimation. part i: Algorithm formulation. *Journal of Atmospheric and Oceanic Technology*, 16(2):189–197, 1999.

B. Anderl, W. Attmannspacher, and G. A. Schultz. Accuracy of reservoir inflow forecasts based on radar rainfall measurements. *Water Resources Research*, 12(2):217–223, 1976.

H. Andrieu. Radar rainfall measurement: From the calibration by raingages to the physically based processing of radar images. *La Houille Blanche*, 2:32–36, 2002.

H. Andrieu and J. D. Creutin. Identification of vertical profiles of radar reflectivity for hydrological applications using an inverse method. part i: formulation. *Journal of Applied Meteorology*, 34(1):225–239, 1995.

H. Andrieu, J. D. Creutin, G. Delrieu, and D. Faure. Use of a weather radar for the hydrology of a mountainous area. part i: Radar measurement interpretation. *Journal of Hydrology*, 193(1-4):1–25, 1997.

D. Atlas, editor. *Radar in Meteorology: Battan Memorial and 40th Anniversary*. American Meteorology Society, Boston, 1990.

D Atlas, C W Ulbrich, F D Marks Jr, E Amitai, and C R Williams. Systematic variation of drop size and radar-rainfall relations. *Journal of Geophysical Research D: Atmospheres*, 104:6155–6169, 1999.

G. L. Austin and L. B. Austin. The use of radar in urban hydrology. *Journal of Hydrology*, 22(1-2):131–142, 1974.

G. L. Austin, A. Bellon, P. Dionne, and M. Roch. On the interaction between radar and satellite image nowcasting systems and mesoscale numerical models. In *Proceedings Symposium on Mesoscale Analysis and Forecasting*, Vancouver, 1987. ESA SP-282, 225-228.

P. M. Austin. Relations between measured radar reflectivity and surface rainfall. *Monthly Weather Review*, 115(5):1053–1070, 1987.

Pauline M. Austin and Alan C. Bemis. A quantitative study of the "bright band" in radar precipitation echoes. *Journal of the Atmospheric Sciences*, 7(2):145–151, 1950.

L J Battan. *Radar Observation of the Atmosphere*. University of Chicago Press, Chicago, 1973.

A. Bellon and G. L. Austin. Accuracy of short-term radar rainfall forecasts. *Journal of Hydrology*, 70(1-4):35–49, 1984.

A. Bellon, S. Lovejoy, and G. L. Austin. Combining satellite and radar data for the short-range forecasting of precipitation. *Monthly Weather Review*, 108(10):1554–1566, 1980.

A. Bellon, G. W. Lee, and I. Zawadzki. Error statistics of vpr corrections in stratiform precipitation. *Journal of Applied Meteorology*, 44(7):998–1015, 2005.

M. Bernard. An approach to determinate stream flow. *Transactions of the American Society of Civil Engineers*, 100(1):347–362, 1935.

A. Berne and W. F. Krajewski. Radar for hydrology: Unfulfilled promise or unrecognized potential? *Advances in Water Resources*, 51:357–366, 2013.

A. Berne and R. Uijlenhoet. Quantitative analysis of x-band weather radar attenuation correction accuracy. *Natural Hazards and Earth System Science*, 6(3):419–425, 2006.

A. Berne, G. Delrieu, H. Andrieu, and J. D. Creutin. Influence of the vertical profile of reflectivity on radar-estimated rain rates at short time steps. *Journal of Hydrometeorology*, 5(2):296–310, 2004a.

A. Berne, G. Delrieu, J. D. Creutin, and C. Obled. Temporal and spatial resolution of rainfall measurements required for urban hydrology. *Journal of Hydrology*, 299(3-4): 166–179, 2004b.

K. J. Beven, R. Lamb, P. Quinn, R. Romanowicz, and J. Freer. Topmodel. In V. P. Singh, editor, *Computer Models of Watershed Hydrology*, pages 627–668. Water Resources Publications, Colorado, 1995.

C. J. Birks, A. P. Bootman, I. Cluckie, and H. Dawei, editors. *Wessex flood-forecasting system*. Hydrological Applications of Weather Radar. Ellis Horwood Ltd., Chichester, 1991.

Asit K. Biswas. The automatic rain-gauge of sir christopher wren, f.r.s. *Notes and Records of the Royal Society of London*, 22(1/2):94–104, 1967.

M. Borga. Accuracy of radar rainfall estimates for streamflow simulation. *Journal of Hydrology*, 267(1-2):26–39, 2002.

M. Borga, E. N. Anagnostou, and E. Frank. On the use of real-time radar rainfall estimates for flood prediction in mountainous basins. *Journal of Geophysical Research D: Atmospheres*, 105(D2):2269–2280, 2000.

M. Borga, F. Tonelli, R. J. Moore, and H. Andrieu. Long-term assessment of bias adjustment in radar rainfall estimation. *Water Resources Research*, 38(11):81–810, 2002.

E. A. Brandes. Optimizing rainfall estimates with the aid of radar. *J. Appl. Meteor*, 14: 1339 –1345, 1975.

E. A. Brandes, G. Zhang, and J. Vivekanandan. Experiments in rainfall estimation with a polarimetric radar in a subtropical environment. *Journal of Applied Meteorology*, 41(6):674–683, 2002.

R. A. Brown, B. A. Flickinger, E. Forren, D. M. Schultz, D. Sirmans, P. L. Spencer, V. T. Wood, and C. L. Ziegler. Improved detection of severe storms using experimental fine-resolution wsr-88d measurements. *Weather and Forecasting*, 20(1):3–14, 2005.

C R Burrows and S S Attwood. *Radio wave propagation; consolidated summary technical report of the Committee on Propagation of the National Defense Research Committee*. Academic Press, New York, 1949.

T. M. Carpenter, K. P. Georgakakos, and J. A. Sperfslagea. On the parametric and nexrad-radar sensitivities of a distributed hydrologic model suitable for operational use. *Journal of Hydrology*, 253(1-4):169–193, 2001.

S. Chumchean, A. Sharma, and A. Seed. Radar rainfall error variance and its impact on radar rainfall calibration. *Physics and Chemistry of the Earth*, 28(1-3):27–39, 2003.

S. Chumchean, A. Sharma, and A. Seed. An integrated approach to error correction for real-time radar-rainfall estimation. *Journal of Atmospheric and Oceanic Technology*, 23(1):67–79, 2006.

G. J. Ciach and W. F. Krajewski. On the estimation of radar rainfall error variance. *Advances in Water Resources*, 22(6):585–595, 1999.

G. J. Ciach, W. F. Krajewski, E. N. Anagnostou, M. L. Baeck, J. A. Smith, J. R. McCollum, and A. Kruger. Radar rainfall estimation for ground validation studies of the tropical rainfall measuring mission. *Journal of Applied Meteorology*, 36(6):735–747, 1997.

C.O. Clark. Storage and the unit hydrograph. *Transactions of the American Society of Civil Engineers*, 110:1419–1446, 1945.

I. Cluckie and M. D. Owens. Real-time rainfall runoff models and use of weather radar information. In V. K. Collinge and C. Kirby, editors, *Weather Radar and Flood Forecasting*. Wiley and Sons, Chichester, UK, 1987.

S. J. Cole and R. J. Moore. Hydrological modelling using raingauge- and radar-based estimators of areal rainfall. *Journal of Hydrology*, 358(3-4):159–181, 2008.

C. Collier and I. Cluckie. A hydrological study of the real-time calibration of radar derived rainfall data. In *Proceedings from the International Conference on Advances in Water Engineering*, University of Birmingham, 1985. Elsevier.

C. G. Collier. Accuracy of rainfall estimates by radar, part ii: comparison with raingauge network (uk). *Journal of Hydrology*, 83(3-4):225–235, 1986.

C. G. Collier. Developments in radar and remote-sensing methods for measuring and forecasting rainfall. *Philosophical Transactions: Mathematical, Physical and Engineering Sciences (Series A)*, 360(1796):1345–1361, 2002.

C. G. Collier. On quality indicators for radar-based river flow forecasts. *Proceedings of the Institution of Civil Engineers: Water Management*, 162(2):115–123, 2009.

C. G. Collier, P. R. Larke, and B. R. May. A weather radar correction procedure for real-time estimation of surface rainfall. *Quarterly Journal of the Royal Meteorological Society*, 109(461):589–608, 1983.

N. A. Cressie and C. K. Wikle. *Statistics for spatio-temporal data*. Wiley, Hoboken, N.J., 2011.

G. Delrieu, L. Hucke, and J. D. Creutin. Attenuation in rain for x- and c-band weather radar systems: Sensitivity with respect to the drop size distribution. *Journal of Applied Meteorology*, 38(1):57–68, 1999.

G. Delrieu, I. Braud, A. Berne, M. Borga, B. Boudevillain, F. Fabry, J. Freer, E. Gaume, E. Nakakita, A. Seed, P. Tabary, and R. Uijlenhoet. Weather radar and hydrology. *Advances in Water Resources*, 32(7):969–974, 2009.

J. C. I. Dooge. A general theory of the unit hydrograph. *Journal of Geophysical Research*, 64:241–256, 1959.

C. W. Downer and F. L. Ogden. Gssha: Model to simulate diverse stream flow producing processes. *Journal of Hydrologic Engineering*, 9(3):161–174, 2004.

C. W. Downer, F. L. Ogden, and A. R. Byrd. Gsshawiki user's manual, gridded surface subsurface hydrologic analysis version 4.0 for wms 8.1. Technical report, Engineer Research and Development Center, 2008.

M. R. Duncan, B. Austin, F. Fabry, and G. L. Austin. The effect of gauge sampling density on the accuracy of streamflow prediction for rural catchments. *Journal of Hydrology*, 142(1-4):445–476, 1993.

K. El-Rayes and O. Moselhi. Impact of rainfall on the productivity of highway construction. *Journal of Construction Engineering and Management*, 127(2):125–131, 2001.

I. Emmanuel, H. Andrieu, and P. Tabary. Evaluation of the new french operational weather radar product for the field of urban hydrology. *Atmospheric Research*, 103: 20–32, 2012.

F. Fabry and I. Zawadzki. Long-term radar observations of the melting layer of precipitation and their interpretation. *Journal of the Atmospheric Sciences*, 52(7):838–851, 1995.

F Fabry, G L Austin, and D Tees. The accuracy of rainfall estimates by radar as a function of range. *Quarterly Journal of the Royal Meteorological Society*, 118:435–453, 1992.

Frederic Fabry, Aldo Bellon, Mike R. Duncan, and Geoffrey L. Austin. High resolution rainfall measurements by radar for very small basins: the sampling problem reexamined. *Journal of Hydrology*, 161(1-4):415–428, 1994.

R. A. Fulton, J. P. Breidenbach, D. J. Seo, D. A. Miller, and T. O'Bannon. The wsr-88d rainfall algorithm. *Weather and Forecasting*, 13(2):377–395, 1998.

Konstantine P. Georgakakos, Theresa M. Carpenter, James A. Cramer, Jason A. Sperfslage, Timothy L. Sweeney, and Dan L. Fread. National system for threshold runoff estimation. In *Proceedings of the Symposium on Engineering Hydrology*, pages 952–957, San Francisco, CA, USA, 1993. Publ by ASCE.

U. Germann. Radome attenuation - a serious limiting factor for quantitative radar measurements? *Meteorologische Zeitschrift*, 8(3):85–90, 1999.

U. Germann and J. Joss. Mesobeta profiles to extrapolate radar precipitation measurements above the alps to the ground level. *Journal of Applied Meteorology*, 41(5): 542–557, 2002.

U. Germann, G. Galli, M. Boscacci, and M. Bolliger. Radar precipitation measurement in a mountainous region. *Quarterly Journal of the Royal Meteorological Society*, 132 (618 A):1669–1692, 2006.

B. W. Golding. Nimrod: A system for generating automated very short range forecasts. *Meteorological Applications*, 5(1):1–16, 1998.

W. H. Green and G. Ampt. Studies of soil physics, part i. - the flow of air and water through soils. *Journal of Agricultural Science*, 4:1–24, 1911.

D. I. F. Grimes and E. Pardo-Igzquiza. Geostatistical analysis of rainfall. *Geographical Analysis*, 42(2):136–160, 2010.

R. E. S. Gunn and J. S. Marshall. The effect of wind shear on falling precipitation. *Journal of Meteorology*, 12(4):339–349, 1955.

Ross Gunn and Gilbert D. Kinzer. The terminal velocity of fall for water droplets in stagnant air. *Journal of the Atmospheric Sciences*, 6(4):243–248, 1949.

U. Haberlandt. Geostatistical interpolation of hourly precipitation from rain gauges and radar for a large-scale extreme rainfall event. *Journal of Hydrology*, 332(1-2): 144–157, 2007.

G. F. Haggett, C. M. Merrick and C. I. Richards, editors. *Quantitative use of radar for operational flood warning in the Thames area*. Hydrological Applications of Weather Radar. Ellis Horwood Ltd., Chichester, 1991.

T. W. Harrold and P. G. Kitchingman. Measurement of surface rainfall using radar when the beam intersects the melting layer. In *Preprints, 16th Conf. on Radar Meteorology*, page 473478. American Meteorological Society, Houston, TX, 1975.

T W Harrold, E J English, and C A Nicholas. Accuracy of radar-derived rainfall measurements in hilly terrain. *Quarterly Journal of the Royal Meteorological Society*, 100:331–350, 1974.

W Heberden. Of the different quantities of rain, which appear to fall, at different heights, over the same spot of ground. *Philosophical Transactions of the Royal Society*, 59, 1769.

P. H. Hildebrand, N. Towery, and M. R. Snell. Measurements of convective mean rainfall over small areas using high-density raingages and radar. *Journal of Applied Meteorology*, 18(10):1316–1326, 1979.

Peter H. Hildebrand. Iterative correction for attenuation of 5 cm radar in rain. *Journal of Applied Meteorology*, 17(4):508–514, 1978.

Walter Hitschfeld and Jack Bordan. Errors inherent in the radar measurement of rainfall at attenuating wavelengths. *Journal of the Atmospheric Sciences*, 11(1):58–67, 1954.

I. Holleman. Bias adjustment and long-term verification of radar-based precipitation estimates. *Meteorological Applications*, 14(2):195–203, 2007.

W. G. Hoyt. *Studies of Relations of Rainfall and Run-off in the United States*. Water-Supply Paper 772. United States Government Printing Office, Washington, 1936.

M Hudlow, R Arkell, V Patterson, P Pytlowany, F Richards, and S G Geotis. Calibration and intercomparison of the gate c-band radars. Technical report, U.S. Department of Commerce, 1979.

P. Jordan, A. Seed, and G. Austin. Sampling errors in radar estimates of rainfall. *Journal of Geophysical Research D: Atmospheres*, 105(D2):2247–2257, 2000.

D. P. Jorgensen, T. R. Shepherd, and A. S. Goldstein. A dual-pulse repetition frequency scheme for mitigating velocity ambiguities of the noaa p-3 airborne doppler radar. *Journal of Atmospheric and Oceanic Technology*, 17(5):585–594, 2000.

J. Joss and Robert Lee. The application of radar-gauge comparisons to operational precipitation profile corrections. *Journal of Applied Meteorology*, 34(12):2612–2630, 1995.

J. Joss and A. Waldvogel. Precipitation measurement and hydrology. In D. Atlas, editor, *Radar in Meteorology*. American Meteorological Company, Boston, 1990.

R. J. Keeler. Signal processing for atmospheric radars. In D. Atlas, editor, *Radar in Meteorology*. American Meteorological Society, Boston, 1990.

R. J. Keeler and R. J. Serafin. Meteorological radar. In M. I. Skolnik, editor, *Radar Handbook, Third Edition*. McGraw-Hill, New York, 2008.

T. Keenan, P. Joe, J. Wilson, C. Collier, B. Golding, D. Burgess, P. May, C. Pierce, J. Bally, A. Crook, A. Seed, D. Sills, L. Berry, R. Potts, I. Bell, N. Fox, E. Ebert, M. Eilts, K. O'Loughlin, R. Webb, R. Carbone, K. Browning, R. Roberts, and C. Mueller. The sydney 2000 world weather research programme forecast demonstration project. *Bulletin of the American Meteorological Society*, 84(8):1041–1054, 2003.

C. Kidd. Satellite rainfall climatology: A review. *International Journal of Climatology*, 21(9):1041–1066, 2001.

M. Kitchen and R. M. Blackall. Representativeness errors in comparisons between radar and gauge measurements of rainfall. *Journal of Hydrology*, 134(1-4):13–33, 1992.

M. Kitchen, R. Brown, and A. G. Davies. Real-time correction of weather radar data for the effects of bright band, range and orographic growth in widespread precipitation. *Quarterly Journal of the Royal Meteorological Society*, 120(519):1231–1254, 1994.

G. E. Klazura and D. A. Imy. A description of the initial set of analysis products available from the nexrad wsr-88d system. *Bulletin - American Meteorological Society*, 74(7):1293–1311, 1993.

V. I. Koren, B. D. Finnerty, J. C. Schaake, M. B. Smith, D. J. Seo, and Q. Y. Duan. Scale dependencies of hydrologic models to spatial variability of precipitation. *Journal of Hydrology*, 217(3-4):285–302, 1999.

W. F. Krajewski. Cokriging radar- rainfall and rain gage data. *Journal of Geophysical Research*, 92(D8):9571–9580, 1987.

T. Kubota, S. Shige, K. Aonashi, and K. Okamoto. Development of nonuniform beam-filling correction method in rainfall retrievals for passive microwave radiometers over ocean using trmm observations. *Journal of the Meteorological Society of Japan*, 87 A:153–164, 2009.

G Kulesa. Weather and aviation: How does weather affect the safety and operations of airports and aviation, and how does faa work to manage weather-related effects? In *The Potential Impacts of Climate Change on Transportation*, Washington, D.C., 2003.

S. A. Lack and N. I. Fox. An examination of the effect of wind-drift on radar-derived surface rainfall estimations. *Atmospheric Research*, 85(2):217–229, 2007.

M. P. Langleben. The plan pattern of snow echoes at the generating level. *Journal of the Atmospheric Sciences*, 13(6):554–560, 1956.

J. K. Lazo, R. E. Morss, and J. L. Demuth. 300 billion served. *Bulletin of the American Meteorological Society*, 90(6):785–798, 2009.

E. Le Bouar, J. Testud, and T. D. Keenan. Validation of the rain profiling algorithm "zphi" from the c-brand polarimetric weather radar in darwin. *Journal of Atmospheric and Oceanic Technology*, 18(11):1819–1837, 2001.

H. Leijnse, R. Uijlenhoet, and A. Berne. Errors and uncertainties in microwave link rainfall estimation explored using drop size measurements and high-resolution radar data. *Journal of Hydrometeorology*, 11(6):1330–1344, 2010.

P. A. Lewandowski, W. E. Eichinger, A. Kruger, and W. F. Krajewski. Lidar-based estimation of small-scale rainfall: Empirical evidence. *Journal of Atmospheric and Oceanic Technology*, 26(3):656–664, 2009.

J. D. Locatelli and P. V. Hobbs. Fall speeds and masses of solid precipitation particles. *J. Geophys. Res.*, 79:2185–2197, 1974.

S. Lovejoy and G. L. Austin. The sources of error in rain amount estimating schemes from goes visible and ir satellite data. *Monthly Weather Review*, 107(8):1048–1054, 1979.

P. V. Mandapaka, W. F. Krajewski, G. J. Ciach, G. Villarini, and J. A. Smith. Estimation of radar-rainfall error spatial correlation. *Advances in Water Resources*, 32(7):1020–1030, 2009.

Glenn Aaron Manley. *Development and Implementation of a Multi-Instrument High-Resolution Weather Monitoring System*. PhD thesis, University of Auckland, 2006.

J. S. Marshall. Interpretation of the fluctuating echo from randomly distributed scatterers. *Canadian journal of physics*, 31(6):962 –994, 1953.

J. S. Marshall and W. McK Palmer. The distribution of raindrops with size. *Journal of the Atmospheric Sciences*, 5(4):165–166, 1948.

J. S. Marshall, R. C. Langille, and W. McK Palmer. Measurement of rainfall by radar. *Journal of the Atmospheric Sciences*, 4(6):186–192, 1947.

Doug McCollor and Roland Stull. Hydrometeorological accuracy enhancement via postprocessing of numerical weather forecasts in complex terrain. *Weather and Forecasting*, 23(1):131–144, 2008.

J. L. Monteith. Evaporation and environment. In *Symposia of the Society for Experimental Biology, XIX*, pages 205–234, 1965.

M L Morrissey, J A Maliekal, J S Greene, and J Wang. The uncertainty of simple spatial averages using rain gauge networks. *Water Resources Research*, 31:2011–2017, 1995.

NASA. National space science data center master catalog, 2012. URL `http://nssdc.gsfc.nasa.gov/nmc/`.

S. P. Neeck, R. K. Kakar, A. A. Azarbarzin, and A. Y. Hou. Global precipitation measurement (gpm) implementation. In *Sensors, Systems, and Next-Generation Satellites XIV*, volume 7826, Toulouse, 2010.

E. L. Neff. How much rain does a rain gage gage? *Journal of Hydrology*, 35(3-4): 213–220, 1977.

J. A. Nystuen. Temporal sampling requirements for automatic rain gauges. *Journal of Atmospheric and Oceanic Technology*, 15(6):1253–1260, 1998.

K. M. O'Conner. River flow forecasting. In D. W. Knight and A. Y. Shamseldin, editors, *River Basin Modelling for Flood Risk Mitigation*, pages 197–213. Taylor & Francis/Balkema, Leiden, 2006.

F. L. Ogden and B. Saghafian. Green and ampt infiltration with redistribution. *Journal of Irrigation and Drainage Engineering*, 123(5):386–393, 1997.

T. Ohtake. Factors affecting the size distribution of raindrops and snowflakes. *Journal of the Atmospheric Sciences*, 27(5):804–813, 1970.

R. Oliveira and D. Ford, editors. *River basin forecasting system for Portuguese rivers*. Hydrological Applications of Weather Radar. Ellis Horwood Ltd., Chichester, 1991.

A. Overeem, H. Leijnse, and R. Uijlenhoet. Measuring urban rainfall using microwave links from commercial cellular communication networks. *Water Resources Research*, 47(12), 2011.

W. L. Patterson. The propagation factor, fp, in the radar equation. In M. I. Skolnik, editor, *Radar Handbook, Third Edition*. McGraw-Hill, New York, 2008.

H. L. Penman. The physical bases of irrigation control. In *Report of the 13th International Horticultural Congress*, London, 1953.

B. Z. Petrenko. The beamfilling algorithm for retrieval of hydrometeor profile parameters from passive microwave measurements. *IEEE Transactions on Geoscience and Remote Sensing*, 39(1):117–124, 2001.

F. Piccolo and G. B. Chirico. Sampling errors in rainfall measurements by weather radar. *Advances in Geosciences*, 2:151–155, 2005.

J. R. Probert-Jones. The radar equation in meteorology. *Quarterly Journal of the Royal Meteorological Society*, 88(378):485–495, 1962.

A. R. Rahimi, A. R. Holt, G. J. G. Upton, and R. J. Cummings. Use of dual-frequency microwave links for measuring path-averaged rainfall. *Journal of Geophysical Research D: Atmospheres*, 108(15):ACL 8–1 – ACL 8–12, 2003.

B. D. Richards. *Flood Estimation and Control*. Chapman and Hall, London, 1944.

M. A. Rico-Ramirez and I. D. Cluckie. Classification of ground clutter and anomalous propagation using dual-polarization weather radar. *IEEE Transactions on Geoscience and Remote Sensing*, 46(7):1892–1904, 2008.

C. N. Ross. The calculation of flood discharge by the use of a time contour plan. *Transactions of the Intitution of Engineers, Australia*, 2:85–92, 1921.

J. W. Ryde. Attenuation of centimeter radio waves and the echo intensities resulting from atmospheric phenomena. *I.E.E., J. Pt. 3A*, 93:101–103, 1946.

J. W. Ryde and D. Ryde. Attenuation of centimetre waves by rain, hail, and clouds. Technical report, General Electric Research Laboratory, Wembley, England, 1944.

N. Sajikumar and B. S. Thandaveswara. A non-linear rainfall-runoff model using an artificial neural network. *Journal of Hydrology*, 216(1-2):32–55, 1999.

M. Sangati, M. Borga, D. Rabuffetti, and R. Bechini. Influence of rainfall and soil properties spatial aggregation on extreme flash flood response modelling: An evaluation based on the sesia river basin, north western italy. *Advances in Water Resources*, 32 (7):1090–1106, 2009.

M. Savina, B. Schppi, P. Molnar, P. Burlando, and B. Sevruk. Comparison of a tipping-bucket and electronic weighing precipitation gage for snowfall. *Atmospheric Research*, 103:45–51, 2012.

W. Schilling. Rainfall data for urban hydrology: what do we need? *Atmospheric Research*, 27(1-3):5–21, 1991.

A. W. Seed. A dynamic and spatial scaling approach to advection forecasting. *Journal of Applied Meteorology*, 42(3):381–388, 2003.

D. Sempere-Torres, C. Corral, J. Raso, and P. Malgrat. Use of weather radar for combined sewer overflows monitoring and control. *Journal of Environmental Engineering*, 125(4):372–380, 1999.

B. C. Seo, W. F. Krajewski, A. Kruger, P. Domaszczynski, J. A. Smith, and M. Steiner. Radar-rainfall estimation algorithms of hydro-nexrad. *Journal of Hydroinformatics*, 13(2):277–291, 2011.

D. J. Seo and J. P. Breidenbach. Real-time correction of spatially nonuniform bias in radar rainfall data using rain gauge measurements. *Journal of Hydrometeorology*, 3 (2):93–111, 2002.

D. J. Seo, J. P. Breidenbach, and E. R. Johnson. Real-time estimation of mean field bias in radar rainfall data. *Journal of Hydrology*, 223(3-4):131–147, 1999.

A. Y. Shamseldin. Application of a neural network technique to rainfall-runoff modelling. *Journal of Hydrology*, 199(3-4):272–294, 1997.

L. K. Sherman. Streamflow from rainfall by unit-graph method. *Engineering News Record*, 108:501–505, 1932.

S. T. Shipley, E. W. Eloranta, and J. A. Weinman. Measurement of rainfall rates by lidar. *Journal of Applied Meteorology*, 13(7):800–807, 1974.

P. E. Shucksmith, L. Sutherland-Stacey, and G. L. Austin. The spatial and temporal sampling errors inherent in low resolution radar estimates of rainfall. *Meteorological Applications*, 18(3):354–360, 2011.

G. A. Shultz. Digital computer solutions for flood hydrograph prediction from rainfall data. In *Unesco-IAHS Symposium on the Use of Analog and Digital Computers in Hydrology*, Tucson, Arizona, 1968.

Catherine J. Smith. The reduction of errors caused by bright bands in quantitative rainfall measurements made using radar. *Journal of Atmospheric and Oceanic Technology*, 3(1):129–141, 1986.

P. L. Smith. Precipitation measurement and hydrology: Panel report. In Atlas D., editor, *Radar in Meteorology*. American Meteorological Society, Boston, 1990.

M. Steiner. Uncertainty of estimates of monthly areal rainfall for temporally sparse remote observations. *Water Resources Research*, 32(2):373–388, 1996.

M. Steiner, J. A. Smith, S. J. Burges, C. V. Alonso, and R. W. Darden. Effect of bias adjustment and rain gauge data quality control on radar rainfall estimation. *Water Resources Research*, 35(8):2487–2503, 1999.

R. E. Stewart, J. D. Marwitz, J. C. Pace, and R. E. Carbone. Characteristics through the melting layer of stratiform clouds. *Journal of the Atmospheric Sciences*, 41(22): 3227–3237, 1984.

C. David Stow, Stuart G. Bradley, Keith E. Farrington, Kim N. Dirks, and Warren R. Gray. A rain gauge for the measurement of finescale temporal variations. *Journal of Atmospheric and Oceanic Technology*, 15(1):127, 1998.

J W Strutt. On the light from the sky, its polarization and colour. *Philosophical Magazine Series 4*, 41(271):107–120, 1871.

L Sutherland-Stacey, P E Shucksmith, and G L Austin. High resolution observation of a small tornado, ardmore, new zealand. *Weather and Climate*, 30:46–53, 2010.

D Tees and G L Austin. The effect of range on the radar measurement of rainfall. In *Hydrological applications of weather radar*, pages 296–304. Ellis Horwood Ltd., West Sussex, 1991.

K. A. Tilford, N. I. Fox, and C. G. Collier. Application of weather radar data for urban hydrology. *Meteorological Applications*, 9(1):95–104, 2002.

M. C. Todd, E. C. Barrett, M. J. Beaumont, and T. J. Bellerby. Estimation of daily rainfall over the upper nile river basin using a continuously calibrated satellite infrared technique. *Meteorological Applications*, 6(3):201–210, 1999.

A.A. Tsonis and G.L. Austin. An evaluation of extrapolation techniques for the short-term prediction of rain amounts. *Atmosphere-Ocean*, 19(1):54–65, 1981.

S Twomey. On the measurement of precipitation intensity by radar. *Journal of Meteorology*, 10:66–67, 1953.

G. J. G. Upton, A. R. Holt, R. J. Cummings, A. R. Rahimi, and J. W. F. Goddard. Microwave links: The future for urban rainfall measurement? *Atmospheric Research*, 77(1-4 SPEC. ISS.):300–312, 2005.

E Vanmarcke. *Random Fields: Analysis and Synthesis (Revised and Expanded New Edition)*. World Scientific Publishing Company, 2010.

J. F. I. Ventura and P. Tabary. The new french operational polarimetric radar rainfall rate product. *Journal of Applied Meteorology and Climatology*, 52(8):1817–1835, 2013.

V. Venugopal, E. Foufoula-Georgiou, and V. Sapozhnikov. Evidence of dynamic scaling in space-time rainfall. *Journal of Geophysical Research D: Atmospheres*, 104(D24): 31599–31610, 1999.

J. Verdin and R. Klaver. Grid-cell-based crop water accounting for the famine early warning system. *Hydrological Processes*, 16(8):1617–1630, 2002.

B. Vieux and N. S. Farajalla. Temporal and spatial aggregation of nexrad rainfall estimates on distributed hydrologic modelling. In *Preprints, Third Int. Conf. on GIS and Environmental Modeling*, page 199204, Santa Fe, NM, 1996. National Center for Geographic Information and Analysis.

B. E. Vieux. *Distributed Hydrological Modeling Using GIS, Second Edition*. Kluwer Academic Publishers, Dordrecht, 2004.

G. Villarini, P. V. Mandapaka, W. F. Krajewski, and R. J. Moore. Rainfall and sampling uncertainties: A rain gauge perspective. *Journal of Geophysical Research D: Atmospheres*, 113(11), 2008.

J. Wang and D. B. Wolff. Evaluation of trmm ground-validation radar-rain errors using rain gauge measurements. *Journal of Applied Meteorology and Climatology*, 49(2): 310–324, 2010.

M. L. Weisman. Convective storms. In J. Holton, J. Pyle, and J. Curry, editors, *Encyclopedia of Atmospheric Sciences 2nd Edition*. Academic Press, 2002.

F. J. Wentz and R. W. Spencer. Ssm/i rain retrievals within a unified all-weather ocean algorithm. *Journal of the Atmospheric Sciences*, 55(9):1613–1627, 1998.

S. M. Wesson and G. G. S. Pegram. Radar rainfall image repair techniques. *Hydrology and Earth System Sciences*, 8(2):220–234, 2004.

P. T. Willis and A. J. Heymsfield. Structure of the melting layer in mesoscale convective system stratiform precipitation. *Journal of the Atmospheric Sciences*, 46(13):2008–2025, 1989.

J. W. Wilson and E. A. Brandes. Radar measurement of rainfall - a summary. *Bulletin American Meteorological Society*, 60(9):1048–1058, 1979.

M. Winchell, H. V. Gupta, and S. Sorooshian. On the simulation of infiltration- and saturation-excess runoff using radar-based rainfall estimates: Effects of algorithm uncertainty and pixel aggregation. *Water Resources Research*, 34(10):2655–2670, 1998.

WMO. Aviation hazards. Technical report, WMO, 2007.

WMO. Status of current and future cgms members' satellites, 2012. URL `http://www.wmo.int/pages/prog/sat/satellitestatus.php`.

J. M. Yuan, K. A. Tilford, H. Y. Jiang, and I. D. Cluckie. Real-time urban drainage system modelling using weather radar rainfall data. *Physics and Chemistry of the Earth, Part B: Hydrology, Oceans and Atmosphere*, 24(8):915–919, 1999.

I Zawadzki. The quantitative interpretation of weather radar measurements. *Atmosphere-Ocean*, 20:158–180, 1982.

I Zawadzki. Factors affecting the precision of radar measurements of rain. In *Preprints, 22nd Int. Conf. on Radar Meteorology*, pages 251–256, Zurich, Switzerland, 1984. American Meteorological Society.

X. Zhang and R. Srinivasan. Gis-based spatial precipitation estimation: A comparison of geostatistical approaches. *Journal of the American Water Resources Association*, 45(4):894–906, 2009.

D. Zhu, D. Z. Peng, and I. D. Cluckie. Statistical analysis of error propagation from radar rainfall to hydrological models. *Hydrology and Earth System Sciences*, 17(4): 1445–1453, 2013.